FORMING SCREEN EFFECT ON ULTRASONIC BEAM FIELD

A Thesis
Presented to
The Academic Faculty

by

John Lyle Fouts

In Partial Fulfillment
of the Requirements for the Degree
Master of Science in the
School of Mechanical Engineering

Georgia Institute of Technology
May 2005

FORMING SCREEN EFFECT ON ULTRASONIC BEAM FIELD

Approved by:

Dr. Cyrus Aidun, Advisor
School of Mechanical Engineering
Georgia Institute of Technology

Dr. Timothy Patterson
School of Mechanical Engineering
Georgia Institute of Technology

Dr. David Orloff
School of Mechanical Engineering
Georgia Institute of Technology

Date Approved: 15 December 2005

Acknowledgements

I would like to thank my advisor, Dr. Cyrus Aidun, for his support throughout this project. I would also like to thank the Department of Energy and the member companies of the fluid dynamics and forming program at the Institute of Paper Science and Technology at Georgia Institute of Technology for their support. I would like to thank Mr. Matthias Messer for his help with the experiments and the other support that he gave. Finally, I would like to thank my wife for her support and help during the pursuit of this endeavor.

TABLE OF CONTENTS

List of Figures

Nomenclature

c	Speed of wave propagation
d	Diameter of sample volume disk
D	Diameter of ultrasonic transducer
$D_r(\gamma)$	Directivity function
Δd	Total distance that the particle travels between the two emissions of ultrasonic energy
f	Frequency
f_D	Doppler shift frequency
f_e	Frequency of the source
f_g	Frequency of the reflected wave from the target particle
f_r	Frequency of the receiver
f_{ra}	Audible noise frequency
f_{sn}	Subsonic noise frequency
f_{un}	Ultrasonic noise frequency
h	Thickness of sample volume disk
I_0	Maximum intensity
I_z	Intensity of the acoustic field
J_1	First order Bessel function of the first kind
k	Wave number
L_{NF}	Length of the near field
P	Distance from the transducer to the target particle
R	Radius of ultrasonic Transducer

T	Period of Time
T_D	The time delay between an emitted burst of ultrasonic energy and the echo received from the target particle
T_{prf}	Time between two emissions of ultrasonic energy
$(T_2 - T_1)$	The time delay between an emitted burst of ultrasonic energy and the echo received from the target particle
v	Velocity
v_r	Velocity of the receiver away from the source
v_s	Velocity of the source in the same direction as v_r.
δ	Half angle of beam divergence
ϕ	Angle between the direction of movement and the effective ultrasonic beam direction
λ	Wavelength

Summary

The aim of this study was to characterize the interaction between a pulsed ultrasonic wave and a paper forming screen for potential development of a smart paper forming sensor to measure velocity profile of the forming jet as it impinges on the wire. To achieve this goal, a Signal-Processing DOP 2000 pulsed ultrasonic Doppler velocimeter was used to generate a pulsed ultrasonic signal. The signal was transmitted and received using four different ultrasonic transducers: a 2 MHz 10 mm, 4 MHz 5 mm, 4MHz 8 mm focused, and 8 MHz 5 mm. The ultrasonic signals were then analyzed in order to determine the ultrasonic beam echo amplitude and shape. These tests were performed with and without various paper forming screens placed between the ultrasonic transducer and an ultrasonic signal target.

To get an understanding of how the ultrasonic signal would perform without any obstructions present, tests were performed to quantify the ultrasonic beam characteristics without the forming screen present. These tests showed that, as expected, all ultrasonic transducers tested produced a conic-shaped ultrasonic beam. The tests also showed that each transducer produced a ringing effect, or saturation region, where no useful measurements could be achieved. The minimum distance between the transducer surface and the target medium that could be realized by the ultrasonic transducers tested was 20 mm, 5 mm, 4 mm, and 8 mm for the 2 MHz, 4 MHz, 4 MHz focused, and the 8 MHz transducers, respectively. The repeatability of the beam shape measurements was also studied. The tests showed that the beam shape varied only slightly from test to test. The measurements were performed at different times and after connecting and reconnecting the transducer and plastic sphere in the test setup.

Two different paper forming screens were utilized to study the interaction of the ultrasonic beam with the forming screens. The tests showed that the ultrasonic signal passing through the forming screens is greatly attenuated causing a sharp decrease in echo amplitude. To overcome the attenuation of the signal, a much

higher amplification of the signal was used causing an increase in the saturation region around the forming screen. This increased the minimum distance that a target had to be away from the forming screen. The minimum measurable distance for ScreenA was 8, 3, and 4 mm for the 2 MHz, 4 MHz, and 4 MHz focused transducers, respectively. The minimum measurable distance for ScreenB was 4 mm for the 4 MHz transducer. The closest distance from the plastic sphere to the screen over the widest range of transducer-screen-distances that produced detectable echoes was achieved with the 4 MHz 5 mm transducer. The 4 MHz transducer turned out to represent a good tradeoff between the high attenuation of the 8 MHz transducer and the low resolution (measurable depth and velocity) of the 2 MHz transducer. The beam shape in the far screen field is very close to the same with and without ScreenA. In the near screen field, there is a common trend of beam convergence (narrowing of beam width) followed by beam divergence (widening of the beam width) as the beam progresses to the far screen field. The tests showed for both ScreenA and ScreenB that there is more variation in beam width when the screen is moved laterally than when it is not moved at all. They also show that even though the pores in the forming screen are very small, they seem to have a great effect on the beam width measurements of the ultrasonic transducer. The echo profiles clearly show that the forming screen creates a large echo at a depth of 40 mm. The figures show no other discernable echoes except in the region around a depth of 80 mm. These echoes are caused by reverberation of the signal. The reverberations from ScreenB are much greater than the reverberations from ScreenA because ScreenB is twice as thick and has a higher mesh count than ScreenA. The reverberated signal caused the echo profile of the small sphere to be flawed when it passed through the position that the reverberated signal occupied. This caused a flaw in the measurements of the beam shape at the point where the reverberated signal was present.

1 Introduction

1.1 Motivation

Ultrasonic techniques are known to be useful in the study of motion detection and hydrodynamic flow. These ultrasonic studies have been traditionally used in the medical field as non-intrusive measurement techniques [3 and 5] and more recently as non-intrusive flow measurement techniques in other types of hydrodynamic flows [7, 11, 21, 22, 26, and 37]. Pulsed ultrasonic Doppler velocimetry (PUDV) systems measures velocity profiles in fluids, including opaque fluids, instantaneously. In the paper forming industry, knowing the instantaneous velocity measurements of the pulp on the forming screen can help optimize the paper forming process. In order to utilize a pulsed ultrasonic Doppler velocimeter to quantify these measurements, the beam shape and profile emitted from the transducer need to be computed. This study will attempt to qualitatively and quantitatively explain the behavior of the ultrasonic signal from various PUDV transducers. It will also attempt to characterize the interaction between a pulsed ultrasonic wave and a paper forming screen for potential development of a smart paper forming sensor to measure velocity profile of the forming jet as it impinges on the wire. This will be accomplished by analyzing the characteristics, specifically the ultrasonic beam shape and behavior as it interacts with a paper forming screen, of several different PUDV transducers. The development of a smart paper forming sensor to measure velocity profile of the forming jet as it impinges on the wire will help enable paper mills to better control, in real time, the quality of the paper produced by the mill by sensing irregularities with the forming jet or wire.

1.2 Background

Ultrasonic Doppler techniques were originally designed in the medical field, but they have since been used in many fields of science and engineering. Originally, the devices were used as imaging devices. One of the imaging devices made it possible to determine flow velocity by measuring the phase difference in upstream and downstream ultrasonic waves [19]. In 1957, Satomura developed a device that would send and receive ultrasonic signals, and used it in the study of cardiac function [33]. This study showed that blood velocity patterns could be detected by the Doppler frequency shift. Other studies showed that the ultrasonic Doppler technique could be used to measure blood flow by mounting transducers directly on blood vessels [13 and 14] and, ultimately, measurement of blood flow transcutaneously [15]. These methods all used the continuous wave Doppler principle. This method used two piezoelectric crystals. One of the crystals continuously emitted the ultrasonic signal and one received the echo of the ultrasonic signal. The received echo was then analyzed for a change in frequency from the emitted signal frequency, and the frequency change was used to estimate the blood flow velocity. Since continuous wave ultrasonic systems emit and receive signals continuously, all vessels or tissue in the path of the ultrasound beam contribute to the Doppler signal obtained by the receiving transducer. The ultrasonic beam becomes sufficiently attenuated at a certain depth due to signal strength and tissue composition. No useful data can be obtained past this point for the system due to the attenuation of the signal. Since the ultrasonic signal is continuous, no specific locations of velocities in the beams can be determined using continuous wave ultrasonic systems, only general flow movement within the total system. The greatest limitation to continuous wave systems is the inability to determine the specific location of the measurement. This limitation was eventually overcome by the use of pulsed wave Doppler systems.

Pulsed wave ultrasonic systems were developed a short time after the development of the continuous wave ultrasonic systems. Pulsed wave ultrasonic systems were first used, like continuous wave ultrasonic systems, with blood flow

measurement [4]. Analytical and mathematical modeling of pulsed ultrasound systems were also performed showing that a useful transcutaneous blood flow meter based on pulsed wave systems was possible and could be designed [6]. Using the pulsed wave ultrasonic system, fluid flow velocities could be determined as well as the velocities specific location in the flow field. This was a great advancement over the continuous wave ultrasonic system because the continuous wave system did not give any spatial information about the given flow field.

The pulsed wave ultrasound method was developed for medical applications, but it has now been used in a wide variety of applications. The method was easily modified to fit non-medical applications. Poiseuille flow and Taylor vortex flow were studied by Takeda using water as the working fluid. He used an external blood flow meter developed for medical use, and found that the blood flow meter worked well for use in non-medical applications. Takeda concluded that the accuracy of the velocity measurement and the resolution in position and time are deeply related to the selection and frequency of ultrasound, its pulse structure, and electronic constants for data acquisition. He also found that, when using water as the working fluid, some reflecting particles must be suspended in the water, and this could disturb or change properties of the flow field [34]. Takeda continued to study the potential for pulsed wave ultrasonic systems and found that the pulsed ultrasonic Doppler method had several advantages over conventional techniques at the time. He concluded that the pulsed ultrasonic Doppler method produced an efficient flow mapping process, had applicability to opaque liquids, and recorded a history of the spatiotemporal velocity field of the flow in question [35 and 36].

Utilizing the pulsed ultrasonic Doppler technique, or ultrasonic Doppler velocimetry (UDV), other applications of flow measurement have been explored. Ozaki et al used the traditional pulsed ultrasonic Doppler method and a novel technique that they developed to improve the time resolution of the pulsed ultrasonic Doppler method. The technique involved a cross-correlation to estimate the time difference between two echo signals of a pair of emissions of

ultrasound pulses in pipe flow. They determined that they could improve the time resolution of the pulsed ultrasonic device from 10 milliseconds to 500 microseconds, and this led them to suggest that the system could be used to measure the spatiotemporal characteristics of turbulent flow [29]. Another application of the pulsed ultrasonic Doppler method was realized by using the method to evaluate the flow rate of a given flow field. Mori et al used UDV to measure and instantaneous velocity profile and its integral to measure the flow rate of the given flow field. They proved the ability to track and measure flow rates of transient flows [27]. Nowak used UDV to study wall shear stress measurements in turbulent pipe flow. He determined the velocity profiles in boundary layers of turbulent water flows using UDV [28]. Kikura, et al used the UDV to study the effect of measurement volume size on turbulent flow measurement. They measured the ensemble-averaged velocity profile, the Reynolds stress, and the flow rate in fully developed turbulent pipe flows in vertical pipes, and they then compared these measurements to measurements made by direct numerical simulation and laser Doppler velocimetry. Kikura et al found that the simulated average data estimated analytically agreed with the measured average data, and that the flow rate measurement using UDV can be applied to the calibration of other flowmeters [23].

One of the greatest advantages of the pulsed ultrasonic Doppler method is its ability to measure the velocity profile of opaque fluids. UDV was used by Brito, et al, to study velocity measurements in liquid gallium in 2001. This was the first known physical velocity measurement for a vortex of liquid gallium [7]. The velocity measurements of liquid gallium lead the way to other measurements of liquid metal flow fields. Eckert and Gerbeth used UDV to study the velocity fields in liquid sodium. They found that the UDV method performed successfully on liquid sodium flow fields at temperature up to 150^{o}C [11]. Kikura et. al used the pulsed ultrasonic Doppler method to study Taylor vortex flow of magnetic fluids. They concluded that the method was a valid technique in the measurement of a magnetic fluid [21]. The application of UDV on multiphase flow was studied by Wang et al. Wang et al found that the ultrasound refraction has influence on the

determination of the measuring location and Doppler angle, and that the attenuation coefficient of the received echo energy in homogeneous liquid-solid systems monotonously increases with the increase of the solid concentration [38].

1.3 Flow Measurement Systems

Quantifying the instantaneous velocity profile of a given flow field is both one the most fundamental and one of the most challenging quantities to realize in the phenomena of fluid flow. The experimental measurement of the instantaneous velocity profile is a reoccurring theme in all engineering disciplines associated with fluid flow [35]. Different flow measurement devices and techniques have evolved over the years to help scientists and engineers quantify the flow of fluids. Some of the more widely used techniques are particle image velocimetry (PIV), particle tracking velocimetry (PTV), laser Doppler velocimetry (LDV), and more recently pulsed ultrasound Doppler velocimetry (PUDV).

Particle image velocimetry (PIV) is a technique in which the position over a set time is recorded for small tracer particles that are introduced into the flow field. This information provides the local fluid velocity of each of the particles in the fluid flow. PIV requires that the fluid flow and test section be optically transparent. Hardware required for a PIV system include an illuminating light source or laser, an image processing computer, and a recording medium such as film, CCD, or holographic plate. Seeding, illuminating particles which vary in size from a few microns to tens of microns in diameter are also needed [1].

Particle tracking velocimetry (PTV) uses tracer particles in fluid flows. The displacement of the tracer particle is recorded in a single image over a period of time [25]. When a particle is illuminated by two bursts of light, it produces two different images on the same frame of film, and the local velocity of the fluid (Eulerian) can be approximated by measuring the distance between the images. PTV requires the same basic hardware as the PIV system described above. This method can produce erroneous measurements if the image streak of the particle is not normal to the light illumination sheet. Generally, the velocity

measurements determined by PTV are about ten times less accurate and less reliable than PIV measurements [25].

Laser Doppler velocimetry (LDV) is a non-intrusive flow measurement technique that records velocity measurements for a given flow field by means of the Doppler effect. LDV works by recording the shift in the Doppler frequency of the fluid flow, and correlating this shift to the fluid flow velocity. Two lasers with equal-intensity, parallel beams (or one laser split into two beams) are refracted through a lens that causes the beams to cross at a common, focused point. Since the laser beams are the same wavelength and intensity, interference patterns occur at the focused point called fringe patterns. The fringe patterns are constructive and destructive, and they are composed of planar layers of low and high intensity light. A fluid flow field 'seeded' with small particles is passed through the intersecting beam's fringe pattern where the particles scatter light in all directions. A photomultiplier collects the scattered light, and the frequency of the scattered light is recorded. The frequency of the scattered light is called the Doppler frequency of the flow and is proportional to the component of the particle's velocity that is perpendicular to the planar fringe pattern caused by the intersecting laser beams [10].

1.4 Ultrasonic Doppler Velocimetry

The three methods described above are only a few of the many popular methods for quantifying velocity profiles for fluid flow. The major downfall to each of these methods is that none of the methods can be used in opaque fluids that are found in many applications. In order to realize velocity profiles in opaque fluids (or fluids obstructed from view by an opaque barrier), other methods must be employed.

The Doppler effect is the underlying principle of laser Doppler velocimetry and ultrasonic Doppler velocimetry. It was first studied by Austrian mathematician and physicist Johann Christian Doppler. The Doppler effect is essentially the change in frequency of an electromagnetic or acoustic wave as a result of change in position of an emitter or receptor [6]. A wave source and a receiver

are both need to observe the Doppler effect. As the wave source approaches the receiver, the perceived frequency of the wave is greater than the actual emitted frequency of the source, and as the wave source moves away from the receiver, the perceived frequency of the wave is less than the actual emitted frequency of the wave source [12]. The apparent frequency of the receiver is given by:

$$f_r = \frac{c - v_r}{c - v_s} f_e \tag{1}$$

where f_e is the frequency of the source, c is the speed of wave propagation, v_r is the velocity of the receiver away from the source, and v_s is the velocity of the source in the same direction as v_r. The velocity v, by convention is considered negative when the source is moving toward the receiver. The Doppler shift frequency, f_D, is realized by rearranging equation 1 to give [39]:

$$f_D = f_r - f_e \tag{2}$$

or:

$$f_D = \left(\frac{c - v_r}{c - v_s} - 1 \right) f_e . \tag{3}$$

The movement of reflecting interfaces can also be studied using the Doppler effect. The wave direction is altered by the reflecting interface in such a way when the source and receiver are stationary that they appear to originate from a virtual source. The distance to the virtual source from the receiver appears to equal the total distance traveled by the waves. This has the same effect as if the source and receiver moved apart at the same velocities equal to that of the reflective surface. This implies that $v_r = -v_s = v$, and the Doppler frequency, $f_{D,}$ is then given by:

$$f_D = -\left(\frac{2v}{c + v} \right) f_e \tag{4}$$

where v is the absolute velocity of the reflector away from the source [39]. In the case where $c >> v$, equation (4) simplifies to [40]:

$$v = -\frac{f_D c}{2 f_e} . \tag{5}$$

The main other situation that arises in Doppler velocimetry is the case when the different velocities do not act along the same straight line. For this case, f_D must be calculated using the appropriate velocity vectors, and only the magnitude (not the algebraic sign) of f_D is important to the Doppler shift detector. In this case, ϕ is defined as the angle between the direction of movement and the effective ultrasonic beam direction, and equation (5) can be modified to encompass velocities not acting along the same line as [40]:

$$v = -\frac{f_D c}{2 f_e \cos\phi}. \tag{6}$$

1.4.1 Continuous Ultrasound Doppler Systems

As mentioned in the previous section, continuous ultrasound Doppler velocimetry was the original Doppler ultrasound method for finding velocities in various flow fields. The continuous ultrasound Doppler method works by finding the Doppler shift frequency produced by the flow field and then relating the shifted frequency to velocity mathematically. The derivation of the mathematical relationship between the Doppler shift frequency of the continuous ultrasound and the velocity profile of the desired flow field is considered below.

The simplest case to consider is one where an ultrasonic transducer is fixed in some medium (v_S = 0) and emits waves of frequency f_e as shown in Figure 1-1. The speed of sound in the medium is defined as c, and a target (particle) in the flow field moves with velocity V^+ (V^+, by convention is considered positive when target is moving away from the transducer). Figure 1-1 shows that the target particle forms an angle of θ_1 with respect to the direction of propagation direction of the ultrasonic wave. Using this configuration, the perceived frequency of the ultrasonic waves by the target particle will be [31]:

$$f_t = f_e - \frac{f_e V^+ \cos\theta_1}{c} \tag{7}$$

In order for the ultrasonic waves to be reflected from the target particle, the acoustic impedance of the target must be different from the acoustic impedance of the surrounding medium. When the two impedances are not the same, the

ultrasonic waves will be partially reflected. The reflected ultrasonic waves can then be recorded by a receiver as shown in Figure 1-1. If the receiver is stationary, the frequency of the ultrasonic waves recorded by the receiver, f_r, is [31]:

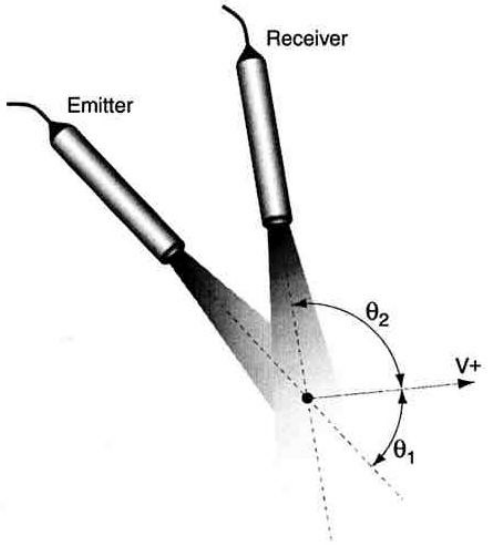

Figure 1-1: Example of transducer setup [31]

$$f_r = f_g + \frac{f_g V^+ \cos\theta_2}{c} \tag{8}$$

where f_g is the frequency of the reflected wave from the target particle. If both the emitter source an the receiver source are stationary in the medium and the vector components of V^+ are substituted for v_r and v_s, equation (8) simplifies to:

$$f_D = \left(\frac{c - V^+ \cos\theta_2}{c - V^+ \cos\theta_1} - 1 \right) f_e \,. \tag{9}$$

In many cases, the velocity of the target is much smaller than the speed of sound in the medium, or $V^+ << c$, and the second order terms of equation (9) can be neglected to yield [31]:

$$f_D = \frac{f_e V^+ (\cos\theta_1 - \cos\theta_2)}{c} \,. \tag{10}$$

Also, as in many cases, if the same transducer is used to emit the ultrasonic signal and to receive the ultrasonic signal, equation (10) simplifies to [31]:

$$f_D = \frac{2 f_e V^+ \cos\theta_1}{c} \tag{11}$$

The basic principle with continuous ultrasound Doppler velocimetry is that when an ultrasonic signal leaves the emitting transducer, it encounters some disturbance in the flow field and is reflected, and then the reflected signal is received by a transducer with a change in its frequency caused by the interaction with the motion in the flow field. The signal is either slightly expanded or slightly compressed from its original frequency. Generally, the separation of the echo signal and the transmitted signal could be made on the basis of difference in time, by separation of the strong transmitted signal form the weak echo or by recognizing the change in the echo-signal frequency caused by the Doppler effect when there is relative motion between radar and target [32]. Velocity is calculated using continuous ultrasound Doppler velocimetry by calculating the Doppler shift frequency in the received signal using equations (9)-(11).

In continuous ultrasound Doppler velocimetry, two ultrasonic transducers are usually used. One transducer is an emitting transducer continuously emitting ultrasonic waves, and one transducer (typically adjacent to the emitting transducer) is a receiving transducer continuously receiving the reflected ultrasonic signals. For simplicity, continuously emitted sinusoidal waves are typically used and then compared to the received frequency of the reflected wave. The Doppler shift is then calculated by multiplying the received signal by a quadrature signal of frequency f_e, the emitted signal frequency. A signal that contains frequency components equal to the sum and difference of the emitted and received signals' frequencies is the result of this calculation. A band-(low)-pass filter is used for removing the higher frequency signal at twice the emitted frequency. The resulting signal after the band-pass filter contains the Doppler shift of the emitted signal and, thus, the velocity encountered in the medium under investigation [25]. Even though only one frequency is present at this time, a continuum of frequencies makes up the received signal. Detecting the most dominant frequency in the signal is the simplest approach to quantifying the

characterization of the flow field in question. Estimating the zero crossing rate of the signal is one technique of characterizing the dominant part of the flow field. The number of times a signal crosses its mean value is counted by a zero crossing detector (a device used for detecting the point where the signal crosses zero in either direction), and this data is used to estimate the frequency of the signal. This method is limited because it works best when the spectrum contains little noise and is essentially monochromatic. A more flexible, accurate and nearly noise free digital implementations consist of an analog front-end, which demodulates the Doppler signal. The signal is then sampled by a pair of analog-to-digital converters and processed by a digital signal processor. A display, or sonogram, of the distribution of velocities can be made by Fourier transforming the received signal and showing the result [17].

The major downfall to continuous ultrasound Doppler systems is the inability to quantify depth of field, or the distance between the ultrasonic transducer and the moving object of study. This means that no information about the distance between the ultrasonic transducer and the object in motion is provided. The benefit to the continuous ultrasound Doppler system is that since the sampling rate is very large, ambiguities in velocity, or aliasing, of the Doppler shifted signal is not a problem [20]. Generally, continuous ultrasound Doppler systems are inexpensive and simple devices, but they do have the problem of leakage of noise of the transmitter and receiver [25].

1.4.2 Pulsed Ultrasound Doppler Velocimetry

An improvement from the continuous ultrasound Doppler velocimetry system described above is the pulsed ultrasound Doppler velocimetry (PUDV) system. Using pulsed ultrasound Doppler systems, the distance between the ultrasonic transducer and the object in motion can be resolved. Pulsed ultrasound Doppler systems operate by sending periodic, short ultrasonic bursts into the medium of interest, and echoes of the ultrasonic signal from objects in the path of the beam are collected continuously by the receiving transducer. Echoes are accepted only for a short period of time following delay that can be adjusted by the

operator. The length of the delay determines approximately the range from which signals are gathered [12]. The emitting (source) transducer sends ultrasonic signals through the test medium at a fixed pulse repetition frequency. This means that it emits a pulse (short burst) of ultrasonic energy periodically. This ultrasonic energy interacts with the test medium causing the energy to be reflected, and the reflected energy is received by the receiving transducer. This received signal is called an echo. So, by sampling the incoming echoes at the same time relative to the emission of the series of bursts at the fixed pulse repetition frequency, the shift in position of the target particles are measured [31]. This allows, in pulsed ultrasound Doppler systems, for a relative measurement of phase shift between pulses received rather than the absolute measurement of frequency recorded using continuous wave Doppler systems.

The relative shift in position of the target particles is the desired quantity for the pulsed ultrasound Doppler system to measure. Figure 1-2 [31] shows a simplified ultrasonic transducer setup where there is only one target particle present along the ultrasonic beam. In Figure 1-2, P is the distance from the transducer to the target particle, and the time delay between an emitted burst of ultrasonic energy and the echo received from the target particle is T_D. If T_D is known, then P would be computed using the equation:

$$P = \frac{cT_D}{2} \tag{12}$$

where c is the sound velocity of the ultrasonic wave in the medium. Since, in nearly all cases, the target particle will not be moving in the axis of the ultrasonic beam, θ is the angle at which the target particle is moving with respect to the ultrasonic beam. Knowing the angle of the target particle with respect to the ultrasonic beam and the amount of time that separates two emissions of the ultrasonic transducer, the variation of depth of the particle, ΔP, can be calculated by the equation:

$$\Delta P = (P_2 - P_1) = \Delta d \cos\theta = vT_{prf} \cos\theta = \frac{c}{2}(T_2 - T_1) \tag{13}$$

where Δd is the total distance that the particle travels between the two emissions of ultrasonic energy, T_{prf} is the time between two emissions of ultrasonic energy,

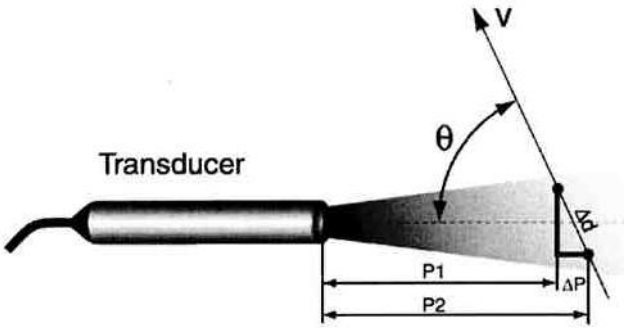

Figure 1-2: Simplified ultrasonic transducer setup [31]

v is the velocity of the particle, and ($T_2 - T_1$) is the time difference, or time delay, between an emitted burst of ultrasonic energy and the received echo of reflected energy from the target particle. The time difference, ($T_2 - T_1$), is always a very short (usually less than a microsecond). The phase shift of the received echo, δ, is given by the equation:

$$\delta = 2\pi\, f_e\,(T_2 - T_1) \tag{14}$$

where f_e is the emitting frequency of the ultrasonic transducer. Using equations (13) and (14), and rearranging to get the velocity of the target particle gives:

$$v = \frac{c(T_2 - T_1)}{2T_{prf}\cos\theta} = \frac{c\delta}{2T_{prf}\cos\theta\; 2\pi\, f_e} = \frac{cf_D}{2\, f_e \cos\theta} \tag{15}$$

where f_D is given by the relation [31]:

$$f_D = \frac{1}{2\pi}\frac{\delta}{T_{prf}}\ . \tag{16}$$

Even though the last result is the same as the Doppler equation, the pulsed ultrasonic Doppler method does not rely on the same Doppler technique as laser Doppler velocimetry or continuous ultrasound Doppler velocimetry. A pulsed ultrasound Doppler-system transmits short bursts of acoustic energy by amplitude modulation of a carrier frequency. The returning signal is sampled at a specific delay time from the transmission of each pulse. As a consequence, the sampled portions of the returning signal correspond to a back-scattered acoustic energy originating from a specific region of space in the ultrasonic field called the

sample volume, whose range from the transducer is determined by the delay time [23]. In laser Doppler velocimetry and in continuous ultrasound Doppler velocimetry the velocity is measured directly by finding the Doppler shift frequency of the target medium in the received signal. In pulsed ultrasound Doppler velocimetry, the velocities are derived from shifts in position of the pulses of ultrasonic energy, not from shifts in the emitted frequency. Ultrasonic pulses are emitted into the target medium or fluid and at the same relative time to the pulse emission a reflected (backscattered) signal is received by the receiving transducer. Since the particles in the target medium or fluid are moving, the displacement of the backscattered signal is detected by the pulsed ultrasound Doppler system. Therefore, it is a shift in the target medium itself that is detected by the pulsed ultrasonic Doppler system, not a shift in the emitted frequency due to the shift of the target medium as in continuous wave systems or laser Doppler systems. This is a very subtle point, but an important one none the less.

1.4.3 Ultrasound

Mechanical vibrations that travel in a host medium are called sound waves. They are coupled modes between medium particles oscillating about equilibrium positions and a traveling sonic wave [25]. The velocity of sound, *c*, in a perfectly elastic material is given by:

$$c = \lambda f = \frac{\lambda}{T} \tag{17}$$

Where λ is the wavelength, f is the frequency, and T is the period of time. At a given temperature and pressure, the velocity of sound in a material is constant. The acoustic spectrum is composed of three major categories: subsonic noise (f_{sn} < 20 Hz), audible noise (20 Hz < f_{ra} < 20 kHz), and ultrasonic noise (f_{un} > 20 kHz) as shown in Figure 1-3 [30]. Subsonic noise is below the range of human hearing, and audible noise is the range of frequencies that are audible to humans. Although the ultrasonic range can be broken down into three categories, the general range of frequencies for ultrasonic applications (non-

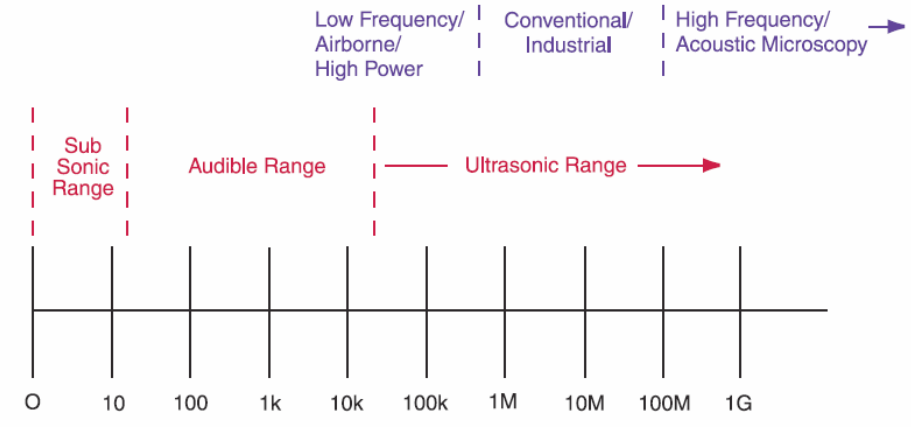

Figure 1-3: Acoustic Spectrum [30]

destructive testing, thickness gauging, etc.) is 100 kHz to 50 MHz [30]. Medical Doppler applications usually use frequencies between 2 MHz and 10 MHz, although some applications call for higher frequencies. This lower limit is determined by the wavelength and the upper limit by acceptable power levels. The spatial resolution decreases as the wavelength of the signal increases, and attenuation rises rapidly with increasing frequency [12]. Due to the fact that ultrasonic energy has a much shorter wavelength than audible sound, ultrasound can be reflected off of small surfaces or particles that are suspended in a testing medium. Since ultrasound has similar properties to and a shorter wavelength than audible sound, it is a useful tool for velocity profile measurement or nondestructive testing of materials [25].

Sonic vibrations travel in wave form. Sonic waves must have an elastic medium such as liquid or solid matter to travel through unlike light which only requires a vacuum. Although other forms of waves exist such as surface and Lamb waves, ultrasound commonly utilizes either longitudinal or shear waves to propagate. Pulsed ultrasound is produced by applying electric pulses to an ultrasonic transducer. The number of pulses produced per second is called the pulse repetition frequency. The spatial pulse length is the length of space over which a pulse occurs, and it is equal to the wavelength times the number of cycles in the pulse. The spatial pulse length decreases with increasing frequency [25].

1.4.4 Ultrasonic Field

In order to utilize these techniques and quantify fluid flow, we first need to investigate the characteristics of the ultrasonic signal emitted from the transducer. As previously stated, the pulsed Doppler system emits short bursts of acoustic energy, and the returning signal from the emitted acoustic energy is sampled at a specific delay time from the initial transmission of energy. This received signal is associated with the acoustic energy that comes from a specific region in the ultrasonic field. This region is called the sample volume, and its range from the transducer is determined by the delay time [23]. The region of the sample volume is shown in Figure 1-4, and it is approximated by a disk of diameter *d* and thickness *h* [41]. This means the special resolution of the system is determined by the sample volume size. The lateral size of the sample volume is determined by the ultrasonic beam size, and the length of the sample volume corresponds to the distance sound travels. The spatial resolution is on the order of the ultrasound wavelength in the wave propagation direction

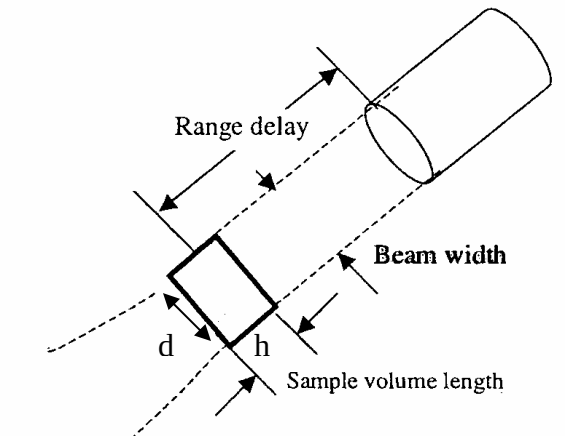

Figure 1-4: Pulsed Doppler system acoustic sample volume [41]

and depends on the width of the ultrasonic beam in the direction perpendicular to the wave propagation direction [7].

Since the ultrasonic sample volume encompasses a three dimensional region in space, when calculating the velocity of a flow field, all particles passing through the sample volume create Doppler signals that are detected by the receiving

transducer. This means that equation (15) that describes the velocity of a single target particle is calculated many times for a given sample volume in a flow field resulting in a spectrum of frequencies containing the Doppler shift of each particle.

The ultrasonic waves generated by an ultrasonic transducer are more or less confined in a narrow cone. As the waves travel in this cone they may be scattered when they touch a particle having different acoustic impedance. The acoustic impedance of a material is the opposition to displacement of its particles by sound. It is given by the product of the speed of sound in the working fluid and the density of the fluid:

$$z = \rho * c \tag{18}$$

In Doppler echography, the object is not to make use of a plane longitudinal wave, but rather an ultrasonic beam that is as thin as possible throughout the measurement depth. The geometry of the acoustic field is governed by the diameter D of the emitter and the wave length, λ, which is equal to the ratio of the speed of sound in the analyzed medium and the emitting frequency. Using Huygen's principle, one may predict the geometry of the acoustic field. In the following approach, an ultrasonic transducer is modeled as a combination of several adjacent point sources, each generating a spherical wave. The typical shape of the ultrasonic field is illustrated in Figure 1-5 [31].

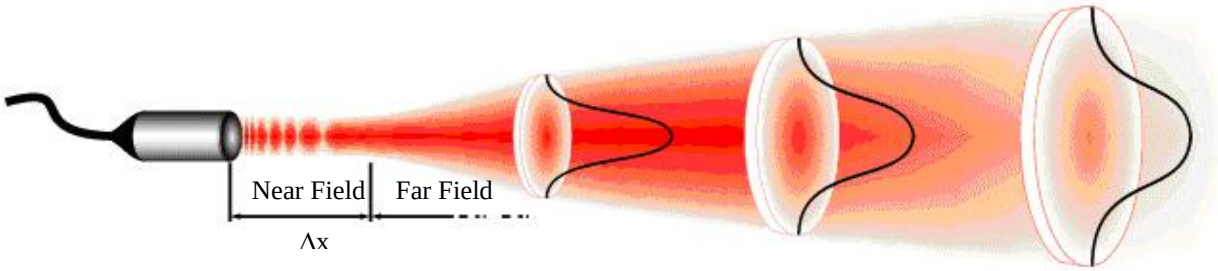

Figure 1-5: Simplified ultrasonic field [31]

The intensity of the acoustic field, I_z, along the axis of a circular ultrasonic transducer of radius r that operates in a piston-like manner is given by:

$$\frac{I_z}{I_0} = \sin^2\left[\frac{\pi}{\lambda}\left(\sqrt{r^2 - \Delta x^2} - \Delta x\right)\right] \tag{19}$$

where I_0 is the maximum intensity, Δx is the distance from the transducer and λ is the wavelength [24]. Two characteristic regions define the acoustic field generated by the ultrasonic transducer. They are the cylindrical near field and the conical far field, and the two fields are separated by the distance of the furthermost maximum of equation (19).

In the near field, or region that is located near the transducer surface, the acoustic field is nearly cylindrical, with a diameter slightly less than the diameter of the emitter. This region is also called the Fresnel zone. The intensity of the acoustic waves oscillates along the axis of the transducer. The echo amplitude goes through a series of maxima and minima (Figure 1-6). The characteristic distances of these oscillations are much smaller than the dimensions of the measured volumes, so they do not significantly affect Doppler information collected in this region. The length of the near field L_{NF} given by [24]:

$$L_{NF} = \frac{4D^2 - \lambda^2}{4\lambda} \tag{20}$$

is determined by the position of the last maximum of the acoustic intensity field. The near field distance is the natural focus of the transducer and a function of the transducer frequency, element diameter (aperture size) and the speed of sound in the medium.

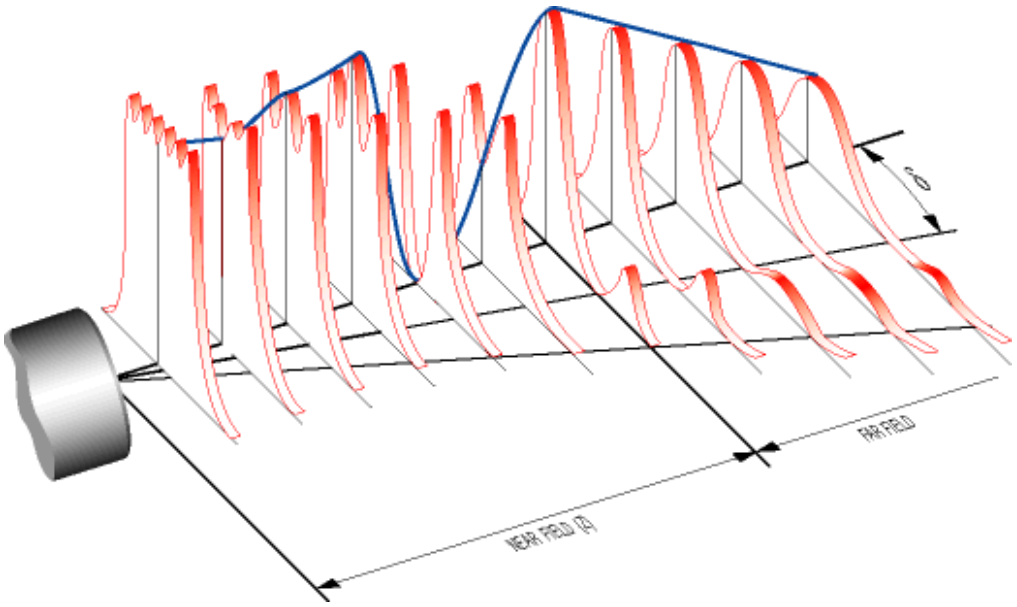

Figure 1-6: Ultrasonic Field [31]

In the far field, the zone lying beyond L_{NF}, the intensity of the acoustic waves along the axis varies as the inverse of the square of the distance form the transducer (according to the inverse-square law for point sources). This region is also called the Frauenhofer zone. Small oscillations appear in the radial direction perpendicular to the axis of propagation, and the sound field pressure gradually drops to zero.

Most of the acoustic energy is contained in a cone-shaped field. The relationship between the acoustic field intensity and the angle of the transducer axis depends on the directivity function [31]:

$$D_r(\gamma) = \frac{2J_1(k\,r\sin\gamma)}{k\,r\sin\gamma} \tag{21}$$

where J_1 is the first order Bessel function of the first kind, r is the radius of the transducer, and k is the wave number. The wave number is given by:

$$k = \frac{2\pi}{\lambda} \tag{22}$$

where λ is the wavelength. The half angle of divergence of the main lobe δ (-6 dB pulse-echo beam spread angle) is characterized by the wavelength and the diameter of the emitting ultrasonic transducer and is given by [31]:

$$\delta = \sin^{-1}\left(\frac{1{,}22\lambda}{D}\right) = \sin^{-1}\left(\frac{1{,}22c}{f \cdot D}\right) \quad (23)$$

Where λ is the wavelength, *D* is the diameter of the ultrasonic transducer, *c* is the speed of sound in the medium, and *f* is the transducer frequency. It can be seen from this equation that beam spread from a transducer can be reduced by selecting a transducer with a higher frequency or a larger element diameter or both.

All transducers have beam spread, and consequently, all ultrasonic beams diverge. In the near field, the beam has a complex shape that usually narrows. In the far field the beam diverges. The divergence of the ultrasonic beam depends on the diameter of the emitter and the wavelength. Most of the time, a compromise between these two parameters has to be established in order to achieve the thinnest beam possible at a defined distance. A higher frequency gives a better axial resolution but also often induces higher attenuation of the ultrasonic waves.

Measurement of the ultrasonic field (transmission zone) of a transducer is undertaken by moving a small detector systematically in the region in front of the transmitting element. The transducer face and the detector are normally immersed in water, although any material that provides acoustic coupling between the transducer and the target medium could be used. Comparisons are made between the fields produced by the small detector and the fields produced by the small detector when various objects are placed between the detector and the transducer, specifically a paper forming screen.

2 Experimental Setup and Procedure

2.1 Ultrasonic Field Measurement Setup:

The pulsed Doppler ultrasound velocimetry instrument DOP2000 model 2125 by Signal Processing was used to measure the ultrasonic field generated by various ultrasonic transducers. The transducers used with this system are both transmitters and receivers. The effect of paper forming screens placed between the ultrasonic transducer and the area of interest (an object reflecting the ultrasonic wave packet emitted by the transducer – in this case: plastic sphere) was evaluated. The sphere was used in order to reflect a source of ultrasonic energy from a single point to the transducer. The ultrasonic transducer and plastic sphere were submerged in water as shown in Figure 2-1. The plastic sphere and the ultrasonic transducer were mounted on xyz-positioners as shown in Figure 2-2. It should be remembered that the beam characteristics measured in water are different from those in water with suspended fibers or particles. Nevertheless, a great deal can be deduced about a beam in water with suspended fibers or particles from a plot obtained in water.

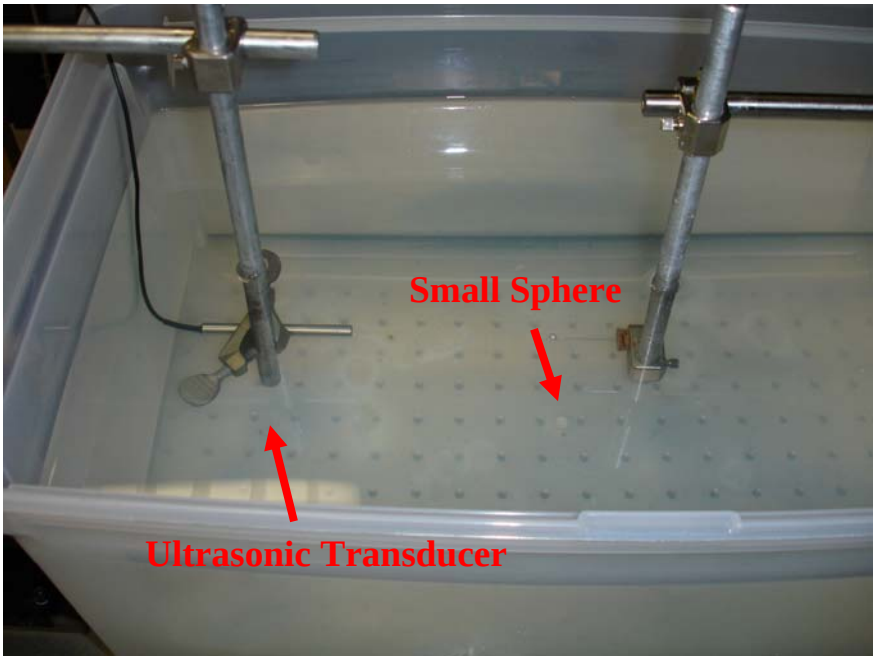

Figure 2-1: Experimental Setup

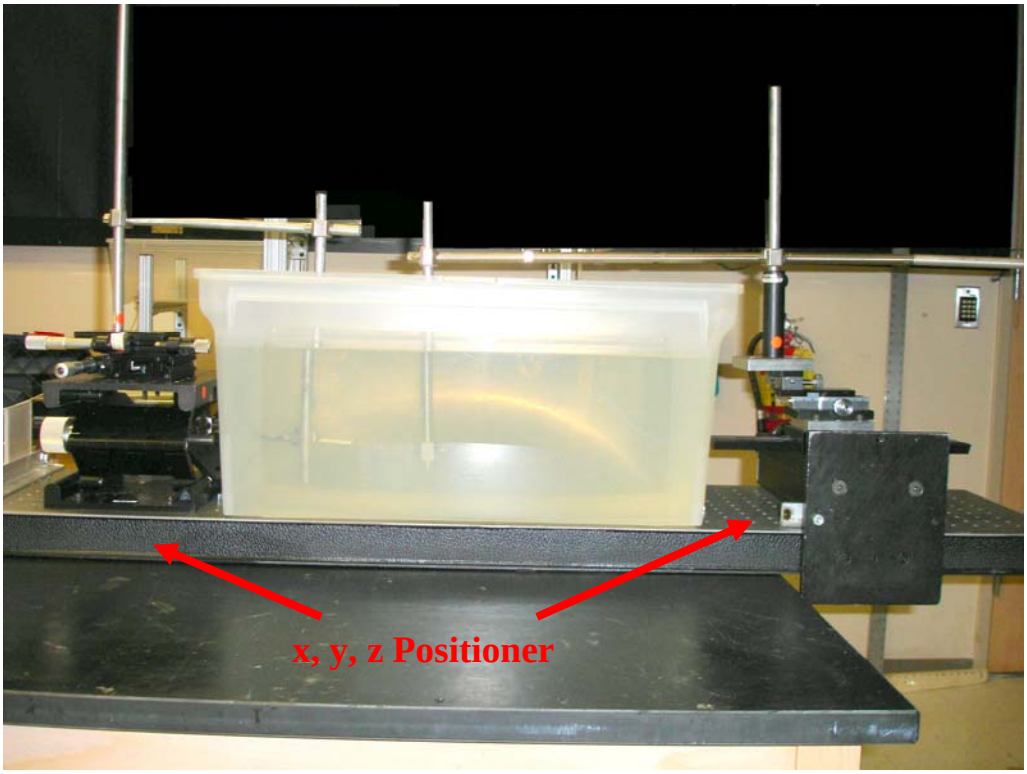

Figure 2-2: Experimental Setup with x, y, and z Positioning

Figure 2-3 shows the basic experimental setup used to measure the ultrasonic field. The distance between the sphere and the surface of the transducer on the x-axis is defined as Δx. The ultrasonic signal propagates along the x-axis; therefore, the ultrasonic beam is symmetric about the x-axis. Y and z are the movements perpendicular to the x-axis, or ultrasonic beam axis.

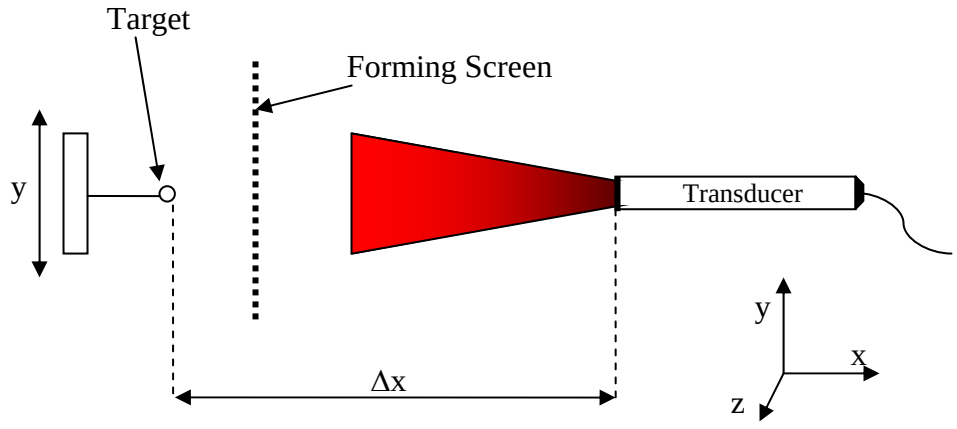

Figure 2-3: Schematic of Beam Measurement test setup

The sphere was attached to a small rigid rod (maximum 1/3 of the diameter of the sphere). The length of the rod was 3 cm. The system, rod, and sphere, are mounted on a xy-table which is capable of positioning the sphere with a minimum resolution of 0.1 mm (Figure 2-2). The system, sphere, and transducer, are completely submerged. Since the maximum distance between the transducer and the plastic sphere in the following tests will be 120 mm, the transducer and plastic sphere were submerged approximately 150 mm below the surface of the liquid. This ensured that the transducer and sphere were surrounded by enough liquid in order to avoid the influence of the free surface of the liquid. If the free surface of the liquid was closer to the transducer or sphere than 120 mm, the liquid surface could cause a false echo, or artifact, in the ultrasonic beam shape experiments.

The measurement of the ultrasonic field generated by an ultrasonic transducer was realized by measuring the intensity of an echo coming from the plastic sphere. By moving the position of the sphere along a line perpendicularly (y-axis) to the axis of the ultrasonic beam (x-axis) the intensity of the echo for different positions of the sphere were measured (it is assumed that the z-axis is symmetric about the y-axis). This data was used to analyze the -3dB and -6dB width of the ultrasonic beam. Figure 2-3 illustrates the principles and experimental setup for the method. After selecting various control parameters, centering and placing the sphere at the desired depth, the ultrasonic field can be measured.

At first, ultrasonic beam measurements of four different transducers were conducted. Then a paper forming screen was placed between the transducer and the plastic sphere (area of interest) as shown in Figure 2-4 and Figure 2-5. Ultrasonic beam measurements of the following transducers were conducted:

- Transducer 1: 2 MHz emitting frequency, 10 mm transducer diameter
- Transducer 2: 4 MHz emitting frequency, 5 mm transducer diameter

- Transducer 3: 8 MHz emitting frequency, 5 mm transducer diameter
- Transducer 4: 4 MHz emitting frequency, 8 mm transducer diameter, focused

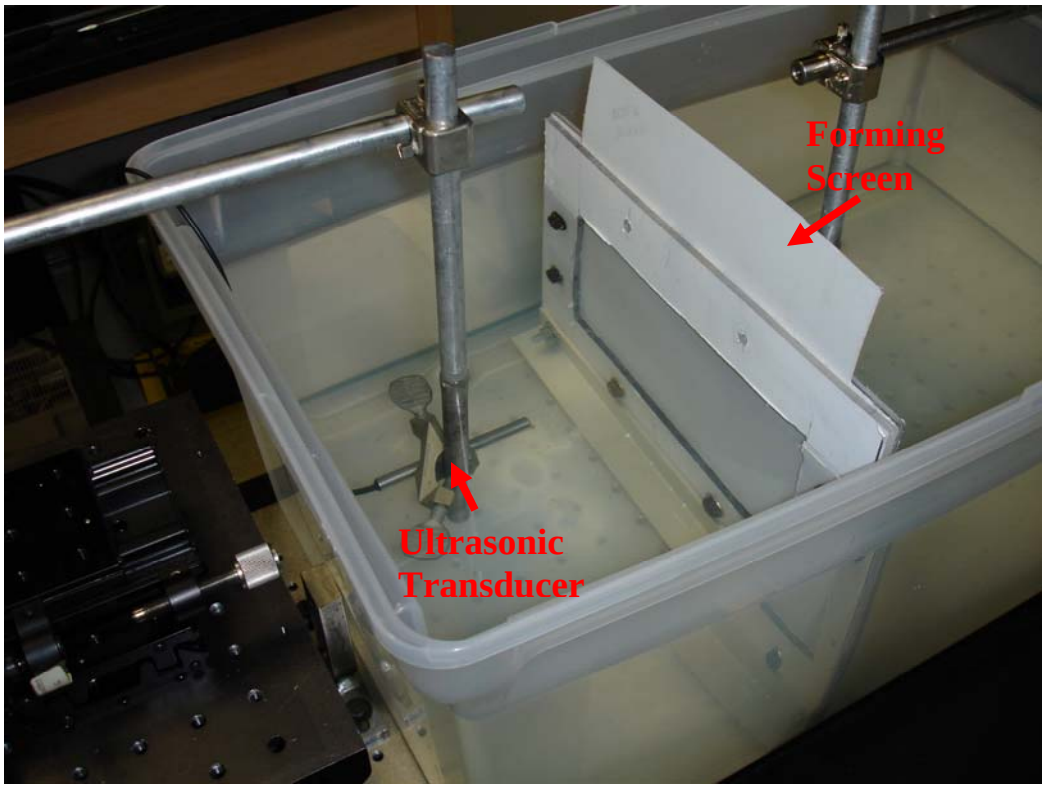

Figure 2-4: Beam Shape Measurement Setup with Forming Screen

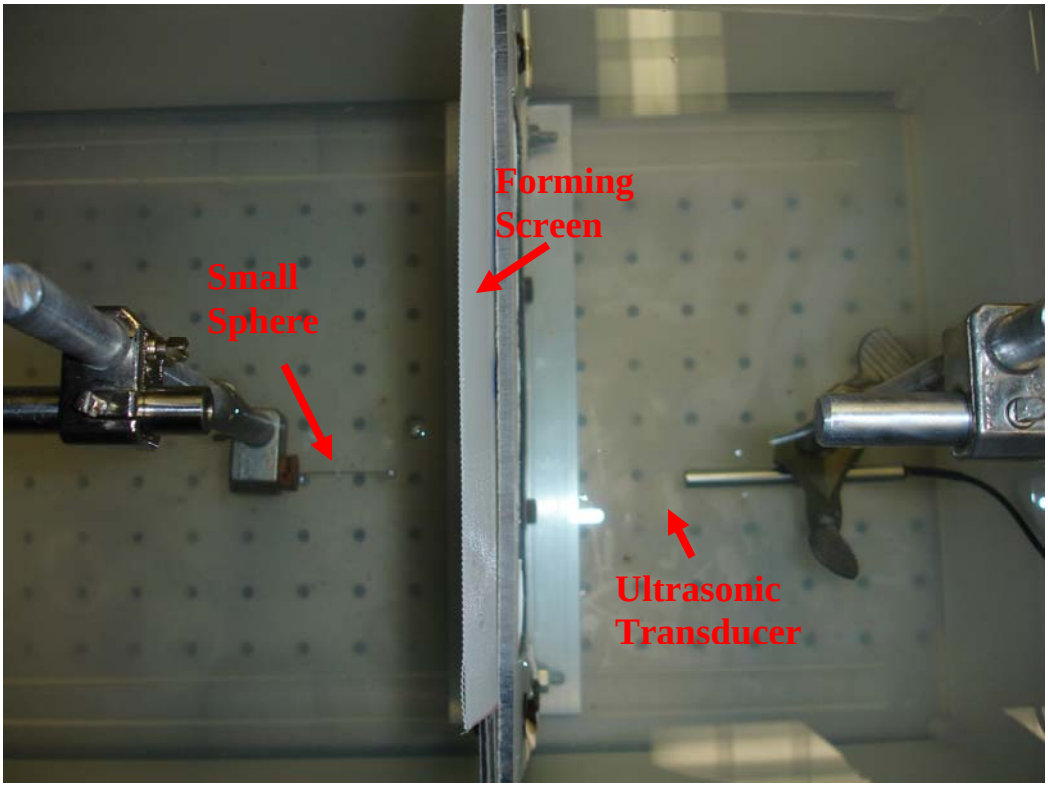

Figure 2-5: Beam Shape Measurement Setup with Forming Screen (Plan View)

The amplitude of the received echo in volt as a function of the distance between the plastic sphere and the transducer center on the y-axis and the general beam divergence of each transducer are presented in the following section. In all echo amplitude plots, the distance between the plastic sphere and the transducer face on the x axis (Δx) is plotted as a function of the distance between the plastic sphere and the transducer center on the y-axis.

2.2 Ultrasonic Field Procedure:

The measurement of the ultrasonic field using the Signal-Processing DOP 2000 was performed using the following procedure as stated in the Signal-Processing handbook [31]:

1. *The test setup should be as described above (Figures 2-1 through 2-5) with an x,y,z-positioner for the transducer and for the target sphere.*

2. *Before entering in the menu dedicated to the measurement of the ultrasonic field, the following procedure must be executed in the supplied software:*
   a. *recall default factory settings;*
   b. *choose emitting frequency corresponding to transducer being used;*
   c. *select a emitting power of "Low";*
   d. *select a burst length of 4 cycles;*
   e. *define overall TGC of 20 dB;*
   f. *select a spatial filter of 1.05mm.*
3. *Enter the ultrasonic field measurement menu found in the "Advanced compute" tab.*
4. *Place sphere in contact with transducer in order to find the center of the ultrasonic beam field in the y and z plane. The sphere should now be centered with the transducer on the x axis*.
5. *Place the sphere at the desired depth, Δx, without moving the y and z directions of the sphere*.
6. *Enter the depth, Δx, in the field labeled "at Z" ("Measure mm" panel) and in "Start at" ("parameters" panel). Also, select a PRF of 1500 and a number of gates equal to 200.* The "Start at" depth can be a few mm lower than the actual depth of the desired measurement, but the closer the desired depth is to the horizontal axis on the echo modulus graph, the better the results that were obtained for this series of tests.
7. *The amplification (TGC and module scale) can now be adjusted in order to obtain a clear and strong echo from the sphere. Take care in identifying clearly the echo from the sphere and not from any of the objects holding the sphere.* The amplitude should be set to the lowest number possible, but the peak of the echo modulus should ideally take up approximately 2/3-3/4 of the horizontal axis of the echo modulus graph.
8. *Once amplification is set, select the number of gates to be 40 (make sure the gates encompass the echo of the sphere on the echo*

modulus graph). Also make sure that any changes in the PRF value (up or down) do not induce changes in the shape or value of the echo from the sphere. If artifacts are present (something other than the sphere), find PRF values where no artifacts appear.

9. *Now you are ready to measure a slice. Define the maximum y distance from the transducer axis from which you will start the measurement and step between the points. Enter these values in their corresponding field in the panel "Measure mm". Be sure that the depth Δx at which the measurement will be realized is also displayed in the corresponding field. Then:*
   a. *Click on the button labeled "Add new slice". A new button labeled "Measure" will appear, and just below this button the y-axis value at which you must place the sphere. Move the sphere to that position.*
   b. *Click on the button "Measure" or press the space bar to record the first point of the slice.*
   c. *Move the sphere a step forward and wait a little bit in order to let the system stabilize. Then press again on the space bar to record a new point*.

   A slice is simply a set of amplitude data points from a certain depth, Δx. For the tests in question, a step size of 0.5 mm was used for a total span of 20 mm.

10. *There is no limit to the number of slices that can be added, but each slice must have a unique depth*. For each slice that is measured, repeat the steps from step 6 above.

3 Ultrasonic Beam Field

Ultrasonic beam measurements are conducted to gain information about the actual beam shape of the given ultrasonic transducers and especially their lateral resolution. These ultrasonic beam measurements will then be used to analyze the effect of porous screens on various measurements. Before investigating the ultrasonic beam shape with porous screens between the transducer and the area of interest (plastic sphere), the beam shape of various transducers is determined with no screen present.

3.1 Echo Amplitude

At a certain distance (minimum distance) between the transducer and the plastic sphere on the x-axis, measurements of the ultrasonic beam shape become impossible due to the transducer's ringing effect. This ringing effect is characterized by a saturation of the transducer preventing measurements. This is indicated by the ultrasonic system showing a strong echo profile in a region of the test medium where there is no object present that could register an echo. When the ultrasonic transducer attempts to take measurements in a saturated region, the DOP 2000 system returns an amplitude value that is several orders of magnitude greater than the amplitude recorded in a region that is not saturated. The system also records a beam width of zero. Further decreasing the Δx beyond this minimum distance between the transducer and the plastic sphere on the ultrasonic beam axis (x-axis) does not yield any useful measurement results of the ultrasonic beam shape. This is due to the fact that the ultrasonic echo of the plastic sphere can not be recognized in between the high echo amplitudes caused by the transducer's ringing effect. Ringing effects following the emission of the ultrasonic wave packet cause a region of strong echoes (saturation) at depths located just after the surface of the transducer. In this region, the ultrasonic field can consequently not be measured. For this study, the region of

high echo amplitudes caused by the transducer's ringing effect is called "saturation region". The distance between transducer and plastic sphere at which the saturation region begins is called the "minimum distance". Increasing the amplification in the instrument consequently increases the transducer's ringing effect; therefore, increasing the amplification increases the saturation region and the minimum distance. This means that the smallest possible amplification level that gives an accurate measurement should be used, especially for measurements that are close to the ultrasonic transducer.

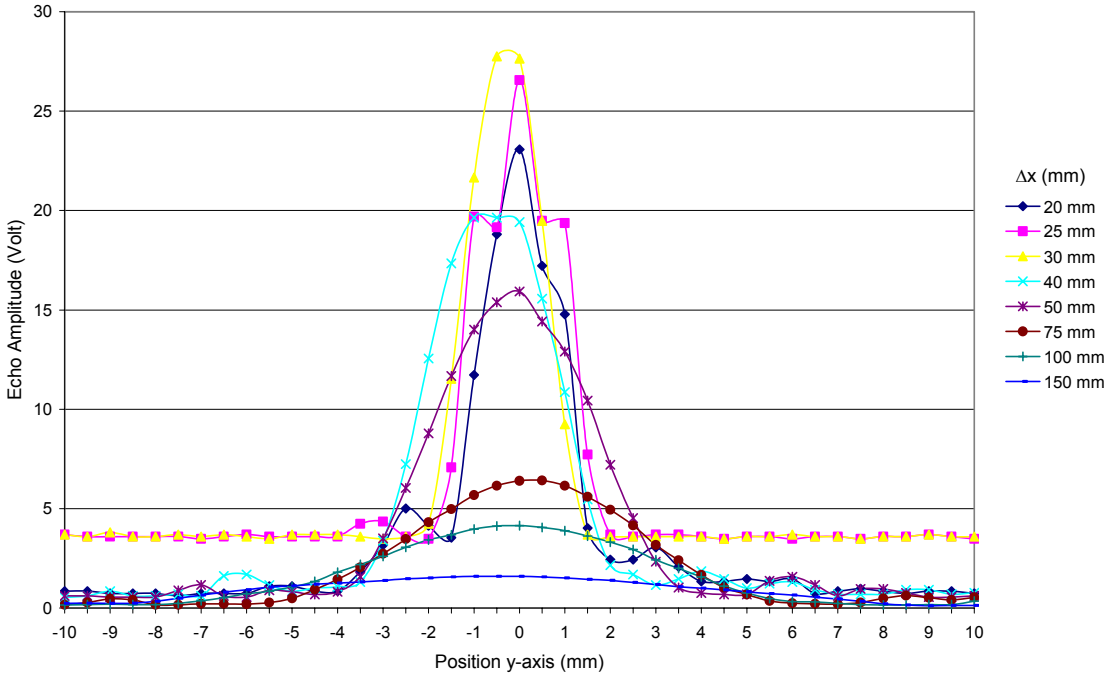

Figure 3-1: Echo Amplitude 2 MHz 10 mm Transducer

Figure 3-1 shows a plot of the amplitude of the 2 MHz 10mm transducer as a function of the position of the plastic sphere. The echo amplitude forms a maximum located on the ultrasonic beam axis (x-axis). As soon as Δx becomes smaller than the minimum distance the overall echo amplitude level increases. Further decreasing Δx leads to a straight line at relatively high echo amplitudes. In this case, the echo of the plastic sphere can not be recognized in between this "saturation region." Therefore, at a certain minimum distance, beam shape measurements become impossible. The DOP 2000 device simply records a value of zero for the width of the beam.

Using a 2 MHz ultrasonic transducer, the saturation region is ideally 10 – 15 mm wide. In the saturation region, no valid measurements are obtained, therefore, when using the 2 MHz ultrasonic transducer, the area of interest had to be at least 15 mm away from the ultrasonic transducer. As shown in Figure 3-1 the smallest Δx measurement recorded was 20 mm due to the fact that the amplitude was larger on the periphery of the beam measurement in comparison to the much smaller values of amplitude on the periphery of the beam measurements for the Δx's that were 30 mm and greater. Further decreasing the Δx for this transducer would result in a much larger value for the amplitude with no change in the value for the entire span of the y-axis. A decrease in Δx would also produce a beam width measurement of zero.

Using a 4 MHz transducer, the region of strong echoes is ideally 3 – 8 mm, depending on the chosen amplification. In this test set-up, the minimum distance is 5 mm for the unfocused 4 MHz (Figure 3-2) and 4 mm for the focused 4 MHz ultrasonic transducer (Figure 3-3), respectively. For the 8 MHz transducer, values of ideally 3 – 5 mm can be obtained, but the minimum distance for the 8 MHz transducer is 8 mm as shown in Figure 3-4. In general, the minimum distance decreases with increasing frequency. Since much stronger attenuation occurs to the ultrasonic signal emitted by the 8 MHz transducer than the ultrasonic signal emitted by the 4 MHz transducer, a higher amplification must used when working with the 8 MHz transducer. This caused the minimum distance of the 8 MHz transducer to increase and is therefore higher than the

minimum distance for the 4 MHz transducer. The amplitude plots show maximum amplitudes of 73 and 325 volt for the 4 MHz and 4 MHz focused transducers, respectively. This shows that the focused transducer receives more energy in its echo from the small sphere than the unfocused transducer. This is due to the fact that the ultrasonic energy emitted from the focused transducer is focused, or more concentrated itself, therefore, more of the ultrasonic energy is reflected back to the transducer by the small sphere causing a much higher amplitude measurement.

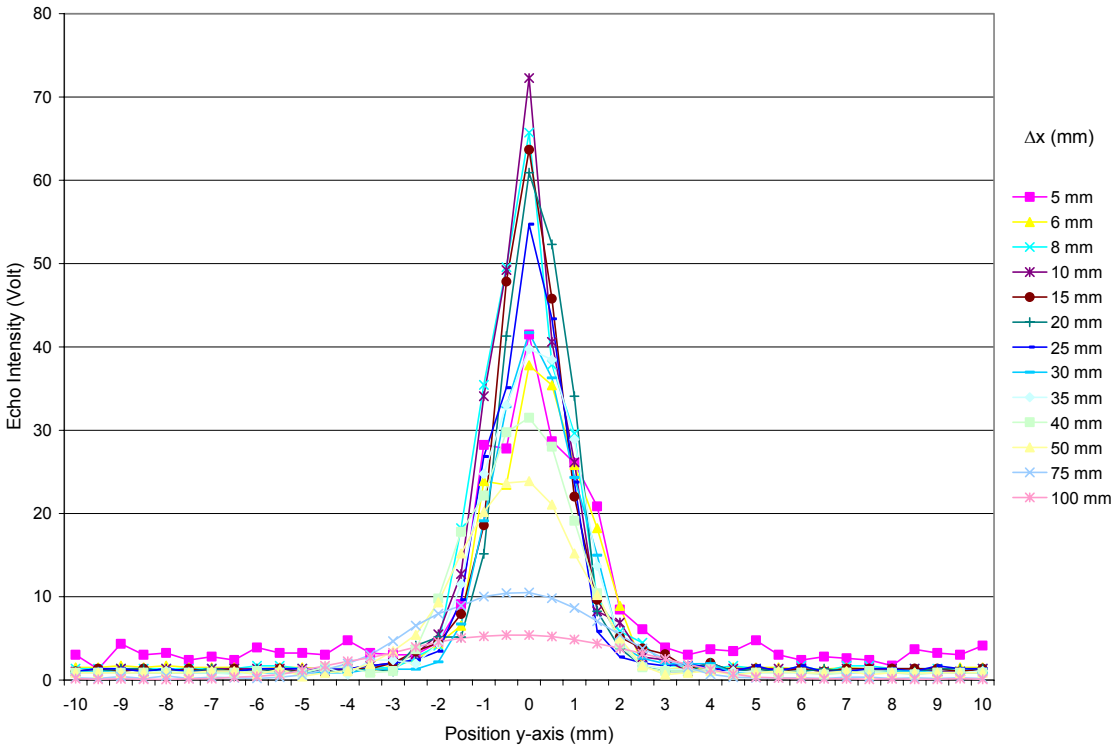

Figure 3-2: Echo Amplitude 4 MHz 5 mm Transducer

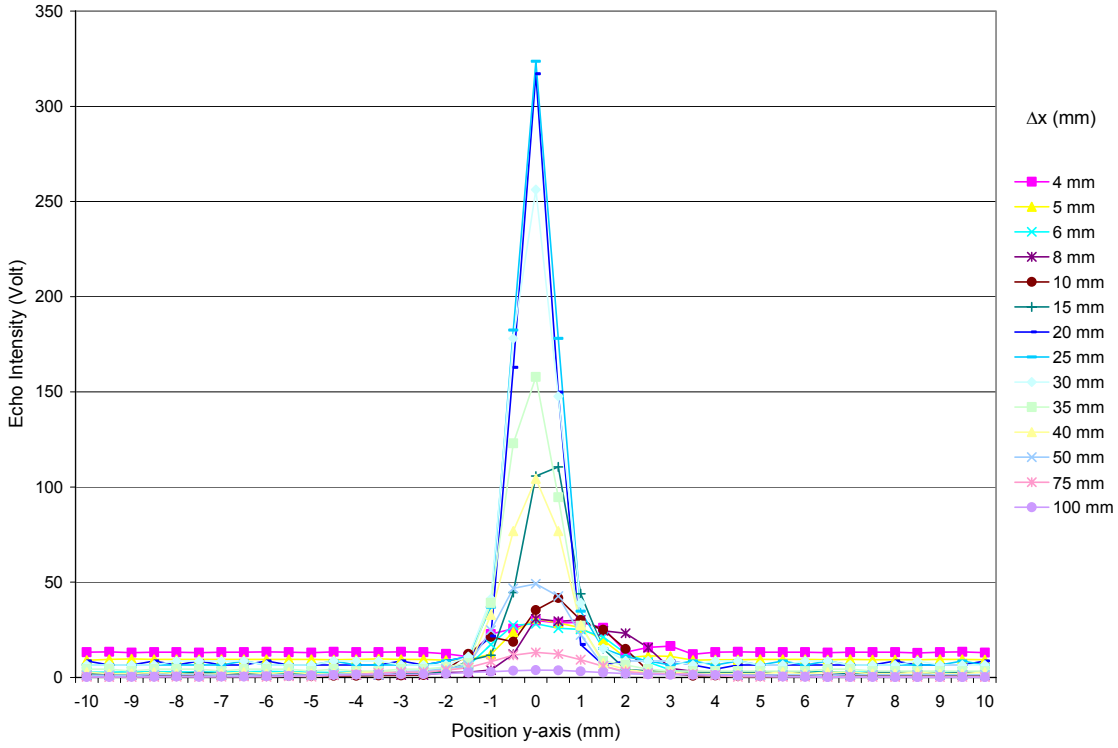

Figure 3-3: Echo Amplitude 4 MHz 8 mm Focussed Transducer

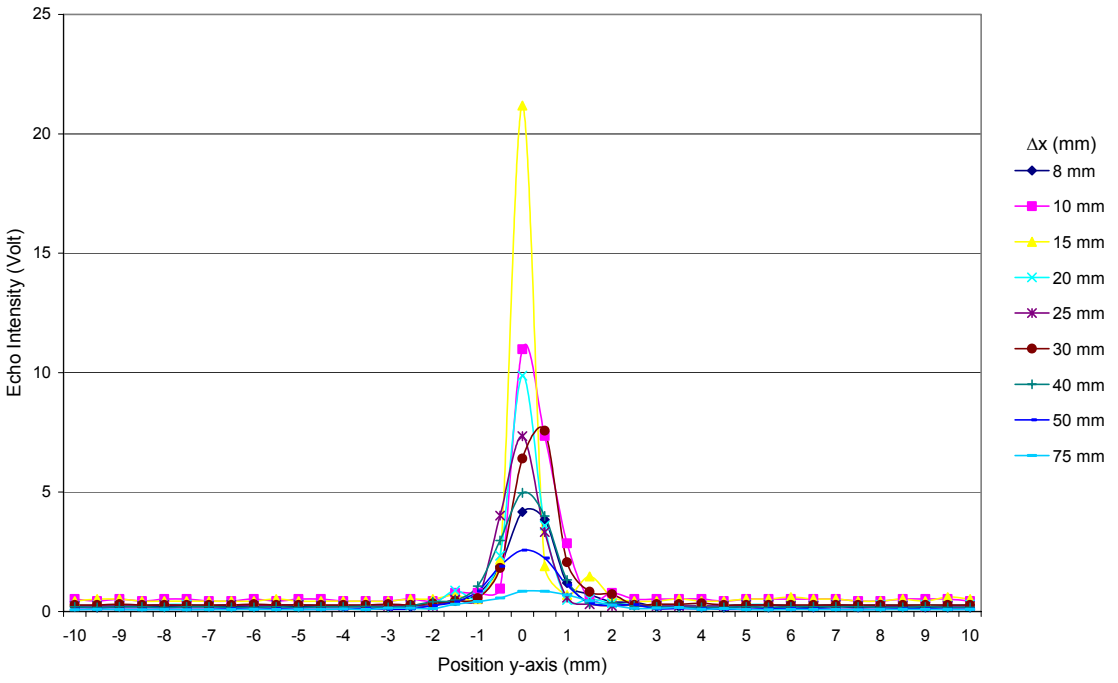

Figure 3-4: Echo Amplitude 8 MHz 5 mm Transducer

3.2 Ultrasonic Beam Shape

Ideally, the ultrasonic beam emitted from the transmitter should be a conic in shape. With no obstructions present in the ultrasonic field, Figures 3-5 through 3-8 show that the ultrasonic beam is, in fact, conic in shape. These figures also show that the beam width in the far field decreases with increasing transducer size (greater aperture). In the same way as beam width, beam divergence decreases with increasing frequency. The half angle of beam divergence (given by the instrument) for the 2 MHz 10 mm transducer is 2.27 degrees, 2.23 degrees for the 4 MHz 5 mm transducer, 1.22 degrees for the 8 MHz 5 mm transducer and 2.33 degrees for the 4 MHz 8 mm focused transducer. This is shown in Table 3-1. Theoretically beam divergence in the far field should be less for larger than smaller diameter transducers [12]. This shows that the half angle of beam divergence is smaller for the unfocused 4 MHz 5 mm than for the focused 4 MHz 8 mm transducer. Consequently, when comparing focused and unfocused ultrasonic transducers the claim that beam divergence in the far field should be less for larger diameter than smaller transducers is not justified. Unfortunately unfocused ultrasonic probes of the same frequency with different diameters were not available to experimentally validate this theoretical claim. Theoretically, for a given transducer frequency the near field length should also be greater for larger diameter transducers, and for a given transducer diameter the near field length should theoretically be greater for higher-frequency transducers [12].

The ultrasonic beam divergence profile of the 2 MHz transducer (Figure 3-5) shows that this transducer is not suitable for measuring velocity profiles in small channels or where measurements are made close to the transducer due to the relatively large minimal measurable distance of 20 mm and the poor lateral resolution. The 2 MHz transducer could be placed at a distance of 20 mm away from the region of interest, but acoustic coupling and anomalies such as wall effects decrease the quality of achieved measurement results. The 4 and 8 MHz transducers (Figure 3-6, Figure 3-7, and Figure 3-8) are best suited for measuring velocity profiles when dealing with small geometries. Due to the

better lateral and axial resolution (smaller beam diameter and short ultrasonic pulse length) of the unfocused 8 MHz transducer, compared to the unfocused 4 MHz transducer, the unfocused 8 MHz transducer is theoretically best suited measurements in small geometries described above (in actuality, when conducting experiments involving forming screens, the unfocused 4 MHz transducer produced the best results as presented in a later section).

Table 3-1: Half-Angle Beam Divergence of Various Transducers

Transducer	Half-Angle Beam Divergence
2 MHz 10 mm	2.27^{o}
4 MHz 5 mm	2.23^{o}
4 MHz 8 mm Focused	2.33^{o}
8 MHz 5 mm	1.22^{o}

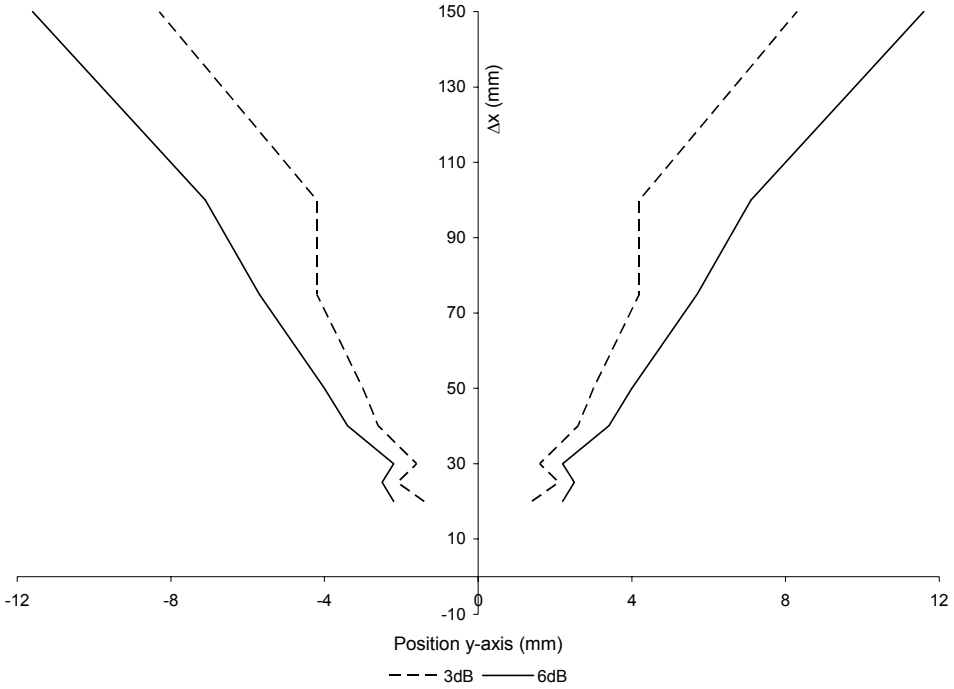

Figure 3-5: Beam Divergence Profile for 2 MHz 10 mm Transducer

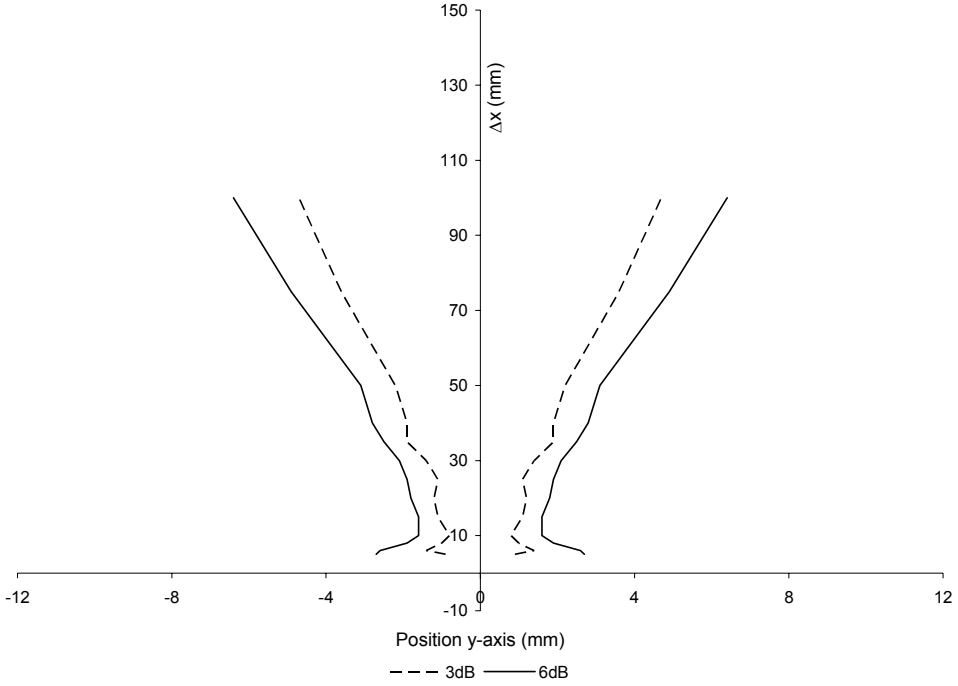

Figure 3-6: Beam Divergence Profile for 4 MHz 5 mm Transducer

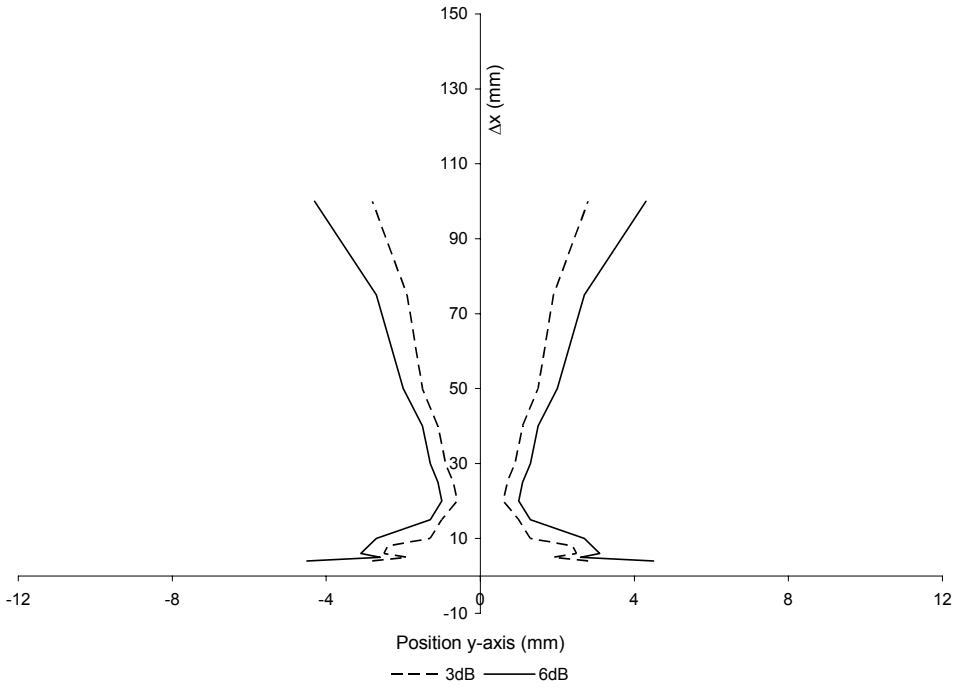

Figure 3-7: Beam Divergence Profile for 4 MHz 8 mm Focused Transducer

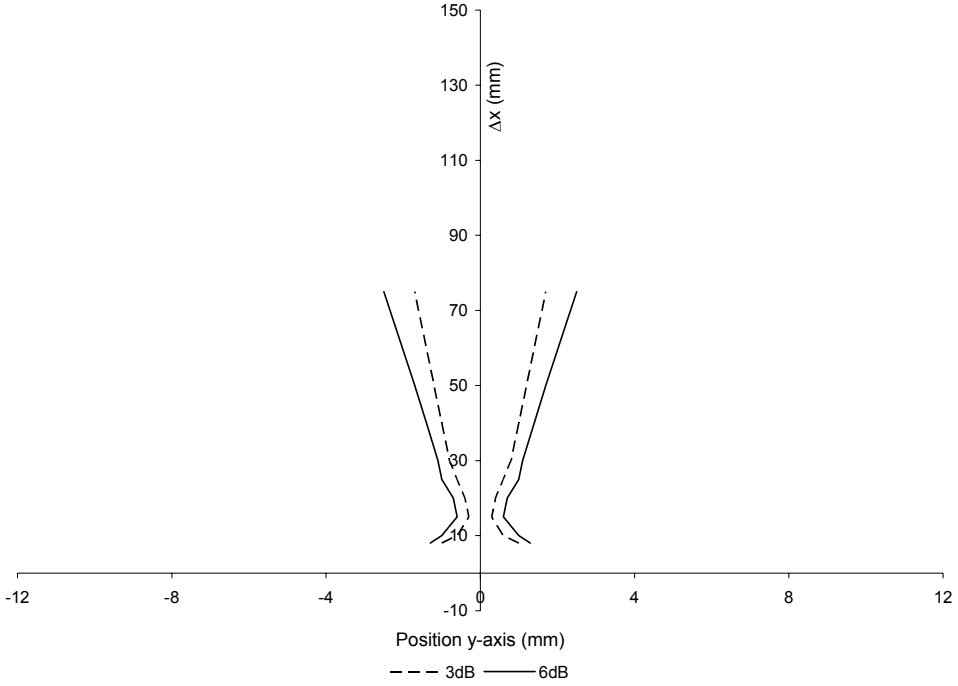

Figure 3-8: Beam Divergence Profile for 8 MHz 5 mm Transducer

A comparison of the beam divergence profiles for the 4 MHz 5 mm and the 8 MHz 5 mm transducers is shown in Figure 3-9. This figure shows that at a given transducer diameter, the beam width decreases with decreasing wavelength because wavelength is inversely proportional to frequency. Beam width consequently decreases with increasing frequency. The fact that for a large ratio of diameter to piezoelectric element thickness the ultrasonic beam is focused can clearly be seen in Figure 3-9. The 4 and 8 MHz transducer both have a transducer diameter of 5 mm. Since the thickness of the piezoelectric element equals half of the desired wavelength, the ratio of the diameter to the piezoelectric element thickness for the 8 MHz 5 mm transducer is larger than for the 4 MHz 5 mm transducer. Therefore, the unfocused 8 MHz 5 mm ultrasonic transducer is focused in contrast to the unfocused 4 MHz transducer.

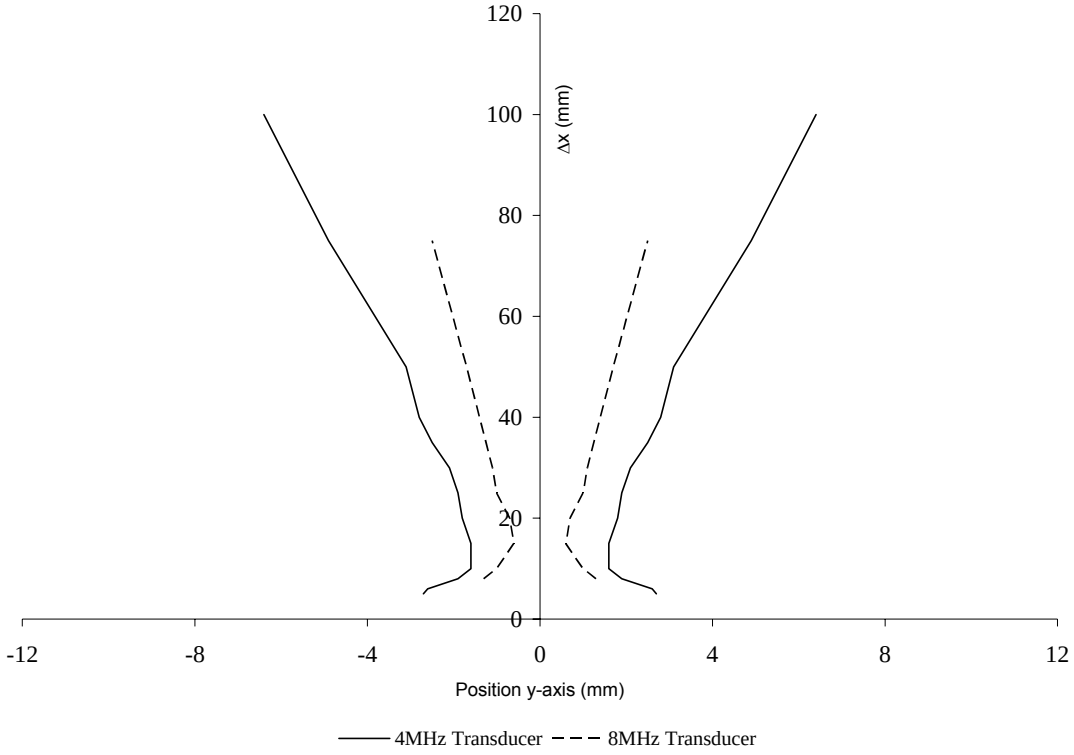

Figure 3-9: Beam Divergence Profiles for the 4 MHz 5 mm and 8 MHz 5 mm Transducers

The focused 4 MHz 8 mm transducer was also compared to the unfocused 4 MHz 5 mm transducer in order to compare measurement results of unfocused and focused ultrasonic transducers. The focal point of the focused 4 MHz 8 mm transducer is approximately 20 mm away from transducer face (Δx of 20 mm). The beam width of the focused transducer is approximately half of the beam width of the unfocused transducer at the focal point as shown in Figure 3-10. Due to focusing the ultrasonic beam and consequently the ultrasonic energy, the amplitude of the received echo from the 4 MHz focused transducer is increased by approximately 500 percent at the focal point and approximately 20 percent at the focal point of the unfocused 8 MHz 5 mm transducer (see Figure 3-2 through Figure 3-4) when compared to the amplitude of the received echo of the 4 MHz unfocused transducer. The focal point of the ultrasonic beam of the unfocused 8 MHz 5 mm transducer (due to the large ratio of diameter to piezoelectric element thickness) is at a Δx of approximately 15 mm. The echo amplitude is of the same order of magnitude before and after the focal point for the focused and unfocused

transducer. The minimal distance at which measurements are possible is of the same order for the focused and unfocused transducer. It can clearly be seen that the beam width in the far field is smaller with the focused transducer (Figure 3-10). This is also due to the larger aperture of the focused transducer.

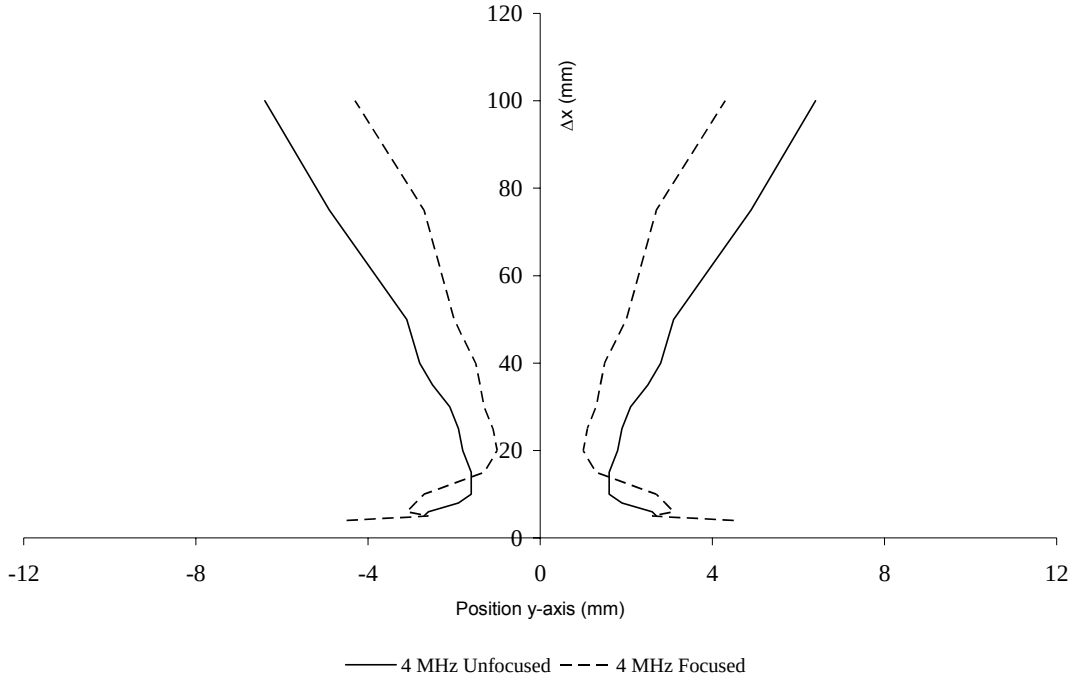

Figure 3-10: Beam Divergence Profiles for the 4 MHz 5 mm and 4 MHz 8 mm Focused Transducers

3.3 Repeatability

Another important characteristic of the beam shape measurements is the repeatability of the tests in question. If, for example, each time the beam shape tests were performed, they were drastically different, there would be no basis to compare the beam shape measurements when the forming screen is present. Figure 3-11, **Figure 3-12**, and Figure 3-13 show beam shape measurements for the 4 MHz 5 mm ultrasonic transducer at 6 dB and 3 dB, respectively. These beam shape measurements were all recorded at different times, and show that the shape of the pulsed ultrasonic beam vary only slightly from test to test. This shows that the beam shape measurements are repeatable, so they can be

compared to the beam shape measurements when obstructions are placed in the path of the ultrasonic signal.

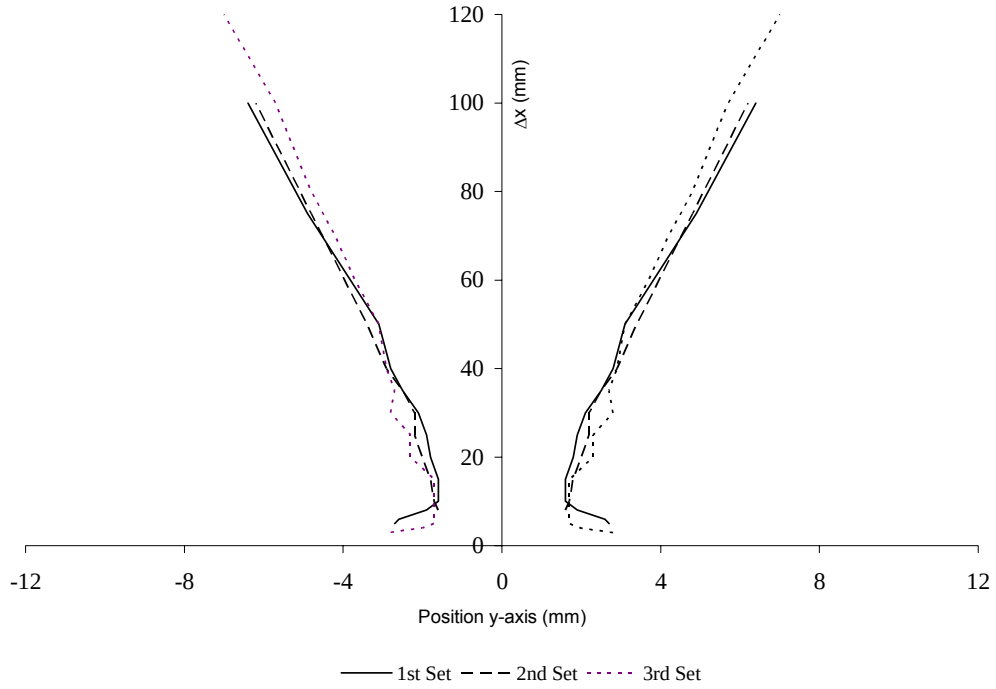

Figure 3-11: Repeatability of Beam Divergence Profiles for the 4 MHz 5 mm Transducer (6 dB)

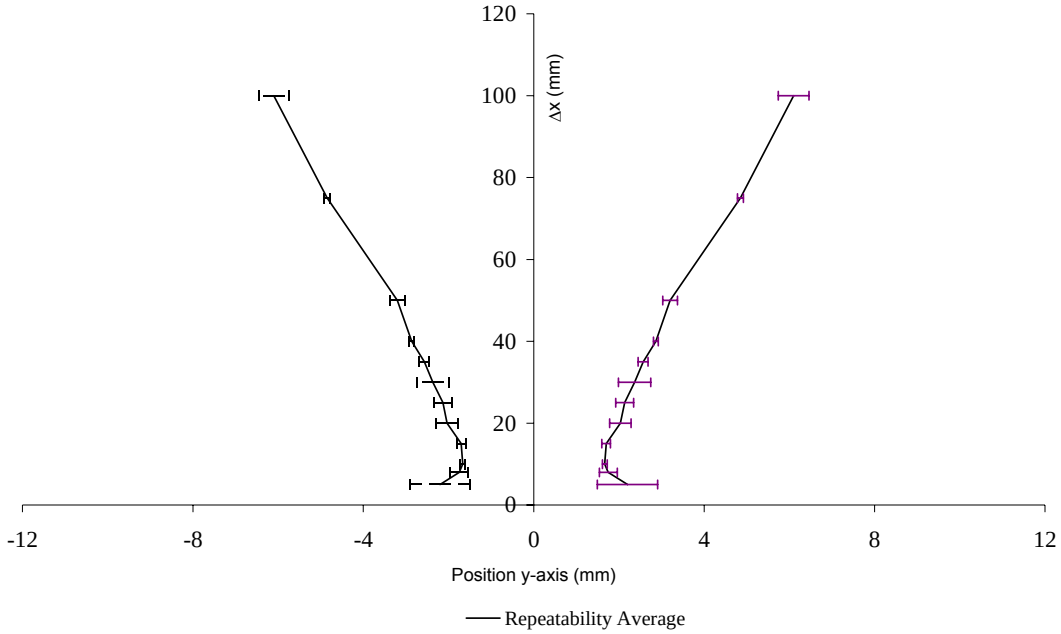

Figure 3-12: Average of Repeatability Profile for 4 MHz 5 mm Transducer with 1 Standard Deviation Error Bars

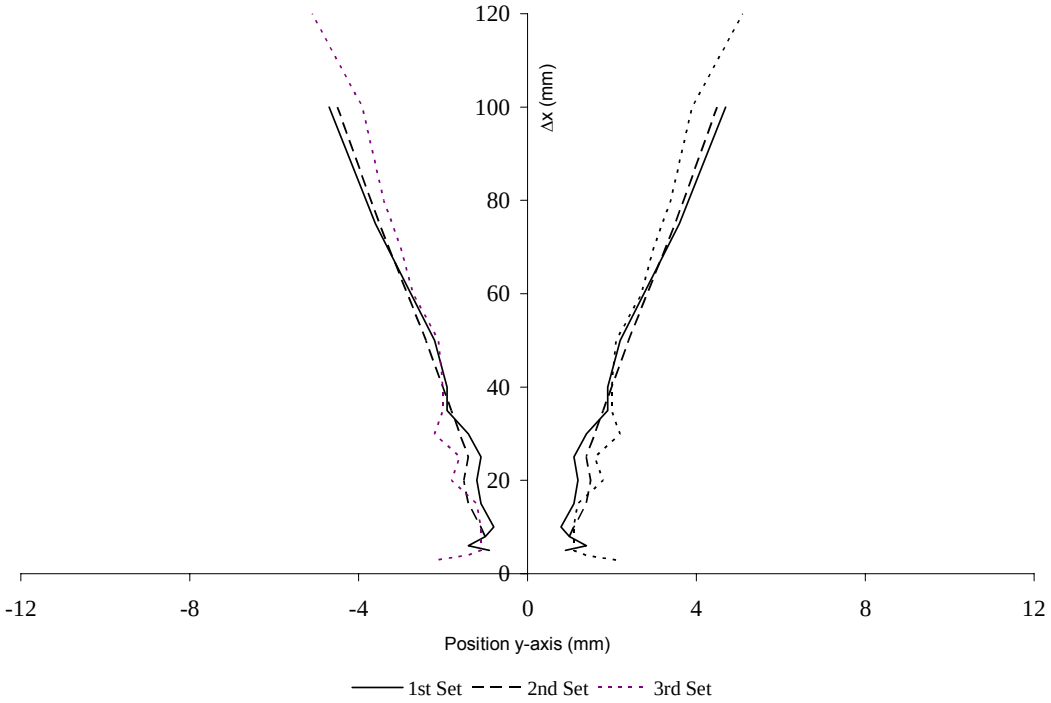

Figure 3-13: Repeatability of Beam Divergence Profiles for the 4 MHz 5 mm Transducer (3 dB)

4 Effect of Forming Screen

In industrial applications measurements of the velocity profile in the area close to forming screens is most important. Therefore, the distance from the screen to the plastic sphere at which the echo of the plastic sphere can still be recognized must be as small as possible. A forming screen is placed at various distances on the x-axis in order to find the smallest measurable plastic sphere-screen distance. In evaluating the measurement results of the forming screen, emphasis is placed on finding the closest distance from the plastic sphere to the screen over the widest range of transducer-screen-distances (Δx) that produces detectable echoes of the plastic sphere behind the forming screen.

4.1 Forming Screen Specifications

Two different forming screens were used in this study, forming screen A (ScreenA) and forming screen B (ScreenB). A microtomographic view of ScreenA is shown in Figure 4-1. ScreenA has the following properties:

- Material: Polyester
- Density Polyester: 1.35 g/cm^3 = 1350 kg/m^3
- Fiber volume: 0.38 cm^3
- Pore volume: 0.36 cm^3
- Porosity: 0.95
- Sample weight (in air): 0.57 g
- Sample weight (in water): 0.873
- Sample volume: 0.74 cm^3
- Apparent density (in air): 0.77 g/cm^3 = 770 kg/m^3
- Apparent density (in water): 1.18 g/cm^3 = 1180 kg/m^3
- Thickness t: 0.022 in = 0.00056 m
- Mesh: 60 wires/inch = 2362 wires/meter

- Pore shape factor: 1 (cylindrical pores ≈ cubical pores)
- Double layer:
    i. Fiber diameter ply 1: 0.2 mm
    ii. Fiber diameter ply 2: 0.4 mm
- Specific flow resistance: 95.5 MKS Rayls
- Sound Speed (Brodeur 1993): 1700 m/s

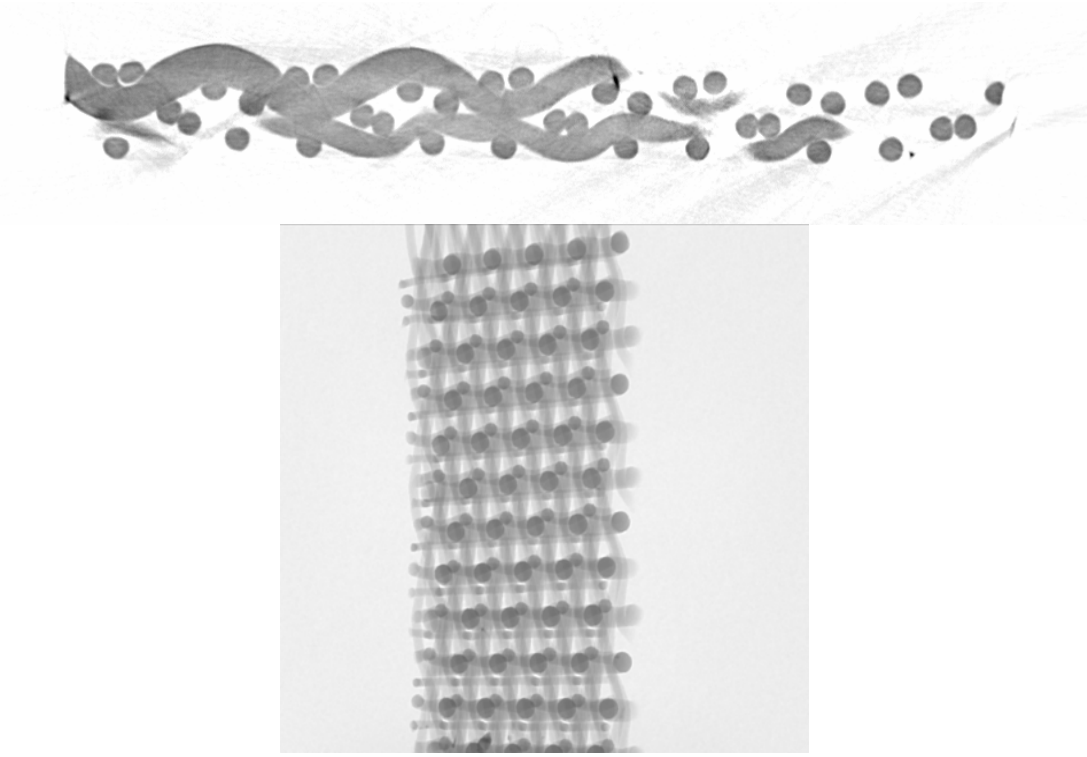

Figure 4-1: Microtomographic Cross-Section View Forming Screen

Forming screen B (ScreenB) was supplied by Albany International. It is fabric number F17263. ScreenB has the following properties:

- Material: Polyester
- Density Polyester: 1.35 g/cm^3 = 1350 kg/m^3
- Thickness t: 0.054 in = 0.00137 m
- Mesh: 94 wires/inch = 3700 wires/meter
- Count: 89 wires/inch = 3503 wires/meter
- Permeability: 493 CFM = 232 liters/second

- Pore shape factor: 1 (cylindrical pores ≈ cubical pores)
- Design: CD125
- Style: TL
- Sound Speed (Brodeur 1993): 1700 m/s.

Table 4-1: Comparison of Transducer Wavelength and Pore Size

Transducer	Wavelength (μm)	Screen Pore Size (μm)
2 MHz 10 mm	750	20 (ScreenA)
4 MHz 5 mm	375	70 (ScreenB)
8 MHz 5 mm	187.5	

4.2 Echo Amplitude and Beam Shape Measurements

Placing a forming screen between the plastic sphere and transducer forces the echo amplitude to decrease due to the absorption and reflection of acoustic energy by the forming screen. When placing a forming screen between the transducer and plastic sphere, the foremost effect seen is a sharp decrease in the amplitude of the echo. A high amplification must be used to clearly recognize the echo coming from the plastic sphere behind the forming screen. For the 2 MHz 10 mm transducer, the decrease in the amplitude of the echo is 60 percent when ScreenA is between the plastic sphere and the transducer. When no screen is present, the maximum amplitude received by the transducer is 28 Volts (Figure 3-1), and when ScreenA is present (20 or 40 mm away from the transducer), the amplitude received by the transducer is 11 Volts. The amplitude plot for the 2 MHz 10 mm transducer when ScreenA is 40 mm away from the transducer is shown in Figure 4-2. This figure shows that the maximum amplitude received by the transducer when ScreenA was present was 11 Volts. For the 4 MHz 5 mm transducer, the decrease in echo amplitude is 93 and 96 percent for ScreenA and ScreenB, respectively, and with the 4MHz 8mm focused

transducer, the decrease in the amplitude of the echo is approximately 94 percent. The maximum amplitude recorded by the 4 MHz 5 mm ultrasonic transducer was 75 Volts when no screen was present (Figure 3-2), 5.5 Volts when ScreenA was present (60 mm away from transducer) as shown in Figure 4-3, and 3 Volts when ScreenB was present (20 mm away from transducer) as shown in Figure 4-4. It should be noted that although there appears to be another maximum value in Figure 4-4 for the transducer measurements at Δx = 23 mm, the measurements taken at Δx = 23 mm were in the region saturated by ScreenB that causes the ringing effect. This means that this slice, or set of measurements, does not give meaningful results. The maximum amplitude recorded by the 4 MHz 8 mm focused ultrasonic transducer with the forming screen absent was 325 Volts (Figure 3-3), and the maximum amplitude that was recorded by the ultrasonic transducer when ScreenA was present was 21 Volts when the forming screen was 20 mm away from the transducer as shown in Figure 4-5. The 8 MHz 5 mm transducer had a decrease of 100 percent in echo amplitude. No results were achieved for the 8 MHz transducer when ScreenA was in place due to the high absorption rate. In all cases, the reduction in amplitude when the forming screen was present was very significant. These trends show that the echo amplitude decreases with increasing frequency since attenuation of acoustic waves increases with increasing frequency. This trend of decreasing echo amplitude with increasing frequency is the reason that the 8 MHz 5 mm transducer did not yield useful results. It simply did not have enough acoustic energy to create a detectable echo. The echo amplitude decreases with increasing distance between the transducer and the screen. All cases show a significant decrease in echo amplitude for the case when the forming screen is between the plastic sphere and transducer. Table 4-2 shows a summary of the maximum echo amplitudes recorded with and without the forming screens present.

Table 4-2: Summary of Echo Amplitudes

ScreenA

Transducer	Maximum Amplitude without Screen Present	Maximum Amplitude with Screen Present	Percent Decrease in Amplitude
2 MHz 10 mm	28 Volts	11 Volts	60%
4 MHz 5 mm	75 Volts	5.5 Volts	93%
4 MHz 8 mm Focused	325 Volts	21 Volts	94%
8 MHz 5 mm	22 Volts	No Data	100%

Screen B

Transducer	Maximum Amplitude without Screen Present	Maximum Amplitude with Screen Present	Percent Decrease in Amplitude
4 MHz 5 mm	75 Volts	3 Volts	96%

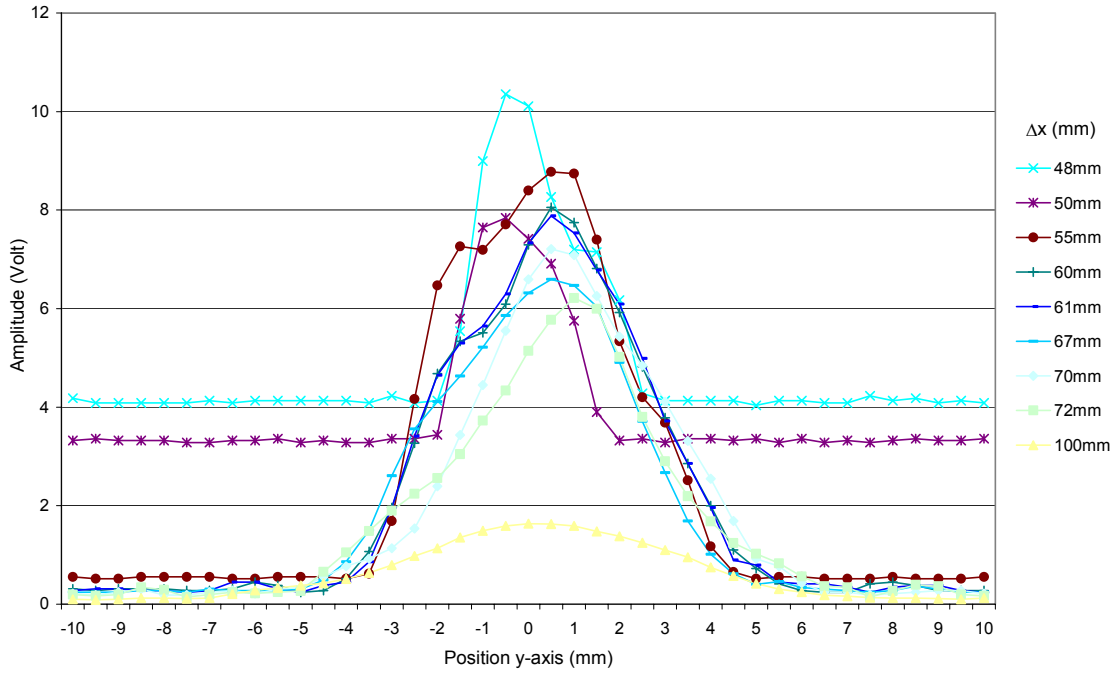

Figure 4-2: Echo Amplitude of 2 MHz 10mm Transducer with ScreenA at $\Delta x = 40$ mm

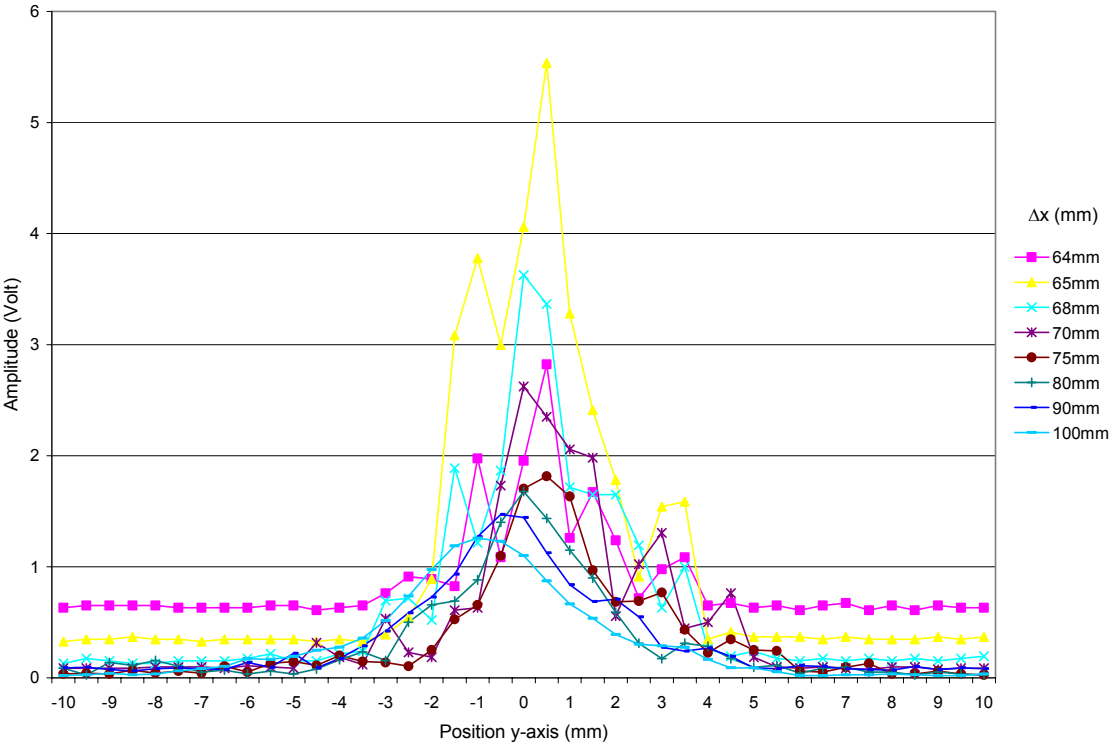

Figure 4-3: Echo Amplitude of 4 MHz 5 mm Transducer with ScreenA at $\Delta x = 60$ mm

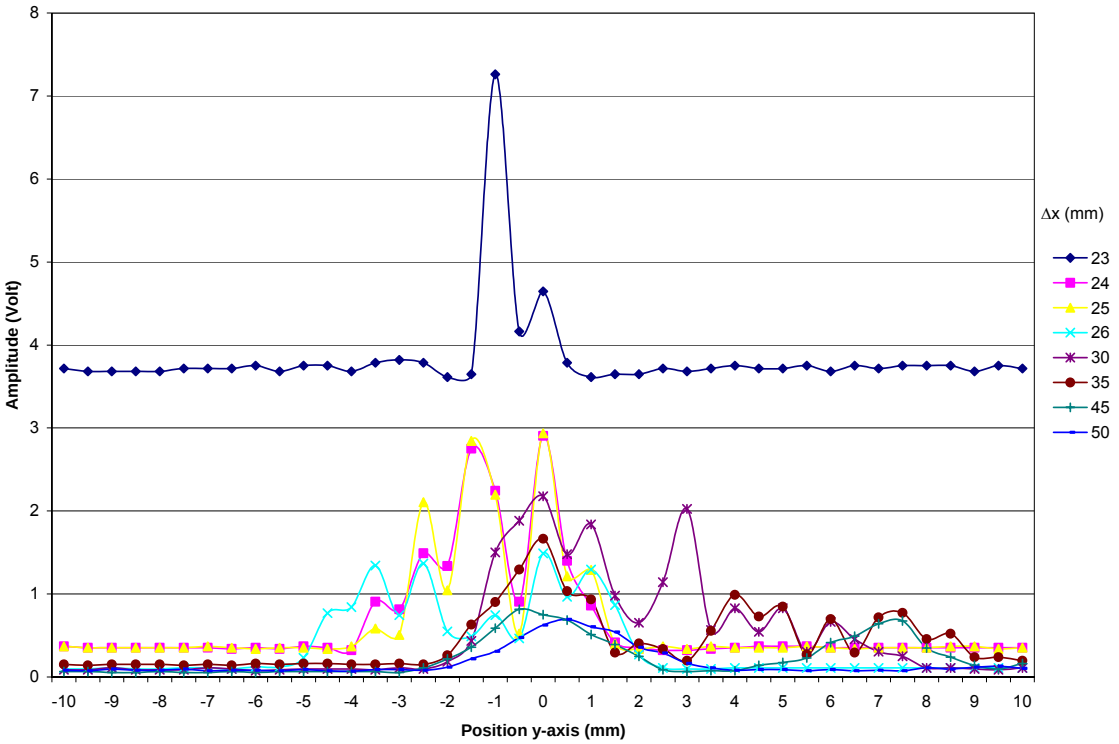

Figure 4-4: Echo Amplitude of 4 MHz 5 mm Transducer with ScreenB at Δx = 20 mm

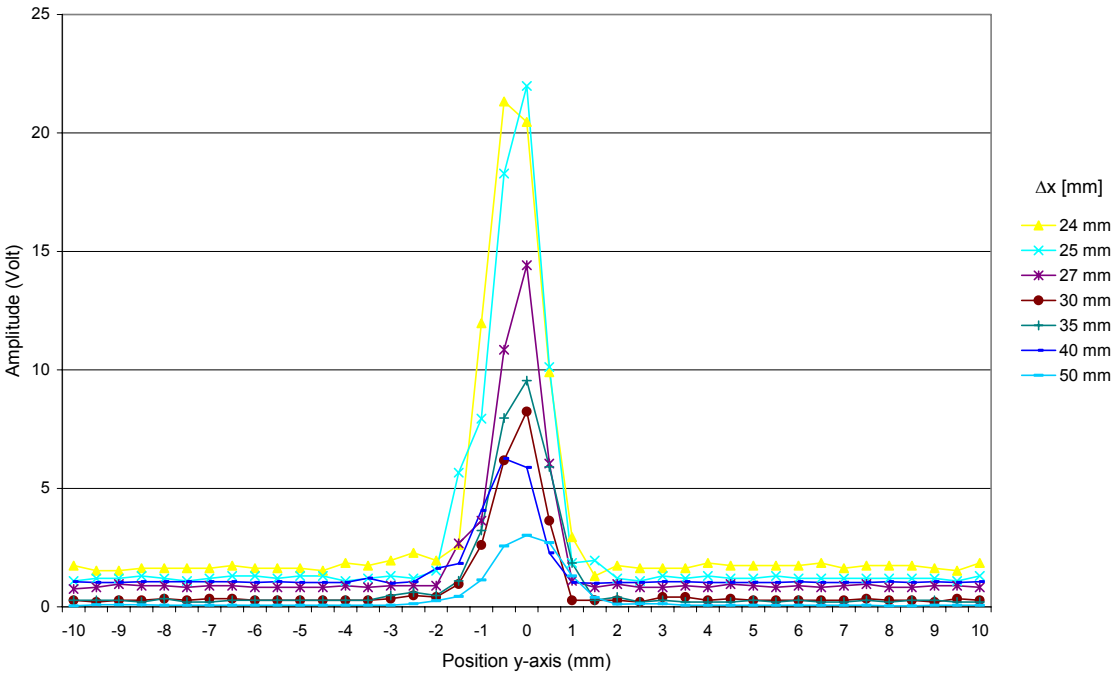

Figure 4-5: Echo Amplitude of 4 MHz 8 mm Focused Transducer with ScreenA at Δx = 20 mm

As the echo amplitude decreases due to the presence of the forming screen, the gain of the system must be increased to achieve a measurable signal. As the gain of the system is increased, the ringing effect increases. This ringing effect causes the minimum measurable distance to increase. This is due to the fact that the region close to the forming screen is saturated. No measurements can be detected by the ultrasonic transducer in this saturated region. For the 2 MHz 10 mm transducer, the minimum measurable distance is 8mm. This is evident from the amplitude profile (Figure 4-2) and from the beam divergence profile (Figure 4-6). The closest that the small sphere could be placed to ScreenA before there was no detectable signal was 8 mm. Any attempt to place the sphere closer to the forming screen did not produce results because the signal received by the transducer was saturated. When the signal is saturated, the DOP 2000 system reads a very high (several orders of magnitude larger than the readings when the signal is not saturated) amplitude reading that is constant across the y-axis and a beam width of zero. While using the 4 MHz 5 mm and the 4 MHz 8 mm focused transducer, minimum measurement distances of 3 mm and 4 mm are achieved, respectively, for ScreenA. Again, these values were evident in the amplitude and beam divergence profiles as shown in Figure 4-3, Figure 4-5, Figure 4-7, and Figure 4-8. The 4 MHz 5 mm transducer also had a minimum measurement distance of 4 mm when ScreenB was in place as shown in Figure 4-4. After only one measurement with the 8 MHz 5 mm transducer, the ultrasonic signal diverged so much that no signal was detected by the device. This is shown in Figure 4-9. Due to high absorption and attenuation of the ultrasonic signal, when using the 8 MHz 5 mm transducer, no results were achieved when the forming screen is placed between the plastic sphere and the transducer. The closest distance from the plastic sphere to the screen over the widest range of transducer-screen-distances that produced detectable echoes was achieved with the 4 MHz 5 mm transducer. The 4 MHz transducer turned out to represent a good tradeoff between the high attenuation of the 8 MHz transducer and the low resolution (measurable depth and velocity) of the 2 MHz transducer.

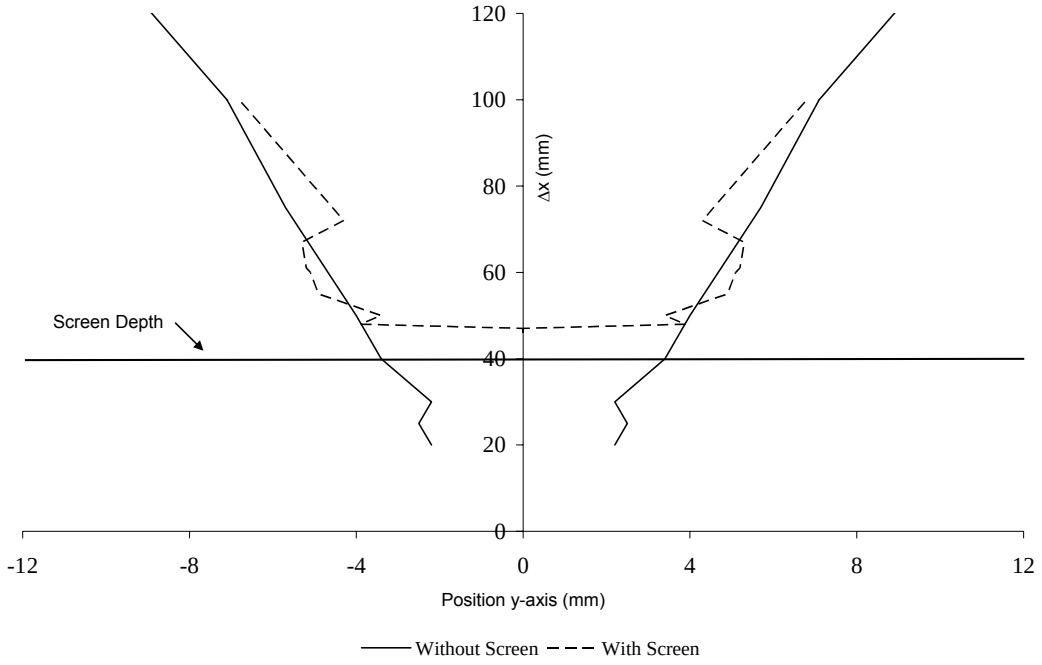

Figure 4-6: Beam Divergence Profile of 2 MHz 10 mm Transducer with ScreenA at Δx = 40 mm (6 dB)

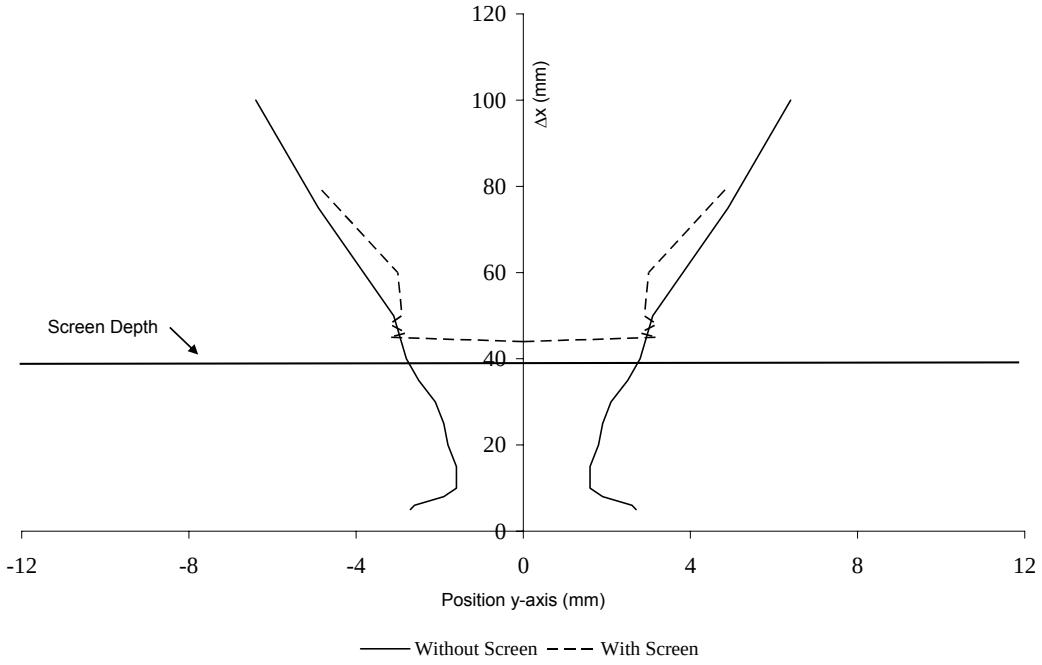

Figure 4-7: Beam Divergence Profile of 4 MHz 5 mm Transducer with ScreenA at Δx = 40 mm (6 dB)

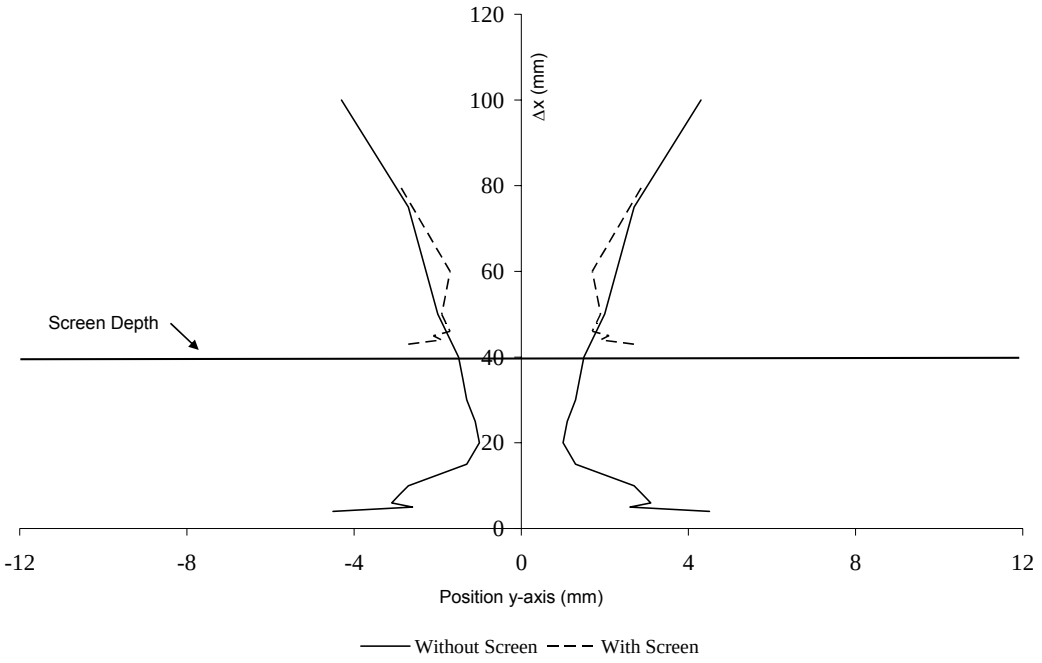

Figure 4-8: Beam Divergence Profile of 4 MHz 8 mm Focused Transducer with ScreenA at Δx = 40 mm (6 dB)

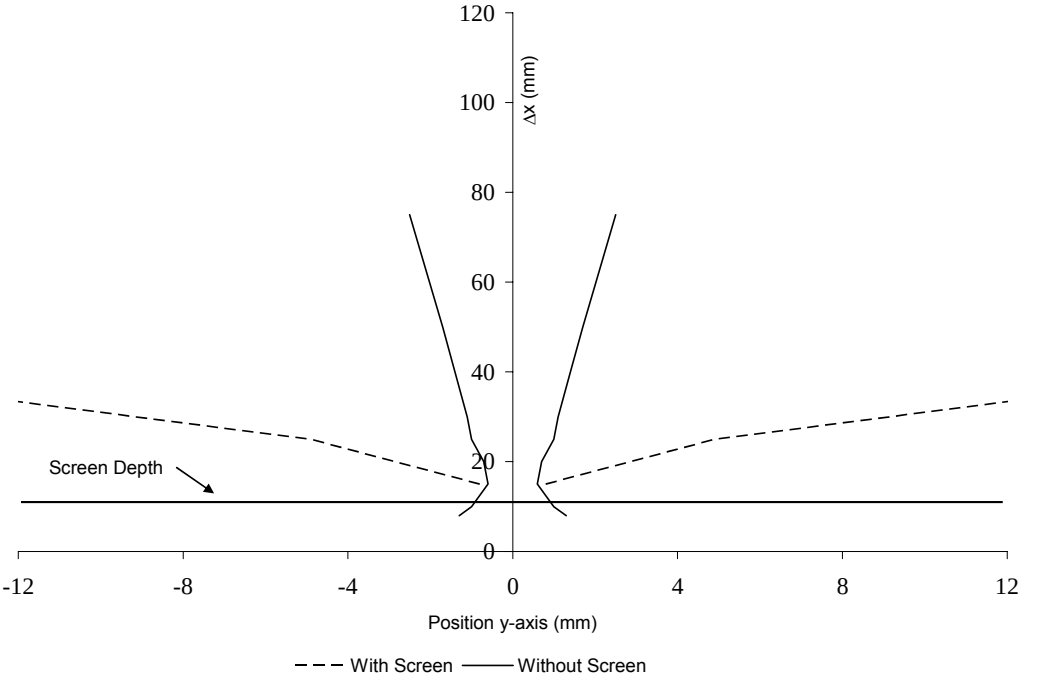

Figure 4-9: Beam Divergence Profile of 8 MHz 5 mm transducer with ScreenA at Δx = 10 mm (6 dB)

The shape of the beam of the ultrasonic transducer changes when the screen is inserted in the field. When the screen is in place between the plastic sphere and the transducer, the beam seems to have two distinct regions. The “near screen field“ is the region on the opposite side of the screen from the transducer, which is approximately 20-40 mm in length for the 2 MHz transducer and 20 mm in length for both of the 4 MHz transducers (focused and unfocused) with ScreenA. The “far screen field“ is the region that is on the opposite side of the screen as the transducer and is past the “near screen field“ (greater than 40 mm for the 2 MHz transducer and greater than 20 mm for the 4 MHz transducers) for ScreenA. In all cases (except for the 8 MHz transducer), the beam shape and width in the far screen field are very close to the same with and without ScreenA as shown in Figure 4-6, Figure 4-7, and Figure 4-8. In the near screen field, there is a common trend of beam convergence (narrowing of beam width) followed by beam divergence (widening of the beam width) as the beam progresses to the far screen field (Figure 4-6, Figure 4-7, and Figure 4-8). The beam width in the near screen field is slightly smaller (typically no more than 2mm) than the beam width when ScreenA is not present. The 3 dB divergence profiles are slightly narrower than the 6 dB divergence profiles in all cases. An example of a 3 dB beam divergence profile is shown in Figure 4-10 for the 4 MHz 5 mm transducer with ScreenA at Δx = 40 mm.

The same trends for beam shape were apparent also when ScreenA was placed 20 mm away from the ultrasonic transducer. The ultrasonic beam converges slightly in the near screen field and then diverges as it passes into the far screen field. For the 4 MHz 8 mm focused transducer, the focal point without the screen is at 20mm, but with ScreenA placed 20 mm away from the transducer, the focal point shifts back approximately 10 mm as shown in Figure 4-11. This does not happen when ScreenA is at any other position that was tested with the 4 MHz focused transducer. Since the far screen field beam width and shape are very similar with and without the screen present, the angle of divergence for the transducers is similar in both cases. With ScreenA in place, the beam shape

changes dramatically with different transducers so the trends are different for different transducers at different screen depths.

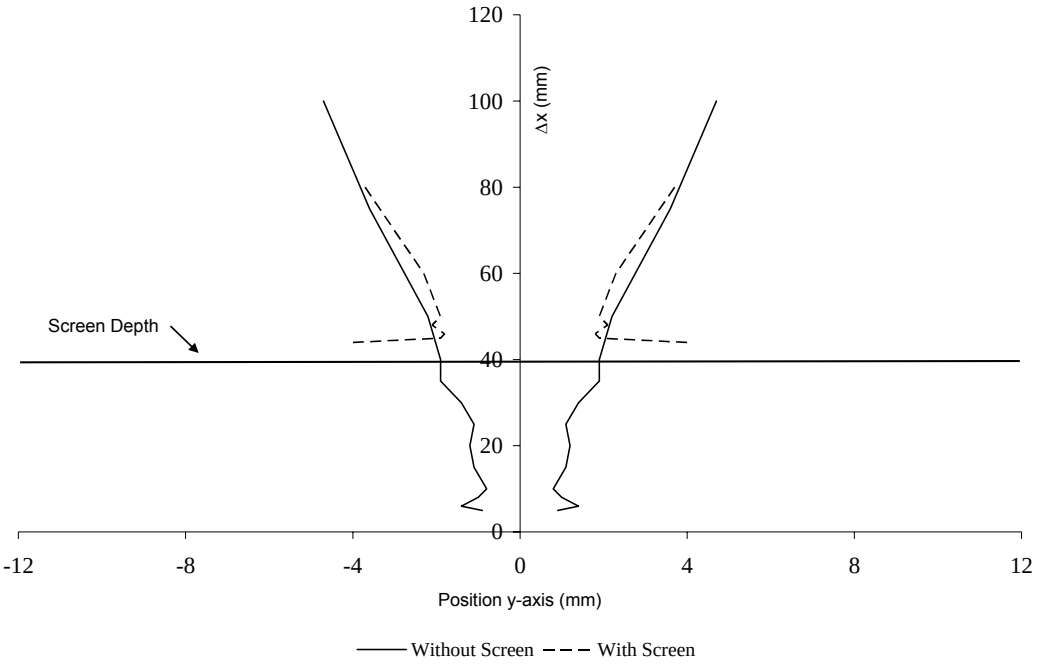

Figure 4-10: Beam Divergence Profile of 4 MHz 5 mm Transducer with ScreenA at Δx = 40 mm (3 dB)

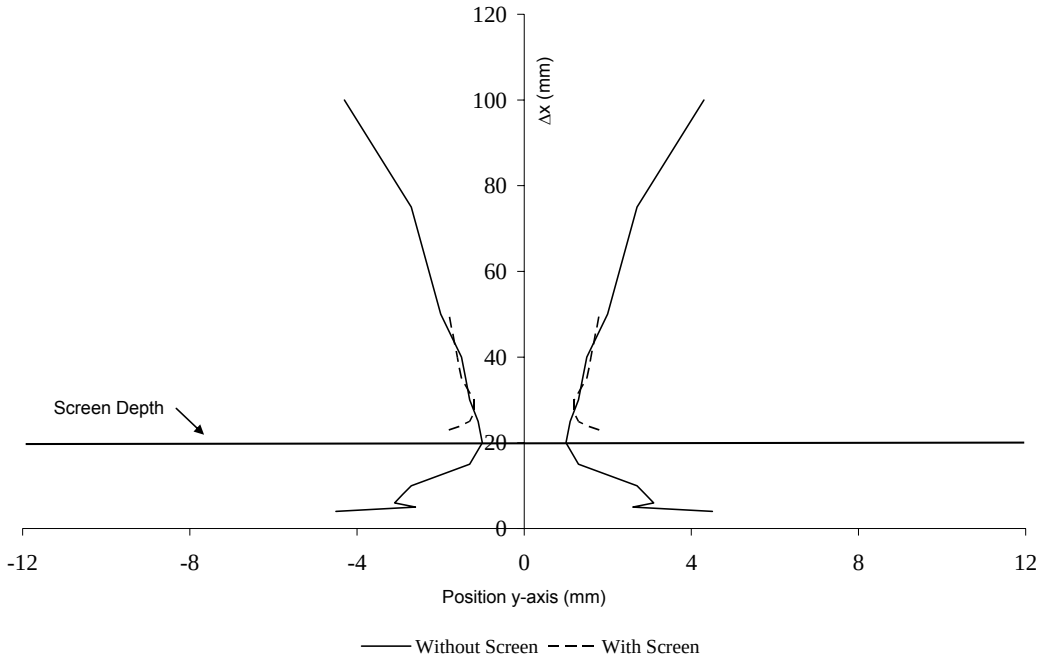

Figure 4-11: Beam Divergence Profile of 4 MHz 8 mm Focused Transducer with ScreenA at Δx = 20 mm (6 dB)

4.3 Modelling of Forming Screen

There are some numerical computations that allow the calculation of the absorption of acoustic energy due to the forming screen, and these would help verify the reduction of echo intensity due to the forming screen. In order to determine the reduction of echo intensity due to the forming screen, the acoustic impedance and the transmission coefficient of the forming screen must be determined. To calculate the acoustic impedance of the forming screen, several approaches were studied.

The first approach was to take the measured apparent density of the forming screen sample, 1.18 g/cm^3, and multiply it by the speed of sound in the forming screen, 1700 m/s, measured by Brodeur [8] to get a vague value of the acoustic impedance. This approach gives the acoustic impedance of the forming screen a value of 2 x 10^6 MKS Rayls. No data was available for the speed of sound for the sample of forming screen used in this study.

The next approach was to try and use numerical models to come up with a value for acoustic impedance of the forming screen. Two numerical models were considered, the Delany-Bazley model which is a fundamental model in the area of sound propagation in fibrous materials and the Allard-Champoux model. The Delany-Bazley model predicted an acoustic impedance that was approximately the same magnitude as water. This would mean that the transmission coefficient was approximately 100% which is not at all realistic. The Allard-Champouc model gave similarly bad results that were not useful (transmission coefficient of ~100%). For reference, both models are described in Appendix C.

Due to the challenge in calculating the acoustic impedance of the forming screen with any reasonable accuracy, the reduction of echo intensity caused by placing the forming screen between the ultrasonic transducer and target sphere could not be calculated. One of the possible solutions of why the numerical results did not yield useful results is that the forming screen has a very high porosity, and the pores in the screen could be saturated with water (the test medium) rather than air. Unfortunately, the echo intensity reduction due to the forming screen for this study is solely based on the measured values using the pulsed ultrasonic Doppler system [25].

4.4 Repeatability Tests

General trends such as beam convergence just past the forming screen and then divergence were seen throughout the forming screen tests, but all tests seemed to have some amount of variation. In the experimental setup of the forming screen tests, the forming screens were mounted in a Plexiglas mount that could be placed in the water bath with the transducer and the small plastic sphere. The forming screen sample was also much larger than the width of the ultrasonic beam emitted from the transducer at the depths that were tested. When placing the forming screen in the water bath, care was taken in each of the tests to have the screen at the same location for each test. The depth of the screen (Δx away from the transducer) was set each time by placing the plastic sphere in contact with the transducer and then backing it to the desired depth of the forming

screen. The forming screen was then introduced into the water bath and placed in contact with the plastic sphere. The depth of the forming screen was then verified using the DOP 2000 ultrasonic system by means of visually inspecting at what depth the echo for the screen occurred. Using these two steps ensured that the forming screen was at the correct depth for every test. Once the depth of the forming screen was set, the screen could be moved laterally approximately 3 mm in either direction along the y-axis. Originally, it was thought that since the voids in the forming screen were so small, slight variation in lateral position would not affect the results of the beam shape measurements. As testing progressed, some questions of repeatability of the tests were raised due to the fact that although the general trends were the same for the beam shape measurements, the measurements themselves were significantly different for each test.

These concerns of repeatability of the measurements prompted a new set of tests that would determine if slight variations in the lateral position of the forming screen would produce different results for the beam shape measurements. Up to this point, the beam measurement tests had not been consecutively performed. Although the conditions were kept as close to the same as possible throughout the tests, there were slight variations in the tests including testing on different days, changing water in the water bath, and remounting the transducer between tests. The new set of tests would all be done on the same day, in the same water bath (without changing the water), and with the ultrasonic transducer and plastic sphere mounted in the exact same positions for each test. The new tests were done with ScreenA and ScreenB. Since the most promising results in the tests leading up to these new tests had been with the 4 MHz 5 mm ultrasonic transducer, it was used for the new set of tests.

4.4.1 ScreenA

For ScreenA, a total of nine different consecutive sets of data were taken. The first three sets of beam shape measurements (sets 1-3, black lines) were taken without moving anything except for the small plastic sphere (in order to generate slices of the beam field). The second three sets of data (sets 4-6, blue lines)

were taken exactly the same as sets 1-3, but the screen was moved 0.5 mm laterally prior to the tests. The third three sets of data (sets 7-9, red lines) were taken with the exact same configuration as sets 4-6 (the previous sets) but waiting 2 hours after set 6 was taken. This last set of tests was meant to determine if the results of the beam shape measurements could be accurately repeated when nothing in the test setup changes. The same depths for the slices (Δx away from transducer) were used for all of the sets of data.

The 6 dB beam divergence profiles for sets 1-3 are presented in Figure 4-12. Set 2 shows a slight variation in beam width at Δx = 70 mm, but otherwise, the beam widths for sets 1-3 are all within an average of 0.4 mm of each other for each measured slice. At Δx = 70 mm the beam width of set 2 is 2.4 mm greater than the beam widths of sets 1 and 3. Figure 4-13 shows the beam divergence profiles for sets 4-6. Set 4 varies by 2.4 mm from sets 5 and 6 at Δx = 75 mm. Sets 4-6 vary by only an average of 0.5 mm at all other measured slices. Figure 4-14 shows the beam divergence profiles for sets 7-9. Set 7 varies by 1.4 mm from sets 8 and 9 at Δx = 45 mm and Δx = 75 mm. The measured beam widths for sets 7-9 all average 0.6 mm for each other for each measured slice other than Δx = 45 mm and Δx = 75 mm.

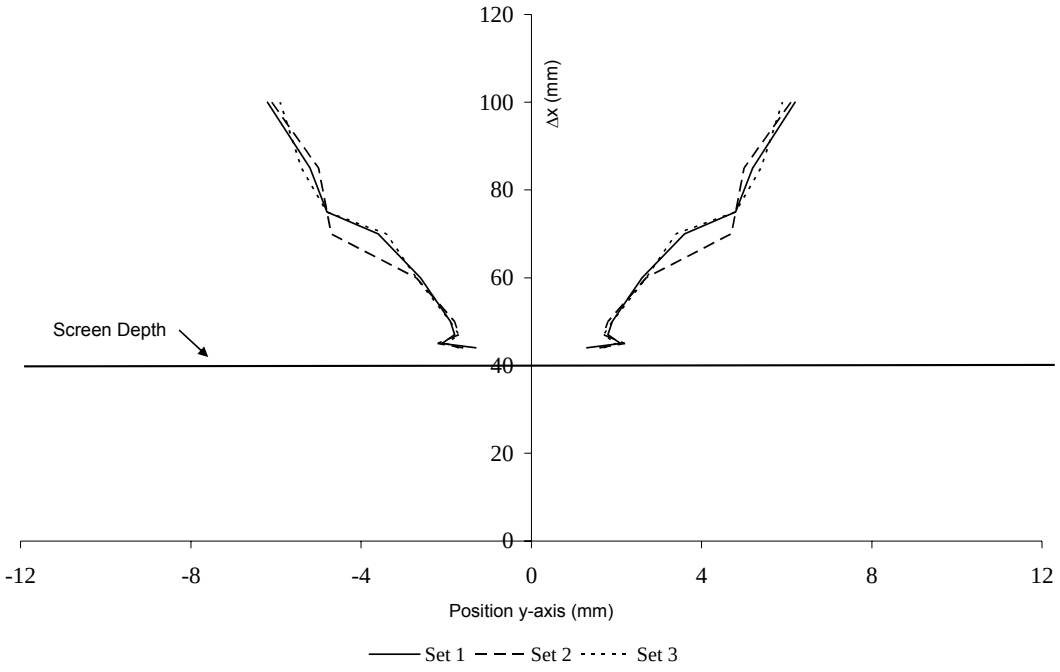

Figure 4-12: Beam Divergence Profile of 4 MHz with ScreenA at Δx = 40 mm (6dB) Sets 1-3

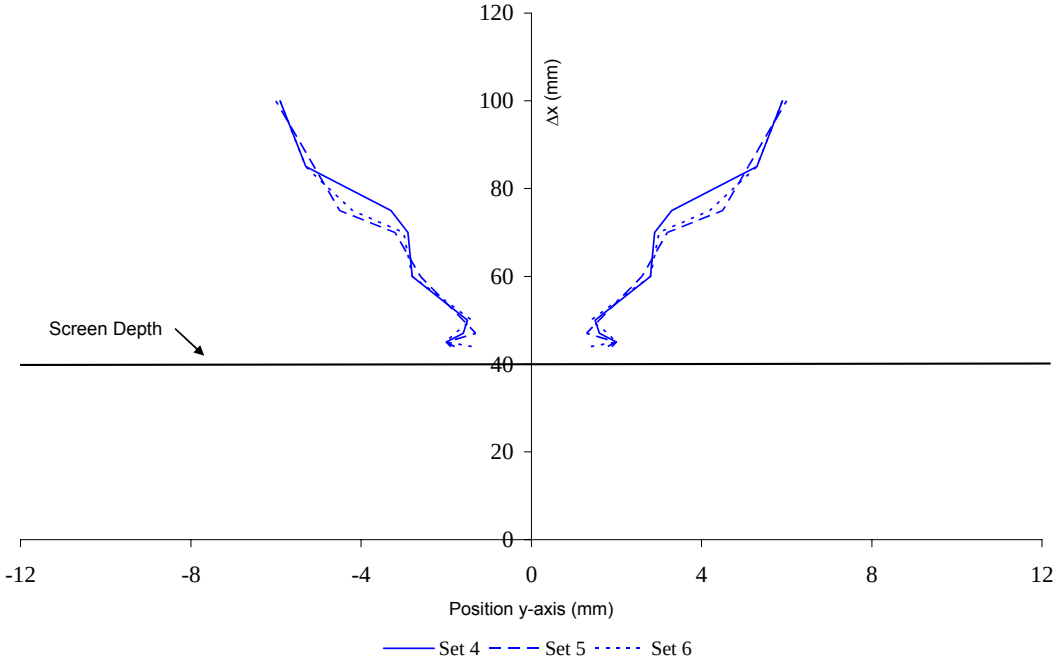

Figure 4-13: Beam Divergence Profile of 4 MHz with ScreenA at Δx = 40 mm (6dB) Sets 4-6

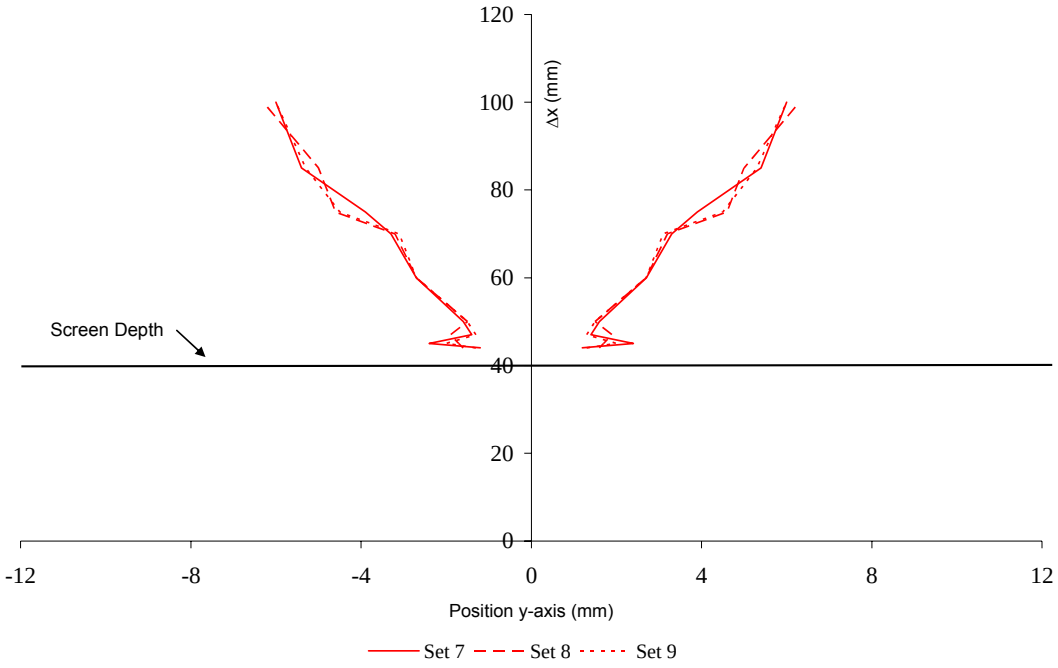

Figure 4-14: Beam Divergence Profile of 4 MHz with ScreenA at Δx = 40 mm (6dB) Sets 7-9

The best way to check and see if the lateral movement of the forming screen caused variation in the beam shape measurements is to look at the relationship between sets 1-6 and sets 4-9. As previously stated, the only difference in the beam shape measurements between sets 1-3 and sets 4-6 was the change (by 0.5 mm) in lateral position (y-axis) of the forming screen. Figure 4-15 shows the beam divergence profiles for sets 1-6. The maximum difference in beam widths are 3.6 mm and 3.0 mm at Δx = 70 mm and Δx = 75 mm, respectively, for sets 1-6. The difference in measured beam widths for sets 1-6 average 0.8 mm for each measured slice other than Δx = 70 mm and Δx = 75 mm. The beam divergence profiles for sets 4-9 are shown in Figure 4-16. The maximum difference in beam widths is 2.6 mm at Δx = 75 mm for sets 1-6. The difference in measured beam widths for sets 4-9 average 0.9 mm for each measured slice other than Δx = 75 mm. Figure 4-17 shows sets 1-9 together on the same beam divergence profile. The maximum difference in the beam divergence measurements was 3.6 mm from sets 2 and 4 at Δx = 70 mm. Consequently,

these two measurements were made when nothing in the experiment had changed except for the lateral screen position.

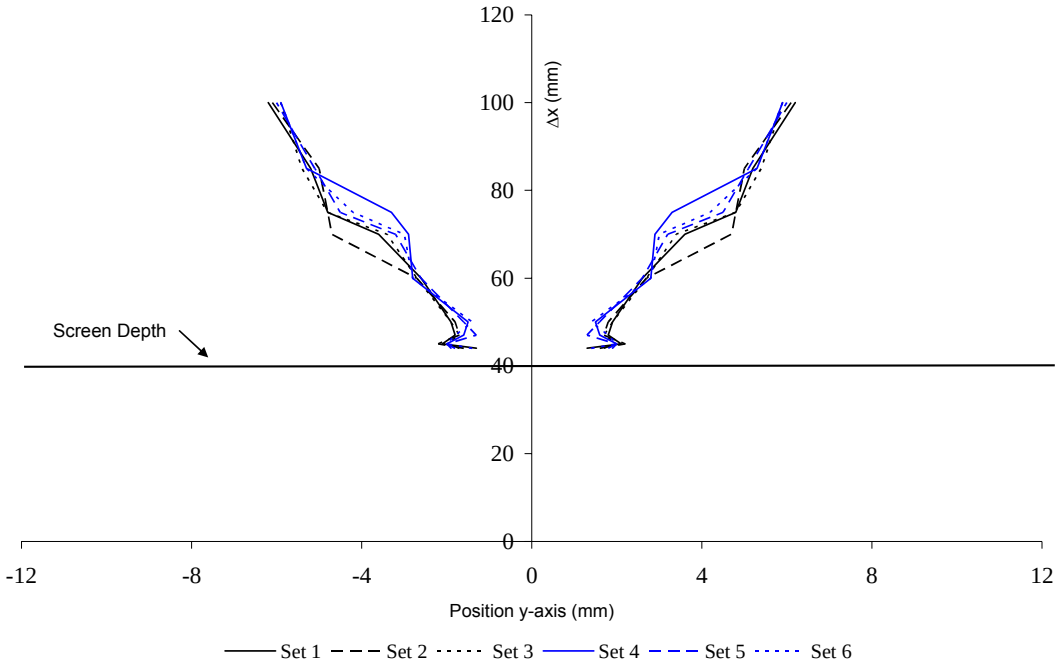

Figure 4-15: Beam Divergence Profile of 4 MHz with ScreenA at Δx = 40 mm Set 1-6 (6dB)

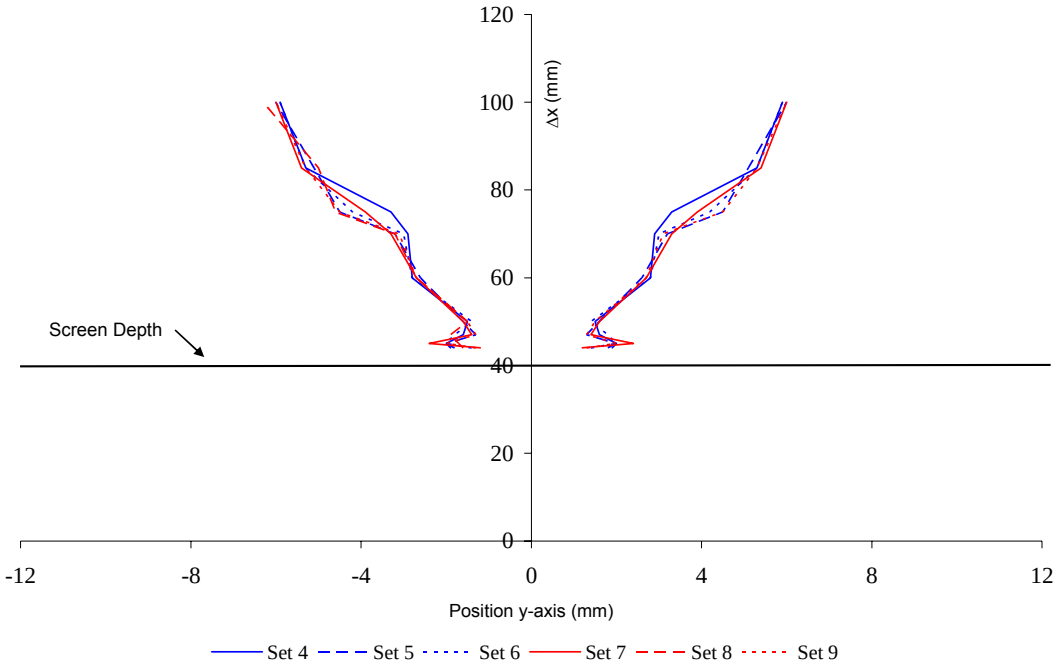

Figure 4-16: Beam Divergence Profile of 4 MHz with ScreenA at Δx = 40 mm Set 4-9 (6dB)

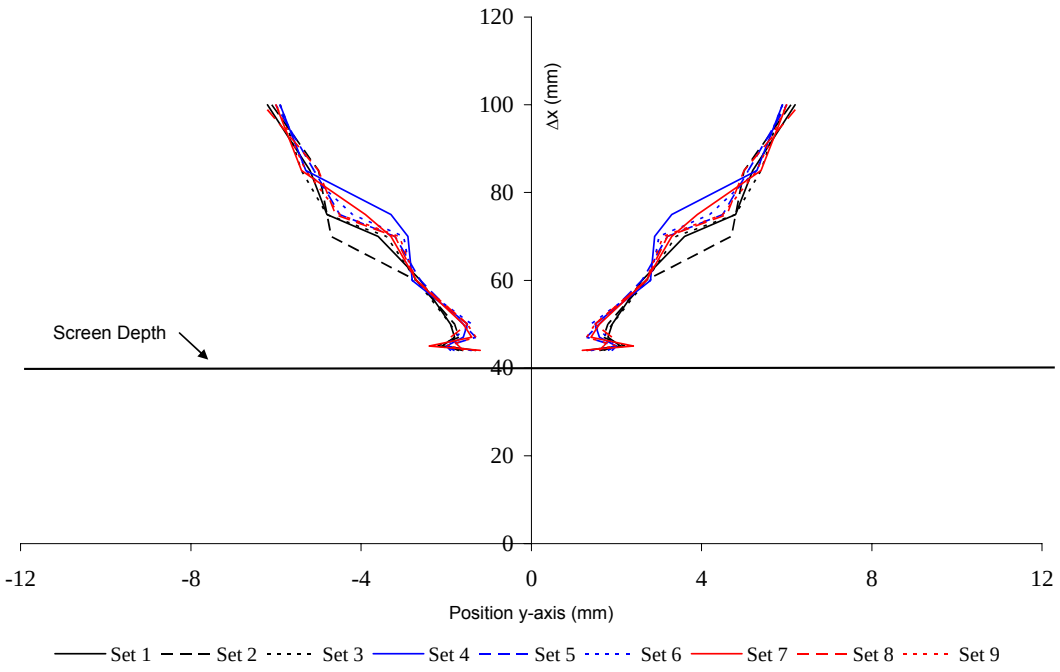

Figure 4-17: Beam Divergence Profile of 4 MHz with ScreenA at Δx = 40 mm Set 1-9 (6dB)

4.4.2 ScreenB

The same general procedure was applied to ScreenB with much more noticeable results. For ScreenB, a total of eight different consecutive sets of data were taken. Like ScreenA, the first three sets of beam shape measurements (sets 1-3, black lines) were taken without moving anything except for the small plastic sphere (in order to generate slices of the beam field). The second two sets of data (sets 4 and 5, blue lines) were taken exactly the same as sets 1-3, but the screen was moved 0.5 mm laterally prior to the tests. The third three sets of data (sets 6-8, red lines) were taken with the exact same configuration as sets 4 and 5 (the previous sets) but waiting 2 hours after set 5 was taken. Again, this last set of tests was meant to determine if the results of the beam shape measurements could be accurately repeated when nothing in the test setup changes, and the same depths for the slices (Δx away from transducer) were used for all of the sets of data.

Figure 4-18 shows the 6 dB beam divergence profile for sets 1-3 with ScreenB. This figure shows a beam divergence profile much different than the previous profiles generated for ScreenA. The most noticeable difference in the profile occurs with measurements made in the Δx = 70 mm to Δx = 85 mm region of the profile. When the DOP 2000 receives a saturated signal from the medium being measured, it typically returns a value of zero for the beam divergence width (the same as if the transducer was experiencing the ringing effect as mentioned in chapter 3). For sets 1 and 2, the DOP 2000 registered a value that was an order of magnitude greater and negative in value for the slice depth of Δx = 75 mm. This is a discontinuity in the data due to a saturated region in the test medium and is analogous to the ringing effect. In set 3 the discontinuity in the saturated region is given a value of zero for the beam width. The general trend in this profile is a divergence of the ultrasonic beam from the screen to a depth of Δx = 60 mm and then a slight convergence followed by another divergence of the ultrasonic beam at Δx = 85 mm and beyond. At depths Δx = 44 mm, Δx = 47 mm, and Δx = 50 mm, the beam widths vary by 3.4 mm for sets 1-3, but at all

other depths (excluding Δx = 75 mm), the beam widths vary by an average of 0.8 mm.

The 6 dB beam divergence profiles for sets 4 and 5 are presented in Figure 4-19. The greatest variation in beam width for these two sets is at Δx = 44 mm and is 5.8 mm. The difference in beam widths for the other measured slices is an average of 0.6 mm. Figure 4-20 shows the beam divergence profile for sets 6-8. The greatest variation in beam width for these two sets is at Δx = 44 mm and Δx = 45 mm and is 5.2 mm. The difference in beam widths for sets 6-8 average 1.0 mm for other measured slices. Figure 4-19 and Figure 4-20show the general trend of convergence of beam shape before divergence as the beam moves farther into the medium past the forming screen.

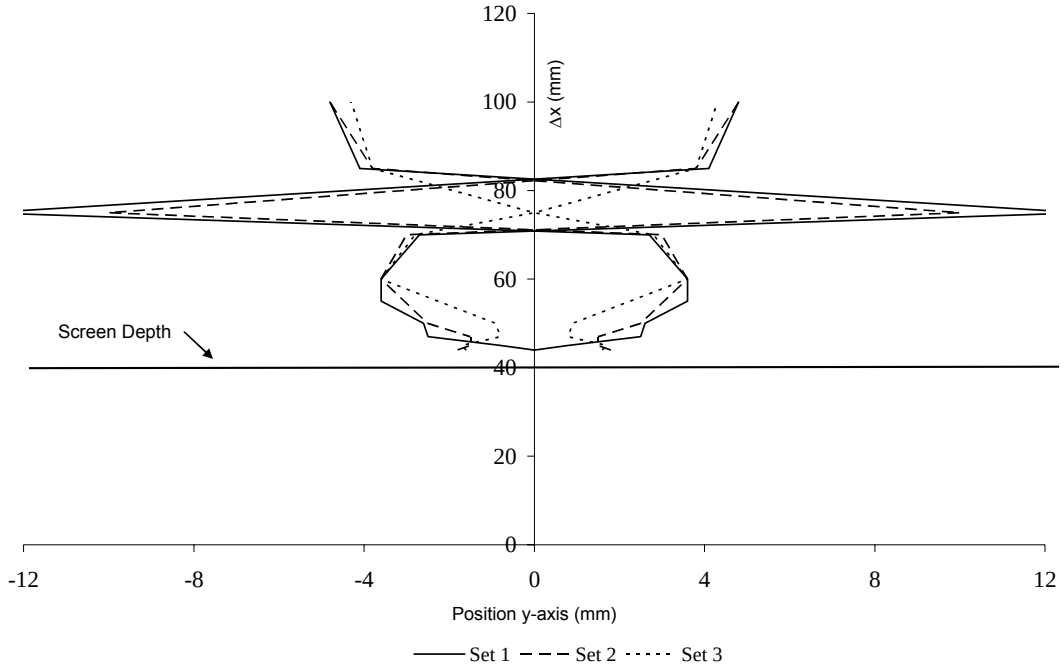

Figure 4-18: Beam Divergence Profile of 4 MHz with ScreenB at Δx = 40 mm (6dB) Sets 1-3

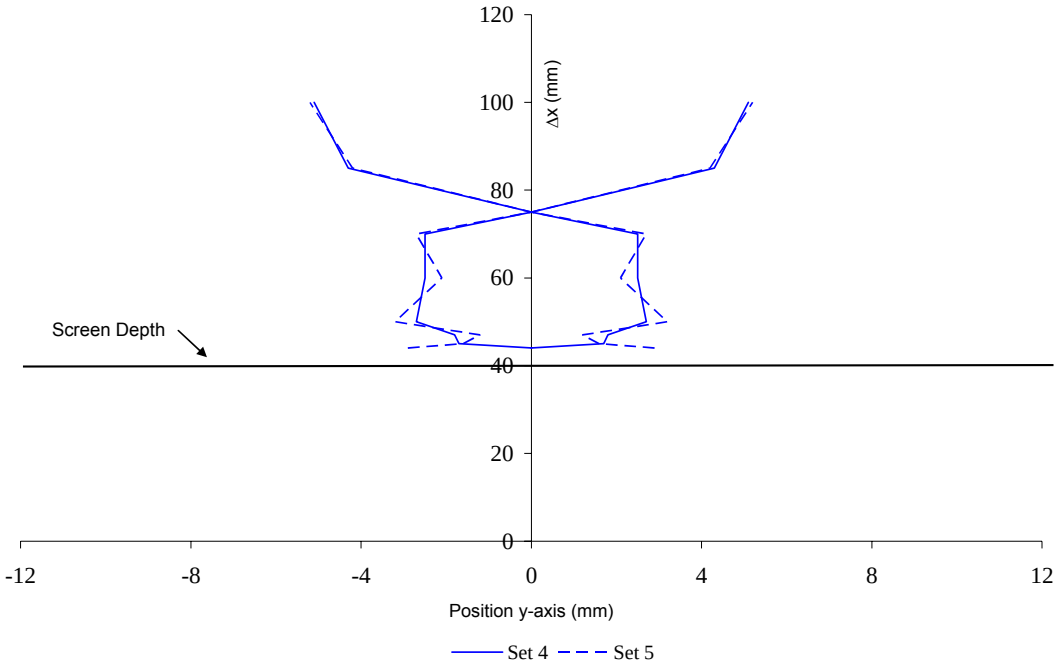

Figure 4-19: Beam Divergence Profile of 4 MHz with ScreenB at Δx = 40 mm (6dB) Sets 5 and 6

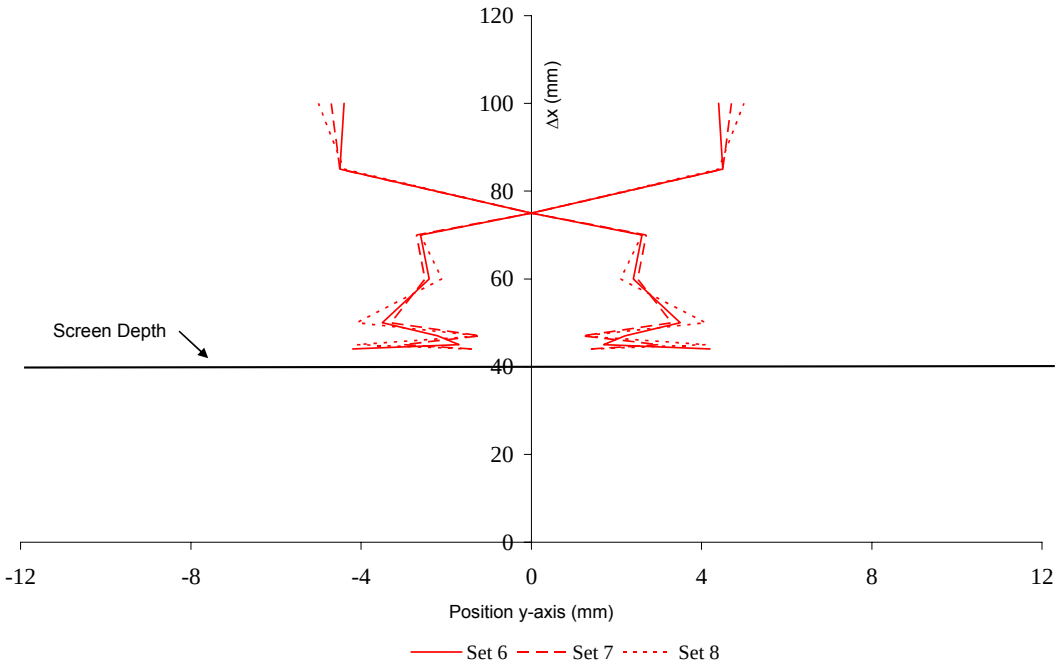

Figure 4-20: Beam Divergence Profiles of 4 MHz with ScreenB at Δx = 40 mm (6dB) Sets 6-8

As with ScreenA, the changes that were made to the forming screen for the different sets of beam shape measurements can be studied for ScreenB. The main two data sets of interest are sets 1-5 and sets 4-8. The only difference in the beam shape measurements between sets 1-3 and sets 4 and 5 was the change (by 0.5 mm) in lateral position (y-axis) of the forming screen. Figure 4-21 shows the beam divergence profiles for sets 1-5. The maximum difference in beam width is 4.6 mm at Δx = 44 mm and Δx = 50 mm, but the difference in beam width for the different sets at all other measured slices averages 2 mm. The beam divergence profiles for sets 4-8 are shown in Figure 4-22. The maximum difference in beam width between the sets is 8.4 mm and 5 mm at Δx = 44 mm and Δx = 45 mm, respectively, and the average beam width difference for each of the other measured slices in the profiles is 1.2 mm. The 6 dB beam divergence profile for sets 1-8 with ScreenB is shown in Figure 4-23. The maximum difference in beam width is 6.6 mm between set 1 and set 8. The other sets average 2.8 mm in variation of beam width between measured slices.

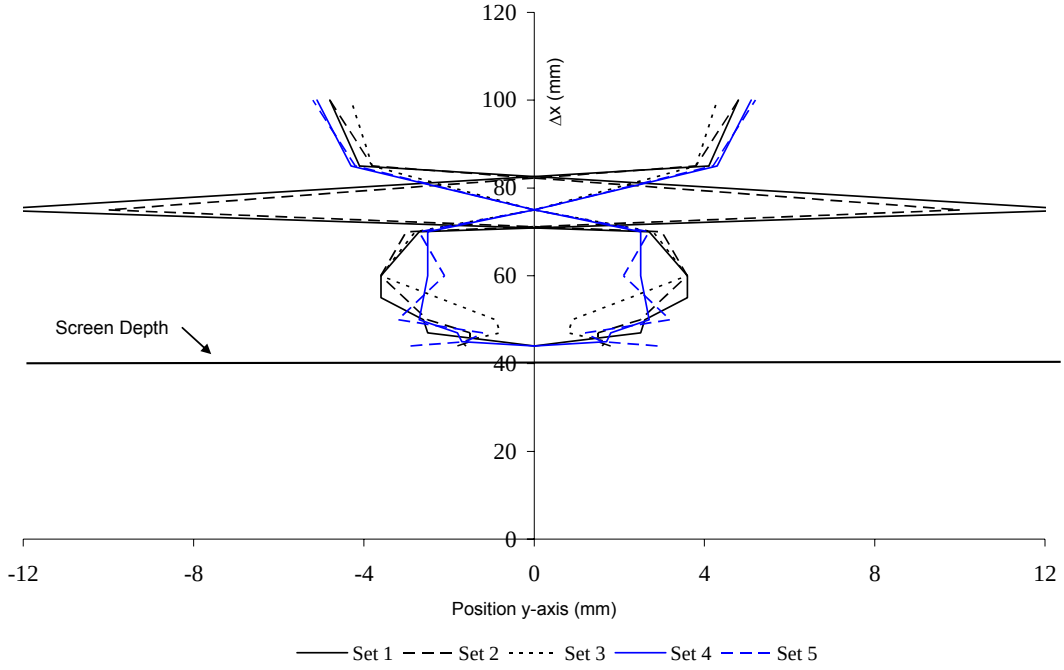

Figure 4-21: Beam Divergence Profiles of 4 MHz with ScreenB at Δx = 40 mm (6dB) Sets 1-5

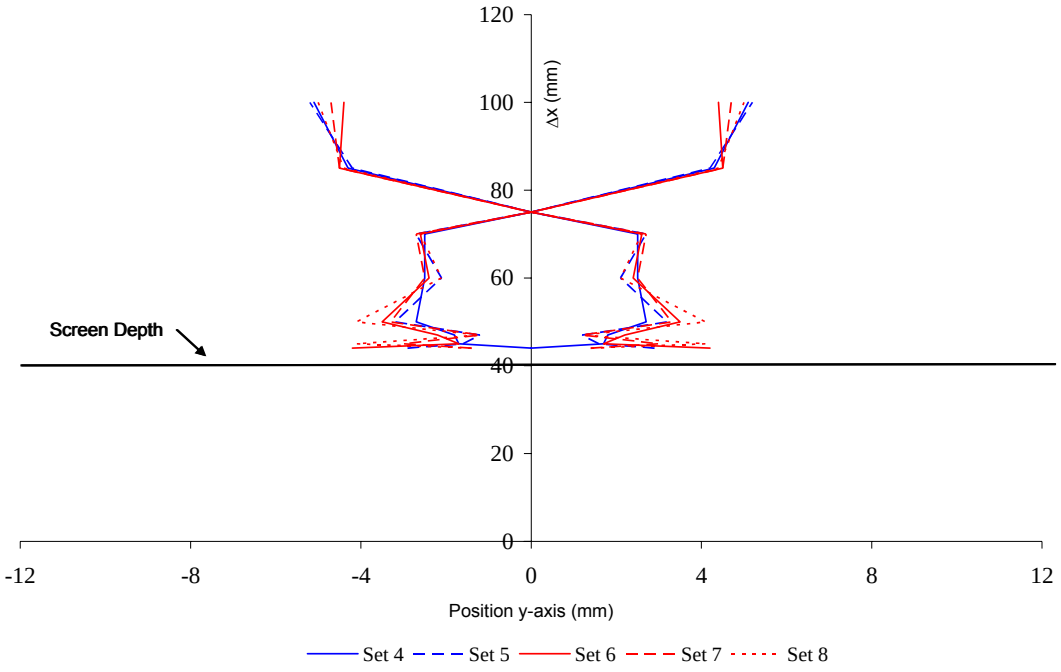

Figure 4-22: Beam Divergence Profiles of 4 MHz with ScreenB at Δx = 40 mm (6dB) Sets 4-8

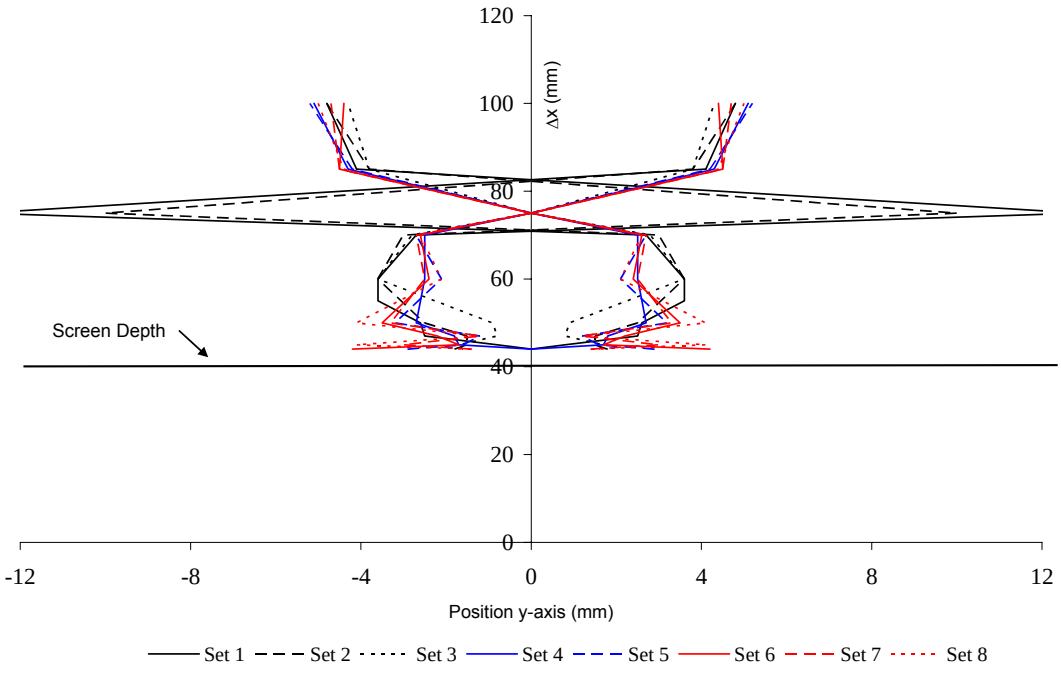

Figure 4-23: Beam Divergence Profiles of 4 MHz with ScreenB at Δx = 40 mm (6dB) Sets 1-8

These tests with ScreenA and ScreenB show that there is more variation in beam width when the forming screen is moved laterally than when it is not moved. They also show that even though the pores in the forming screen are very small, they seem to have a great effect on the beam width measurements of the ultrasonic transducer. The greatest variation in the beam widths for ScreenA is at the depth Δx = 70 mm. The greatest variation in the beam widths for ScreenB is very close to the forming screen, usually at Δx = 44 mm, but there is also a large variation in beam width and a saturated region around Δx = 75 mm. These depths are where the maximum variation in beam width is for each screen, but for both screens the largest variance in beam width between the sets is at Δx = 44 mm and Δx = 70 mm. It should be noted that beam width values for the discontinuity due to the saturated region in the test medium for ScreenB at Δx = 75 were not included in the beam width analysis. This is because there was a discontinuity at this point in the measurements due to a saturated region in the test medium.

4.5 Artefacts

The phenomenon experienced by the ultrasonic system when studying ScreenB at Δx = 75 mm is most likely due to artefacts. False, multiple, or misleading information by the ultrasonic system or interaction with an adjacent test medium by the ultrasonic system is defined as an artefact. Artefacts come from the ultrasonic system experiencing refraction, shadowing, enhancement, or reverberation of the ultrasonic signal. Refraction simply causes a mirror image of the object in the test medium. The reduction of echo intensity due to a structure that reflects or attenuates the original signal is called shadowing. The opposite of shadowing is enhancement, or an increase in echo intensity due to a structure that does not reflect or attenuate the ultrasonic signal. The results of shadowing and enhancement are that the echoes received from the ultrasonic signal are too small and too large, respectively.

Reverberation is caused by multiple echoes being reflected from the same object. If a strong echo returns to a transducer surface, the transducer receives most of the energy of the echo, but some of the signal can be reflected off of the transducer surface. This reflected signal travels to the same object that it encountered originally and causes a second echo that the transducer receives. This means that one pulse of ultrasound produces two echoes from the same object in the test medium. The inherent delay in the second signal causes the ultrasonic system to display a second image of the same object at twice the original depth. This results in the placement on the image of reflectors that are not real. They are placed beyond the second real reflector at separation intervals equal to the separation between the first and second real reflectors [16].

Figure 4-24 and Figure 4-25show the echo intensity profile from the forming screen tests for ScreenA and ScreenB, respectively, placed at Δx = 40 mm in the water bath. No objects are present in the water bath except the forming screen and the ultrasonic transducer. These echo profiles clearly show that the forming screen creates a large echo at a depth of 40 mm. They also show the ringing effect by the transducer in the region very close to the transducer. This region is from a depth of zero out to a depth of approximately 7 mm. No useful measurements can be attained in this region of the test medium without modification to the test setup. The figures show no other discernable echoes except in the region around a depth of 80 mm. These echoes are caused by reverberation of the signal. Some of the original signal is reflected by the forming screen, and this reflected signal returns to the transducer surface. As the reflected signal gets to the transducer surface, some of the signal is received by the transducer, and some of the signal is reflected by the transducer surface. The signal encounters the forming screen again and then returns to the transducer. Since the transducer received two signals from the same object, it perceives the fact that there are two echoes. One of the echoes is in the correct position (Δx = 40 mm), and one of the echoes is at twice the depth of the original echo (Δx = 80 mm).

Figure 4-24 shows a small echo, and Figure 4-25 shows a much more defined echo. These echoes can definitely influence any measurements around the Δx = 80 mm region if the forming screens are present. ScreenB is approximately twice as thick and has a higher mesh count (number of wires per inch) than ScreenB. This allows ScreenA to let more of the ultrasonic signal pass through than ScreenB, and consequently, ScreenB reflects more of the signal back to the transducer surface. Since more of the signal is reflected back to the transducer surface by ScreenB than ScreenA, a stronger signal reflects off of the transducer surface into the test medium, and a larger echo profile is produced by the returning signal. This is the reason that the echo at a depth of 80 mm is much larger for ScreenB than for ScreenA.

These echoes at Δx = 80 mm act in the same way in the beam shape measurement tests as the forming screen. Since the ultrasonic system perceives an object at Δx = 80 mm, the information received from that region will be flawed. This means that if an object passes through this region, the signal received by the ultrasonic transducer will contain a combination of the reverberated signal and the true signal reflected by the object. This combination of the signals causes the ultrasonic system to output data similar to the data that it gives in a saturated region or from the ringing effect. This is the reason that the variation in beam shape measurements was greatest around the Δx = 80 mm region of the test medium. Although the reverberation effects could be seen in the beam shape measurements for ScreenA, the problems encountered for the beam shape measurements with ScreenB at Δx = 75 mm can definitely be attributed to the reverberation of the ultrasonic signal.

For comparison, Figure 4-26 shows ScreenB placed at Δx = 20 mm in the same test setup as above. The effects of reverberation can again clearly be seen at twice the screen's depth, or Δx = 40 mm. In this case, the perceived echo is much larger than the case when the forming screen was at a depth of 40 mm because the signal travels a shorter distance and is attenuated less.

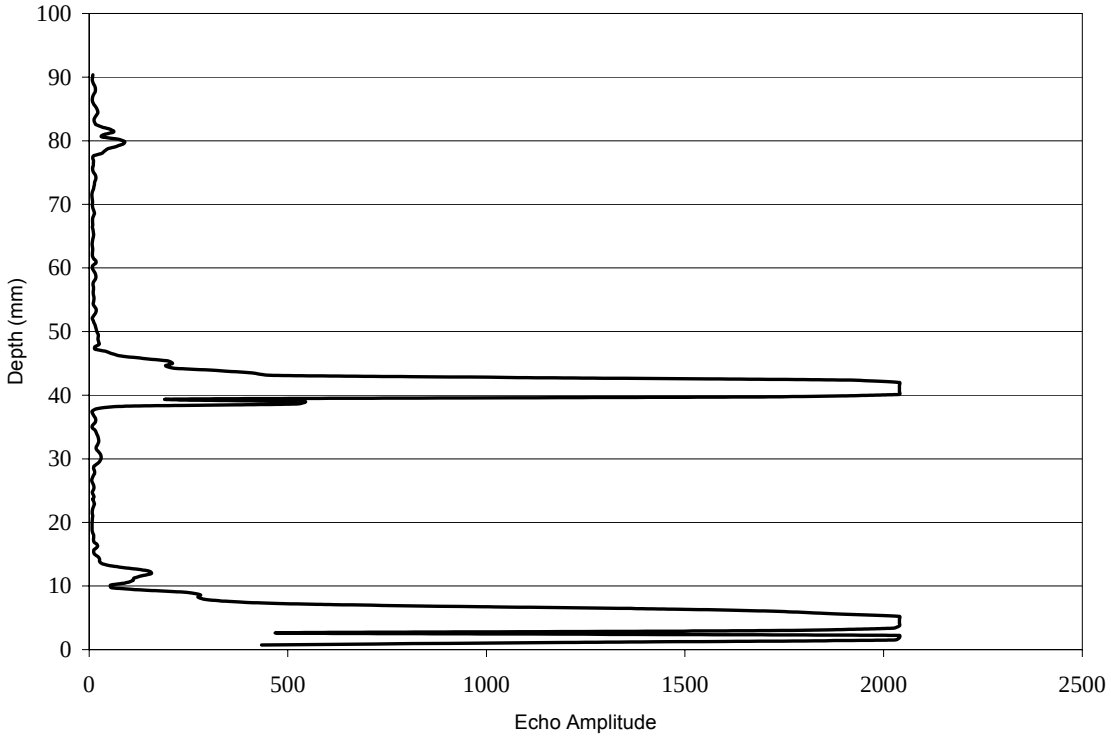

Figure 4-24: Echo Intensity with 4 MHz Transducer and ScreenA at $\Delta x = 40mm$

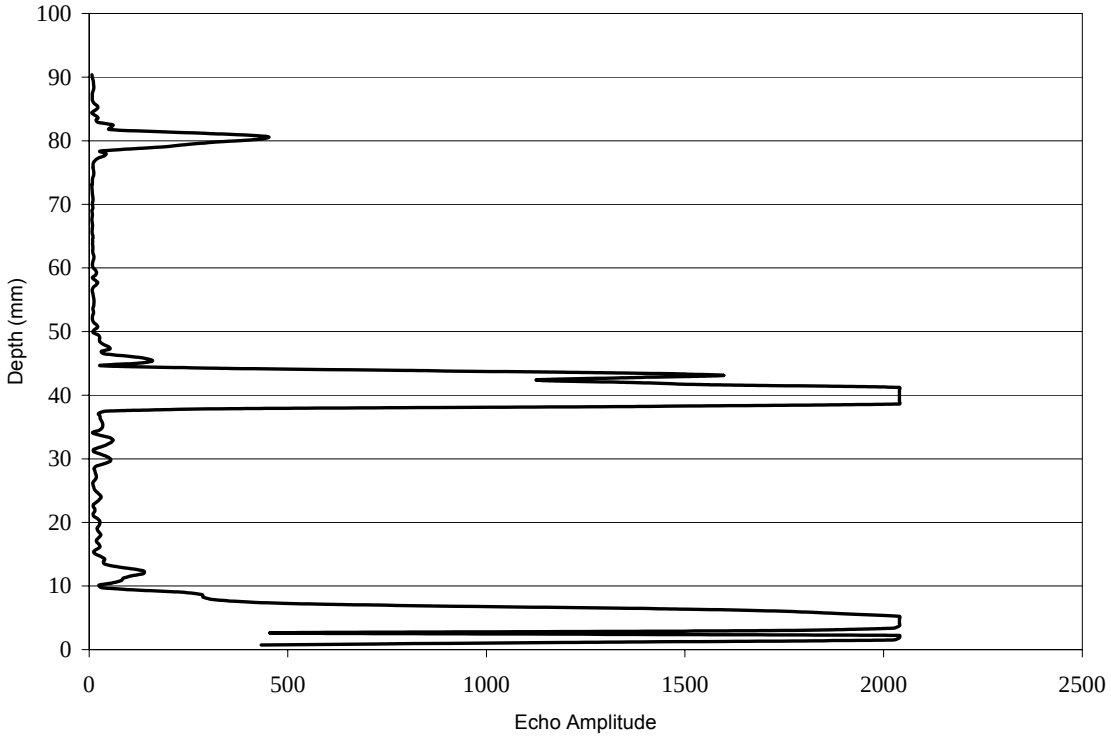

Figure 4-25: Echo Intensity with 4 MHz Transducer and ScreenB at $\Delta x = 40mm$

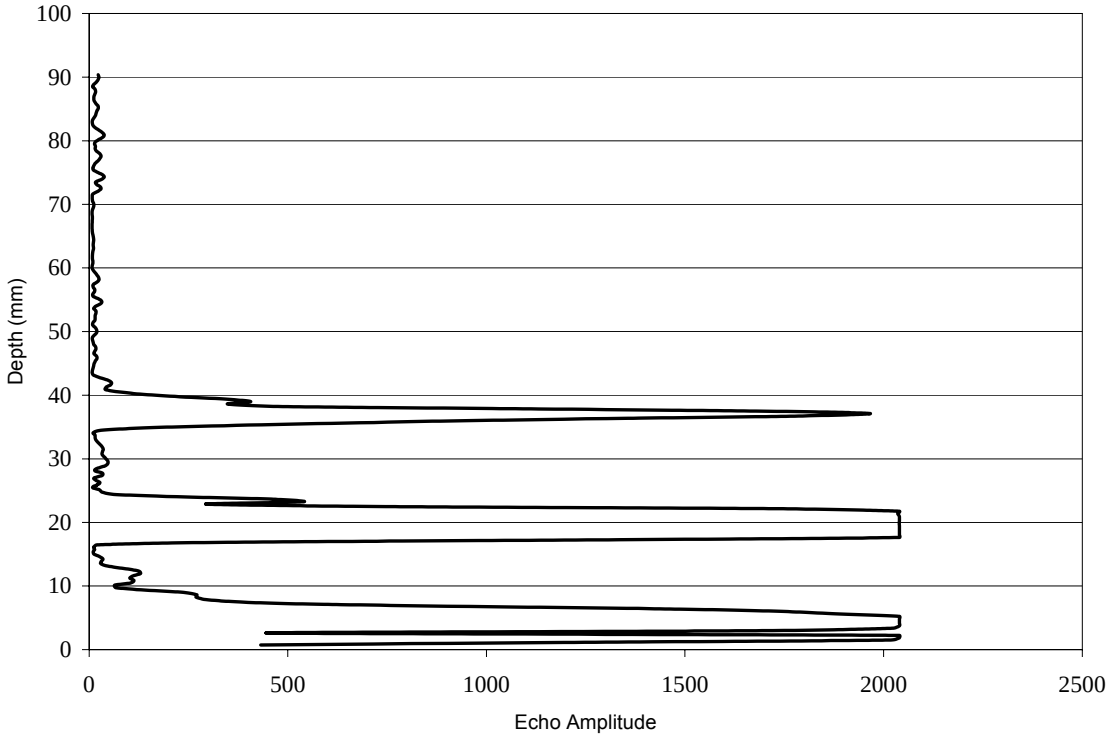

Figure 4-26: Echo Intensity with 4 MHz Transducer and ScreenB at Δx = 20mm

5 Conclusion and Future Work

5.1 Conclusions

The original aim of this study was to characterize the interaction between a pulsed ultrasonic wave and a paper forming screen. To achieve this goal, a Signal-Processing DOP 2000 pulsed ultrasonic Doppler velocimeter was used to generate a pulsed ultrasonic signal. The signal was transmitted and received using four different ultrasonic transducers: a 2 MHz 10 mm, 4 MHz 5 mm, 4MHz 8 mm focused, and 8 MHz 5 mm. These ultrasonic transducers were held in place by a xyz-positioner in a water bath. A small plastic sphere which was also mounted on a xyz-positioner was used as a target in the water bath. The plastic sphere was used to laterally traverse the water bath (perpendicular to the ultrasonic beam propagation direction) and reflect an echo of the ultrasonic signal. The echoes were then analyzed in order to determine the ultrasonic beam amplitude and shape. These tests were performed with and without various paper forming screens placed between the ultrasonic transducer and the plastic sphere.

5.2 Ultrasonic Beam Field

5.2.1 Echo Amplitude

Ultrasonic beam shape measurements were performed in the water bath with the DOP 2000 in order to have a basis of what the beam shape of the various ultrasonic transducers would look like with no obstruction in the path of the ultrasonic beam. As expected, all ultrasonic transducers tested produced a conic-shaped ultrasonic beam. These tests also provided information about the measurement volume of each of the ultrasonic transducers. They showed that each transducer produced a ringing effect, or saturation region, where no useful measurements could be achieved. This region is just in front of the face of the transducer, and its distance varies by transducer. This ringing effect caused a

"minimum distance" from the surface of the transducer to which measurements could be realized. Increasing the amplification of the DOP 2000 increases the ringing effect and consequently, the minimum distance. The minimum distance for the ultrasonic transducers tested was 20 mm, 5 mm, 4 mm, and 8 mm for the 2 MHz, 4 MHz, 4 MHz focused, and the 8 MHz transducers, respectively. This meant that the closest point the ultrasonic beam measurements could start to the transducer in question was the minimum distance for the transducer.

5.2.2 Beam Shape Measurements

The ultrasonic beam field measurements also showed that the beam width decreases with increasing frequency of the ultrasonic transducer. This is due to the fact that wavelength is inversely proportional to frequency. When comparing the 4 MHz 5 mm transducer to the 4 MHz 8 mm focused transducer, the beam width of the focused transducer is approximately half of the beam width of the unfocused transducer at the focal point. The focal point of the focused transducer is approximately 20 mm from the transducer face. Consequently, the amplitude of the received echo from the focused transducer is approximately 500 percent greater at the focal point than the received amplitude from the unfocused 4 MHz transducer.

The repeatability of the beam shape measurements was also studied. The tests showed that the beam shape varied only slightly from test to test. The measurements were performed at different times and after connecting and reconnecting the transducer and plastic sphere in the test setup.

5.3 Ultrasonic Field with Forming Screen Present

The ultimate goal of this study was to look at the interaction of the pulsed ultrasonic beam with a paper forming screen, specifically the amplitude and beam divergence profiles for various transducers. The distance from the screen to the plastic sphere at which the echo of the plastic sphere can still be recognized is desired to be as small as possible in order to get accurate beam shape measurement close to the forming screen. A forming screen is placed at

various distances on the x-axis in order to find the smallest measurable plastic sphere-screen distance. Two different forming screens were used in this study.

5.3.1 Echo Amplitude

The ultrasonic signal is greatly attenuated as it passes through the forming screen causing a great decrease in the amplitude of the echo. The attenuation is caused by absorption and reflection of the ultrasonic signal by the forming screen. This means that much higher amplification must be used when studying the ultrasonic field through a forming screen. This increase in amplification causes an increase in the ringing effect and the saturation region around the forming screen. This in turn increases the minimum distance that the target sphere can be placed from the forming screen. ScreenA caused a decrease in echo amplitude of 60, 93 94, and 100 percent for the 2 MHz, 4 MHz, 4 MHz focused, and 8 MHz transducers, respectively, when compared to the echo amplitudes when the forming screen was not present. ScreenB caused a decrease in echo amplitude of 96 percent for the 4 MHz transducer when compared to the echo amplitude when the forming screen was not present. No results were achieved for the 8 MHz transducer when ScreenA was in place due to the high absorption rate. This test showed that the echo amplitude decreased with increasing frequency since the attenuation of the acoustic wave increases with increasing frequency. All cases showed a significant decrease in echo amplitude when either of the forming screens were present in the test medium.

The minimum measurable distance was defined as the minimum distance between the target sphere and the forming screen that would still produce a measurable signal. The minimum measurable distance for ScreenA was 8, 3, and 4 mm for the 2 MHz, 4 MHz, and 4 MHz focused transducers, respectively. The minimum measurable distance for ScreenB was 4 mm for the 4 MHz transducer. The closest distance from the plastic sphere to the screen over the widest range of transducer-screen-distances that produced detectable echoes was achieved with the 4 MHz 5 mm transducer. The 4 MHz transducer turned out to represent a good tradeoff between the high attenuation of the 8 MHz

transducer and the low resolution (measurable depth and velocity) of the 2 MHz transducer.

5.3.2 Beam Shape Measurements

Placing the forming screen in the ultrasonic beam field caused great changes in the shape of the ultrasonic beam. The “near screen field“ is defined as the region on the opposite side of the screen from the transducer, which is approximately 20-40 mm in length for the 2 MHz transducer and 20 mm in length for both of the 4 MHz transducers (focused and unfocused) with ScreenA. The “far screen field“ is defined as the region that is on the opposite side of the screen as the transducer and is past the “near screen field“ (greater than 40 mm for the 2 MHz transducer and greater than 20 mm for the 4 MHz transducers) for ScreenA. In all cases the beam shape and width in the far screen field are very close to the same with and without ScreenA. In the near screen field, there is a common trend of beam convergence (narrowing of beam width) followed by beam divergence (widening of the beam width) as the beam progresses to the far screen field.

5.3.3 Modeling

Numerical modeling of the calculation of the absorption of acoustic energy due to the forming screen would help verify the reduction of echo intensity due to the forming screen as seen in the test measurements. The Delany-Bazley model and the Allard-Champoux model were used to find the acoustic impedance of the forming screen. Both models estimated that the acoustic impedance of the forming screen was the same magnitude as that of water which would mean that the forming screens would have a transmission coefficient of 100 percent. Unfortunately, this is not a realistic conclusion; therefore, the only calculation of the reduction of the echo amplitude caused by the forming screen is from the experimental measurements.

5.3.4 Repeatability Test

Repeatability tests were performed due to slight variations in the beam shape measurements. General trends such as beam convergence just past the forming screen and then divergence were seen throughout the forming screen tests, but all tests seemed to have some amount of variation. An experiment was produced that could test for the variation in the lateral movement of the forming screen in the water bath. Three tests were conducted on both ScreenA and ScreenB. The first test consisted of 3 sets of beam shape measurements where nothing in the experiment was moved except for the small plastic sphere (in order to generate slices of the beam field). The second test consisted of three sets for ScreenA and 2 sets for ScreenB of beam shape measurements where nothing changed from the first test except the screen was moved 0.5 mm laterally prior to the tests. The third test consisted of three sets of beam shape measurements where nothing changed from the second test except 2 hours was allowed to pass between the test 2 sets and the test 3 sets. This last test was meant to determine if the results of the beam shape measurements could be accurately repeated when nothing in the test setup changes. The tests showed for both ScreenA and ScreenB that there is more variation in beam width when the screen is moved laterally than when it is not moved at all. They also show that even though the pores in the forming screen are very small, they seem to have a great effect on the beam width measurements of the ultrasonic transducer. The greatest variation in the beam widths for ScreenA is at the depth $\Delta x = 70$ mm. The greatest variation in the beam widths for ScreenB is very close to the forming screen, usually at $\Delta x = 44$ mm, but there is also a large variation in beam width and a saturated region around $\Delta x = 75$ mm.

5.3.5 Artefacts

Reverberation, a type of artefact, is caused by multiple echoes being reflected from the same object. Echo intensity profiles from the forming screen tests were studies to check for reverberation from the forming screens. No objects are present in the water bath except the forming screen and the ultrasonic

transducer. These echo profiles clearly show that the forming screen creates a large echo at a depth of 40 mm. The figures show no other discernable echoes except in the region around a depth of 80 mm. These echoes are caused by reverberation of the signal. The reverberations from ScreenB are much greater than the reverberations from ScreenA because ScreenB is twice as thick and has a higher mesh count than ScreenA. The reverberated signal caused the echo profile of the small sphere to be flawed when it passed through the position that the reverberated signal occupied. This caused a flaw in the measurements of the beam shape at the point where the reverberated signal was present.

5.4 Future Work

The experiments done for this study should help with the understanding of the interaction of the acoustic field with paper forming screens. Future work to be addressed might include:

- More ultrasonic field measurements on different forming screen samples to develop a better understanding of the forming screen structure and characteristics,
- The study of the interaction of other transducers with forming screens,
- Develop a numerical model to calculate the transmission coefficient of the forming screen,
- Velocity measurement of flow over a forming screen,
- Velocity measurements of pulp on an operational forming screen.

The main limitation to overcome with this research if it is to be of use in industrial applications is the problem of acoustic coupling. The ultrasonic transducer must be coupled with the flow field in some fashion in order to achieve velocity measurements. This could present a problem due to the high speed movement of forming screens.

Appendix A

Technical Specifications Pulsed Ultrasound Doppler Velocimetry System [31]

The digital ultrasonic synthesizer (Figure A-0-1) can generate any emitting frequencies between 0.45 MHz and 10.5 MHz. Associated to this performance, the DOP2000 includes a variable spatial resolution filter that allows to adapt the size of the sampling volume to the application and therefore improves the signal to noise ratio of the measurements.

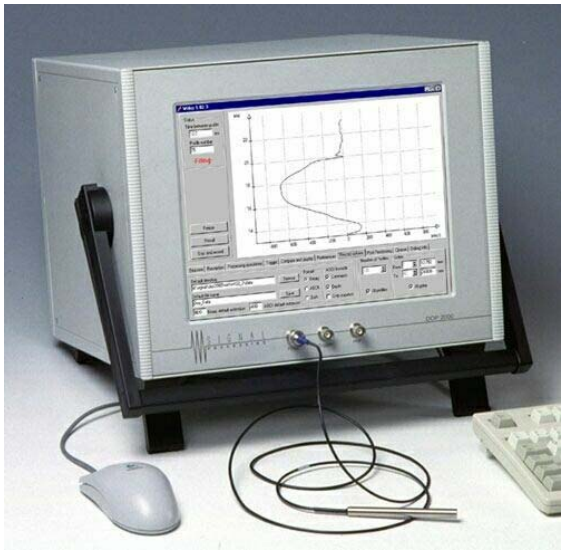

Figure A-0-1: Digital Ultrasonic Synthesizer [31]

All the ultrasonic parameters (Frequency, PRF, Tgc..) and the processing conditions (number of gates, filters ...) are set by the user. The smart trigger capability of the instrument allows to synchronize the acquisition to any periodic or non periodic event. This high flexibility applies to the 10 channels multiplexer and up to 32'000 profiles could be recorded in binary and/or ASCII format.

If desired, the DOP2000 can record simultaneously two types of data profiles, such as the velocity profiles and the Doppler energy profiles. A separate emitter output connector enables to use two different transducers for emission and reception.

Operating in a Windows 9x® environment, the measured profiles are displayed on screen and are recorded in its internal memory or send through the build-in Ethernet connection to any storage device within few milliseconds.

Technical specifications DOP2000 Model 2125

Emission:

Emitting frequencies	from 0.45 MHz to 10.5 MHz, step of 1 kHz
Emitting power	3 levels
Burst length	2, 4 or 8 cycles
PRF	between 64 µs (48 mm) and 10’500 µs (7'875 mm), step of 1 µs

Reception:

Number of gates	between 3 and 1000, step of 1 gate
Position of the first channel	movable by step of 250 ns
Amplification (TGC)	Uniform, Slope, Custom
	Slope mode exponential amplification between two defined depth values. Value at both depths variable between -40dB and +40dB
	Custom mode user's defined values between -40dB and +40dB in cells. Variable number, size and position of the cells.
Sensitivity	>-100 dBm

Resolution:

Lateral resolution	defined by the transducer
Longitudinal resolution	minimum value of 0.85 s (0.64 mm) depends on spatial filter and burst length. (approximate value, defined at 50% of the received)
Spatial filter	from 50 KHz (3.9 mm) to 300 KHz (0.7 mm) , step of 50 KHz
Display resolution	distance between the center of each sample volume selectable between 0.25 s (0.187 mm) and 20 s (15 mm), step of 0.25 s
Velocity resolution	1 LSB (maximum = 0.0091 mm/s; minimum = 91.5 mm/s), Doppler frequency given in a signed byte format

Ultrasonic Processor:

Doppler frequency	computation based on a correlation algorithm
Wall filter	stationary echoes removed by IIR high-pass filter 2nd order
Number of emissions per profile	between 1024 and 8, any values
Detection level	5 levels of the received Doppler energy may disable the computation
Acquisition time per profile	depends on PRF and number of emissions per profile, minimum arround 2 to 3 ms
Filters on profiles	moving average: based on 2 to 32000 profiles, zero values included or rejected median, based on 3 to 32 profiles
Maximum velocity	11.72 m/s for bi-directional flow, 2 times more for unidirectional flow (at 0.5 MHz)
Velocity scale	variable positive and negative velocity range.

Computation:

Compute and display	velocity profile Doppler energy echo modulus velocity profile with echo modulus or Doppler energy velocity profile with velocity versus time of one selected gate velocity profile with flow rate versus time (circular section assumed) velocity profile with real time histogram echo modulus with real time histogram Doppler energy with real time histogram power spectrum of one selected gated
Statistics	mean, standard deviation, minimum, maximum
Velocity component	automatic computation of the projected velocity component
Replay mode	replays a recorded measure from the disk
Utility	freeze/run mode

Advanced features:

	measurement of the ultrasonic field
	extended velocity range (aliasing correction). Option

	acquisition of I and Q signals (8000 values can be recorded)
	acquisition in real time of a complet 3 dimensional velocity field (UDVF mode). Option
	emission and reception can be realized on separated connectors

Trigger:

Input	external signal (TTL) or keyboard action
Configuration parameters	high, low level, internal pull-up 4 K
Delay	between 1 and 10'000 ms, step of 1ms
Acquisition procedure	selectable number of blocks of profiles automatic record capability

Memory/Files:

Internal memory	variable size, memorization from 2 to 32000 profiles
Configuration parameters	10 saved configurations
Data file	Binary (include: ASCII short info blocks, comments, all parameters, all data profiles) ASCII(statistical information available)

Environment*(may be changed):*

Operating system*	Windows® 95 or 98
Processor*	VIA Eden 400MHz
RAM*	128 MBytes (up to 512 Mbytes in option)
Storage devices*	Hard disk 20 GBytes 1'44 MBytes Floppy CD-ROM Read/Write (40x/12x/48x)
Screen	12.4" TFT Color display (800x600) VGA
Communication	2 serial ports 1 parallel port (printer port) 1 Ethernet 10 base T, RJ45 1 external SGVA (simultaneous with TFT) 2 PS2 port (mouse and keyboard) 1 USB (Rev 1.10, type A)

US interface	Echo, (max 0.7 Vp), output impedance of 50 ohm, BNC TTL high level pulse of 100 ns at each emission, BNC Logic level trigger input, pull up by 330 ohm, BNC US probe In/Out, BNC US emission connector, BNC
Power supply	220-110 VAC, selectable, 50 - 60 Hz
Humidity	=< 80%
Temperature	5 - 35 °C
Size	340x265x305 cm
Weight	13 Kg

Options:

Multiplexer	10 probes, internal or external multiplexer
Sound speed unit	measure the sound velocity within 2%

* may be adapted to the market
All values computed with a sound velocity of 1500 m/s (water),in the direction of the ultrasonic beam

Appendix B

Technical Specifications Ultrasonic Transducers [31]

Technical Specifications Ultrasonic Transducers

Technical specifications of ultrasonic transducers are given in Figure B-1 and B-2.

Frequencies and diameters:

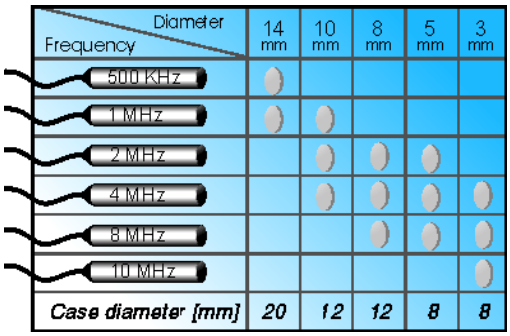

Figure B-0-1: Available Ultrasonic Transducers Signal Processing [31]

Cases:

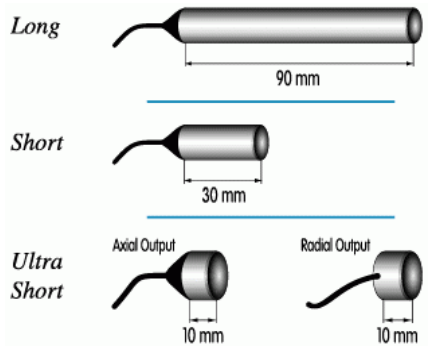

Figure B-0-2: Available Cases Ultrasonic Transducers Signal Processing [31]

Technical specifications

Maximum pressure :	1.5 bars
Impedance :	Matched around 50
Cable type :	RG174
Cable length :	1.5 m (other length upon request)
Cable output :	Axial, Radial available on Ultra-Short Execution
Connector :	BNC
Housing :	Stainless Steel
Front surface :	Epoxy

Appendix C

Delany-Bazley-Model and Allard-Champoux-Model [25]

The Delany-Bazley-Model and the Allard-Champoux-Model were used to model the acoustic impedance of the porous forming screen. Both models and the results are described in the following.

DELANY-BAZLEY MODEL (MIKI CORRECTION)

The equations of Delany and Bayley, presented for the first time in 1970, have since been widely used to describe sound propagation in fibrous materials. These laws have been used in various applications such as sound attenuation in ducts, room acoustics, the calculation of transmission loss through walls, and primarily in models describing sound propagation above various types of ground. Slightly different but similar laws were later suggested to handle specific fibrous materials, and also to improve the low-frequency behavior of the Delany and Bazley equations. The geometry of fibrous materials, in spite of its apparent simplicity has however not been taken into account in these works [2].
The power laws of Delany and Bazley involve eight adjustable parameters that are the same for all fibrous materials. According to Delany and Bazley, the acoustic impedence is predicted by:

$$Z = R + iX = \rho_0 c_0 \left[1 + AF^{\alpha} + iBF^{\beta}\right]$$

with the constants:

A = 0.057

B = 0.087

α = - 0.75

β = - 0.732

Delany-Bazley-Model

where f is the frequency, ρ_0 is the density of the fluid, $\sigma = \Delta p/(U\ l)$ is the flow resistivity, Δp is the pressure drop, U is the fluid velocity, l is the material thickness, c_0 is the speed of sound in the fluid and the constant F is $\rho_0 f/\sigma$.

In general, knowledge of the flow-resistance of a material permits the relevant acoustic impedance to be predicted, although care must be taken to ensure that a representative value of flow-resistance is used, as many practical materials are subject to considerable variation between and within batches. However, for many purposes high accuracy is not required for instance, in the initial design stages where selection of a potentially suitable absorbing material is the objective. Unfortunately, manufactures do not usually include data on flow-resistance in their technical literature. It is emphasized that the purpose of these flow resistivity measurements (see appendix) is solely to provide an indication of the order of magnitude of the flow-resistance to be expected for a given material. Manufacturers do not necessarily control the flow-resistance of their product and it will usually be necessary to sample-test a specific material before final evaluation. The main factors influencing the flow-resistance of fibrous materials are the fiber size and the bulk density, and it is known that for given fiber size the relation between bulk density and flow-resistance approximates closely to a simple power law [10].

The formulas given above were implemented in the following MATLAB code [25] to calculate the acoustic impedance from 2 to 8 MHz.

```
%Acoutic Impedance Description of the Forming Screen

clear all

%Forming screen roperties:
rhop=1620; %density of polyester in kg/m3
Omega=0.95; %porosity
sigmae=95.5; %specific flow resistivity in MKS-Rayls
l=0.00056; %thickness in m
sigma=sigmae/l; %flow resistivity in MKS-Rayls/m

%Fluid properties:
rho0=1000; %density of water in kg/m3
c0=1482; %speed of sound in water at 20 degree celsius in m/s


%Specific Acoustic Impedance Zs

%a) Delany-Bazley model:

N1=2000000;
N2=8000000;
f=N1:1:N2; %frequency in Hertz

A=0.057;
B=0.087;
```

```
F=f.*rho0/sigma; %Non-dimensional frequency
alpha=-0.750;
beta=-0.732;
Zs=rho0*c0*(1+A*F.^alpha+i*B*F.^beta);

figure(1)
subplot(2,2,1)
semilogx(f,real(Zs),'b')
xlabel('Frequency [log]')
ylabel('Real Part Spec. Ac. Impedance')
title('Delany-Bazley Model')

subplot(2,2,2)
semilogx(f,imag(Zs),'b')
xlabel('Frequency [log]')
ylabel('Imaginary Part Spec. Ac. Impedance')
title('Delany-Bazley Model')

hold on
```

The results are shown in Figure C-1 and discussed in chapter 4.3.

ALLARD-CHAMPOUX-MODEL

Jean-F. Allard and Yvan Champoux developed new expressions that can be used instead of the phenomenological equations of Delany and Bazley. They provide similar predictions in the range of validity of these equations, and in addition are valid at low frequencies where the equations of Delany and Bazley provide predictions that are not physically possible. These new expressions have been worked out by using the general frequency dependence of the viscous forces in porous materials proposed by Johnson et al. [18], with a transportation carried out to predict the dynamic bulk modulus of air. The model used suggests how sound propagation in fibrous materials can depend both on the diameter of the fibers and on the density of the material [2].

Typical fibers are modeled here as infinite circular-cylindrical rods of radius r that lie in planes parallel to the surface of the layers. Only the case where the velocity of the fluid for from the fibers is perpendicular to the direction of the fibers is considered here. The detailed description of the model which will be used to describe the propagation of sound through the porous forming screen and the

derivation of the equations which will be applied in the following can be found in the paper of Allard et al. [2]. The acoustic impedance *Z* is:

$$Z = \sqrt{\rho_b(\omega)\, K_b(\omega)}$$

Effective dynamic density of material ρ_b:

$$\rho_b(\omega) = \rho_0 \left[1 - \frac{\sqrt{1 - \frac{i\omega\tau}{2}}}{i\omega\tau} \right]$$

Effective dynamic bulk modulus K_b:

$$K_b(\omega) = \gamma P_0 \left[\gamma - \frac{\gamma - 1}{1 - \frac{\sqrt{1 - i\omega 2N\tau}}{i\omega 4N\tau}} \right]$$

Allard-Champoux-Model

where ρ_0 is the density of the fluid, $\omega = 2\pi f$ is the angular frequency, τ equals ρ_0/σ, $\sigma = 4\Omega\sigma_e/S_f^2$ is the flow resistivity, $\Omega = V_p/V_S$ is the porosity (V_p is the volume of the sample and V_S is the volume of the fibers), σ_e is the specific flow resistivity, S_f is the pore shape factor, γ is the ratio of the specific heats, P_0 is the atmospheric pressure and *N* is Prandtl number.

The predictions obtained from the laws of Delany and Bazley as well as from Allard and Champoux, are very similar in the range of validity of the laws of Delany and Bazley. The expressions given by Allard and Champoux are, however, also valid at low frequencies and can be used to describe the steady flow of air through fibrous media. The Allard-Champoux-model predicts a dependence of the dynamic density and the bulk modulus as a function of the bulk density of the material and the diameter of the fibers, that can be neglected at low frequencies, but is measurable at high frequencies.

The formulas given above were implemented in the following MATLAB [25] code to calculate the acoustic impedance from 2 to 8 MHz.

```
%Acoutic Impedance Description of the Forming Screen

clear all

%Forming screen roperties:
rhop=1620; %density of polyester in kg/m3
Omega=0.95; %porosity
sigmae=95.5; %specific flow resistance in MKS-Rayls
l=0.00056; %thickness in m
s=1; %pore shape factor
sigma=sigmae/l; %flow resistivity in MKS-Rayls/m



%Fluid properties:
rho0=1000; %density of water in kg/m3
c0=1480; %speed of sound in water at 20 degree celsius in m/s
cpw=4.186; %specific heat at constant pressure for water in J/(gK)
cvw=4.186; %specific heat at constant volume for water in J/(gK)
gamma=cpw/cvw; %heat capacity ratio
P0=101300; %atmospheric pressure
N=7; %Prandtl number for water


%Specific Acoustic Impedance Zs (real and imaginery part of the specific acoustic
impedance)

%b)Allard-Champoux Model:

N1=2000000;
N2=8000000;
i=sqrt(-1);

for j=N1:100000:N2 %frequency in Hertz
    f(j)=j;
    omega=f(j)*2*pi;
    tau=rho0/sigma;
    rhob=rho0*(1+((1/(i*2*pi))*(1/(tau*f(j)))*(1+i*pi*(tau*f(j)))^0.5));
    Kb=gamma*P0*(gamma-((gamma-1)/(1+(1/(i*8*pi*N))*(1/(tau*f(j)))*((1+i*pi*
       (tau*f(j)))^0.5)*((1+i*pi*4*N)^0.5))));
    Zs(j)=(rhob*Kb)^0.5;
end

figure(1)
subplot(2,2,3)
semilogx(f,real(Zs),'b')
xlabel('Frequency [log]')
ylabel('Real Part Spec. Ac. Impedance')
title('Allard-Champoux Model')

subplot(2,2,4)
semilogx(f,imag(Zs),'b')
xlabel('Frequency [log]')
ylabel('Imaginary Part Spec. Ac. Impedance')
title('Allard-Champoux Model')

hold on
```

The results are shown in Figure C-1 and discussed in 4.3.

RESULTS OF THE DELANY-BAZLEY-MODEL AND ALLARD-CHAMPOUX-MODEL:

Results of the Delany-Bazley-Model and the Allard-Champoux-Model are given in Figure C-1.

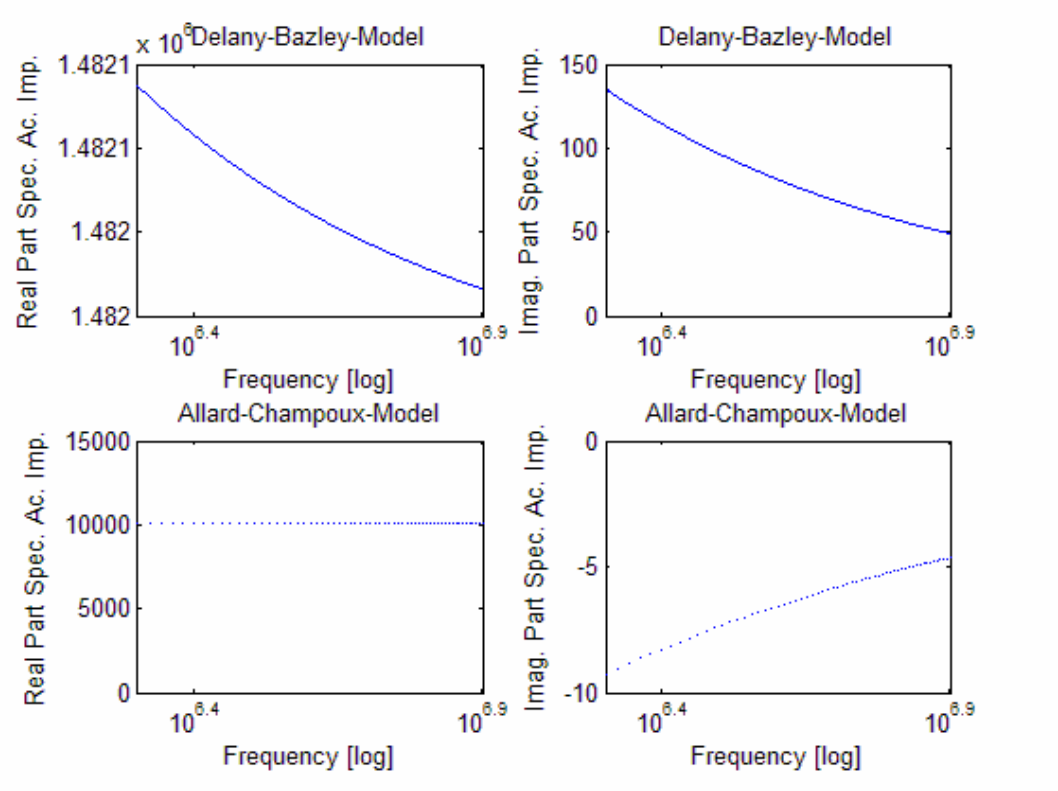

Figure C-0-1: Results Acoustic Impedance Models [25]

References

1. Adrian, R. J. (2004). "Twenty Years of Particle Image Velocimetry." 12th International Symposium on Applications of Laser Techniques to Fluid Mechanics.

2. Allard, J.-F.; Champoux, Y. (1992). "New Empirical Equations for Sound Propagation in Rigid Frame Fibrous Materials." Journal of the Acoustical Society of America 6: 91.

3. Baker, D. W. (1965). "The Doppler Shift Principle Applied to Flow and Displacement Measurement, Proceedings of the 18th Annual Conference on Engineering in Medicine and Biology.

4. Baker, D. W. (1969). “Transcutaneous pulse Doppler techniques.” Proceedings of the 14th annual scientific conference of the American Institute of Ultrasound in Medicine.

5. Baker, D. W. (1970). “Pulsed ultrasonic Doppler blood flow sensing.” IEEE Transactions on Sonics and Ultrasonics SU 17(3): 170-185.

6. Baker, D. W. (1973). "Characteristics and Mathematical Modeling of the Pulsed Ultrasonic Flowmeter." Medical and Biological Engineering(July): 404-421.

7. Brito, D.; Nataf, H. C.; Cardin, P.; Aubert, J.; Masson, J. P. (2001). "Ultrasonic Doppler Velocimetry in Liquid Gallium." Experiments in Fluids 31(6): 653-663.

8. Brodeur, P.H. and Lewis, E.L., "Ultrasonic Characterization of Forming Fabrics", *Tappi J.* 77(4): 137-143 (1994).

9. Delany, M. E.; Bazley, E. N. (1970). "Acoustical Properties of Fibrous Absorbent Materials." Applied Acoustics 3.

10. Durst F., Melling A. and Whitelaw J. H., (1981). “Principles and Practice of Laser Doppler Anemometry.” Academic Press, London.

11. Eckert, S.; Gerbeth, G. (2002). "Velocity Measurements in Liquid Sodium by Means of Ultrasound Doppler Velocimetry." Experiments in Fluids 32(5): 542-546.

12. Evans, D. H.; McDicken, W. N. (2000). "Doppler Ultrasound - Physics, Instrumentation and Signal Processing." Wiley.

13. Franklin, D.L.; Baker, D.W.; Ellis, R.M.; Rushmer, R.F., (1959). “A pulsed ultrasonic flowmeter." Institute of Radio Engineers Transactions on Medical Electronics. v ME-6, n 4: 204-206.

14. Franklin, D.L.; Baker, D.W.; Rushmer, R.F., (1962). "Pulsed ultrasonic transit time flowmeter." IRE -- Transactions on Bio-Medical Electronics v BME-9, n 1: 44-40

15. Harding, D.C.; Rushmer, R.F.; Baker, D.W., (1967). “Thermal transcutaneous flowmeter.” Medical and Biological Engineering v 5, n 6: 623-626

16. Jawad, I. A. (1996). "A Practical Guide to Echocardiogrpahy and Cardiac Doppler Ultrasound." John Wiley & Sons, Inc.

17. Jensen, J. A. (1996). "Estimation of Blood Velocities Using Ultrasound." Cambridge University Press.

18. Johnson, D.L.; Koplik, J.; and Dashen, R. (1987). "Theory of dynamic permeability and tortuosity in fluid-saturated porous media." Journal of Fluid Mechanics 176: 379-402.

19. Kalmus, H.P (1954). “Electronic flowmeter system.” Review of Scientific Instruments v 25, n 3: 201-206

20. Kerut, E. K.; McIlwain, E. F.; Plotnick, G. D. (1996). "Handbook of Echo-Doppler Interpretation." John Wiley & Sons, Inc.

21. Kikura, H.; Takeda, Y.; Durst, F. (1999). "Velocity Profile Measurement of the Taylor Vortex Flow of a Magnetic Fluid Using the Ultrasonic Doppler Method." Experiments in Fluids 26(3): 208-214.

22. Kikura, H.; Takeda, Y.; Sawada, T. (1999). "Velocity Profile Measurements of Magnetic Fluid Flow Using Ultrasonic Doppler Method." Jorunal of Magnetism and Magnetic Materials 201: 276-280.

23. Kikura, H.; Yamanaka, G.; Aritomi, M. (2004). "Effect of Measurement Volume Size on Turbulent Flow Measurement Using Ultrasonic Doppler Method." Experiments in Fluids 36(1): 187-196.

24. Kino, G. S. (1987). "Acoustic Waves: Devices, Imaging and Analog Signal Processing." Engelwood Cliffs, N.J., Prentice-Hall.

25. Messer, M. (2005). “Pulsed Ultrasonic doppler velocimetry for measurement of velocity profiles in small channels and capillaries.” Master Thesis, Georgia Institute of Technology.

26. Mordant, N. P., Pinton, J. F.; Michel, O. (2002). "Time-Resolved Tracking of a Sound Scatterer in a Comlex Flow: Nonstationary Signal Analysis and Applications." Journal of the Acoustical Society of America 112: 108-118.

27. Mori, M.; Takeda, Y.; Taishi, T.; Furuichi, N.; Aritomi, M.; Kikura, H. (2002). "Development of a novel flow metering system using ultrasonic velocity profile measurement." Experiments in Fluids 32: 153-160.

28. Nowak, M. (2002). "Wall shear stress measurement in a turbulent pipe flow using ultrasound Doppler velocimetry." Experiments in Fluids 33: 249-255.

29. Ozaki, Y.; Kawaguchi, T.; Takeda, Y.; Hishida, K.; Maeda, M. (2002). "High time resolution ultrasonic velocity profiler." Experimental Thermal and Fluid Science 26: 253-258.

30. Panametrics, I. (2004). "Technical Notes." http://www.panametrics-ndt.com/ndt/ndt_transducers/downloads/transducer_technotes.pdf.

31. Signal-Processing (2004). "Introducing Ultrasonic Doppler Velocimetry." www.signal-processing.com.

32. Skolnik, M. I. (1990). "Radar Handbook." McGraw-Hill.

33. Satomura, S. (1957). "Ultrasonic Doppler method for the inspection of cardiac functions." Journal of the Acoustical Society of America , v 29, n 11: 1181-1185

34. Takeda, Y. (1986). "Velocity Measurement by Ultrasound Doppler Shift Method." International Journal Heat and Fluid Flow 7(4): 313-318.

35. Takeda, Y. (1995). "Velocity Profile Measurement by Ultrasonic Doppler Method." Experimental Thernal and Fluid Science 10(4): 444-453.

36. Takeda, Y.; Kikura, H. (1998). "Measurement of mercury flow by ultrasonic Doppler method." Proceeding of 1998 ASME fluid engineering division summer meeting, June 21-25, Washington, DC, USA: FEDSM98-5074.

37. Takeda, Y. (1999). "Ultrasonic Doppler Method for Velocity Profile Measurement in Fluid Dynamics and Fluid Engineering." Experiments in Fluids 26(3): 177-178.

38. Wang, T.; Wang, J.; Ren, F.; and Jin, Y. (2003). "Application of Doppler ultrasound velocimetry in multiphase flow." Chemical Engineering Journal 92: 111-122.

39. Wells, P. N. T. (1969). "Physical Principle of Ultrasonic Diagnosis." Academic Press.

40. Wells, P. N. T. (1977). "Biomedical Ultrasonics." Academic Press.

41. Xu, H. (2003). Measurement of Fiber Suspension Flow and Forming Jet Velocity Profile by Pulsed Ultrasonic Doppler Velocimetry. Atlanta, Institute of Paper Science and Technology. Ph.D.